3̶ᵧ̶ᵧ̶1̶ᴐ̶

NAME OF AUTHOR/*NOM DE L'AUTEUR*___Michael Danyluk_____

TITLE OF THESIS/*TITRE DE LA THÈSE*___Two Photon Sequential Absorption Spectroscopy of the___

___Iodine Molecule_____

_____

UNIVERSITY/*UNIVERSITÉ*_____McMaster_____

DEGREE FOR WHICH THESIS WAS PRESENTED/
  *GRADE POUR LEQUEL CETTE THÈSE FUT PRÉSENTÉE*____Ph.D._____

YEAR THIS DEGREE CONFERRED/*ANNÉE D'OBTENTION DE CE DEGRÉ*____1978_____

NAME OF SUPERVISOR/*NOM DU DIRECTEUR DE THÈSE*____Dr. G.W. King_____

DATED/*DATE*__May 29, 1978____ SIGNED/*SIGNÉ*____

PERMANENT ADDRESS/*RÉSIDENCE FIXE*____1239 - 21 Ave____

____CALGARY, ALTA._____

TWO-PHOTON SEQUENTIAL ABSORPTION

SPECTROSCOPY OF THE IODINE MOLECULE

by

MICHAEL D. DANYLUK, MSc.

A Thesis

Submitted to the School of Graduate Studies

in Partial Fulfilment of the Requirements

for the Degree

Doctor of Philosophy

McMaster University

1978

TWO-PHOTON SPECTROSCOPY OF IODINE

DOCTOR OF PHILOSOPHY (1978)　　　　　McMASTER UNIVERSITY
　　　　　　　　　　　　　　　　　　　　Hamilton, Ontario

TITLE:　　　　　Two-Photon Sequential Absorption Spectros-
　　　　　　　　copy of the Iodine Molecule

AUTHOR:　　　　Michael Donald Danyluk, B.Sc. (University of
　　　　　　　　　　　　　　　　　　　　　　　　Calgary)

　　　　　　　　　　　　　　　　　　M.Sc. (University of
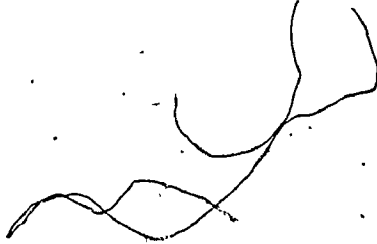　　　　　　　　　　　　　　　　　　　　　　Calgary)

SUPERVISOR:　　Professor G. W. King

NUMBER OF PAGES:　xiv, 170

ABSTRACT

Two independently tunable dye lasers have been
used to examine under high resolution two-photon sequen-
tial absorption processes for molecular iodine. One laser
was used to pump selected rotational levels of the B state
while the second laser excited transitions from the pumped
level(s) to excited states of higher energy. Five separate
electronic states which have ion-pair character have been
examined in the 5 to 5.5eV energy region and their spec-
troscopic constants evaluated. Two of the excited states
have 0_g^+ symmetry as identified by rotational analysis; the
remaining three are either 0_g^+, 1_g^+, or possibly 2_g^+. At
least three of these excited gerade states have been
shown to likely contribute to previously reported emission
spectra of iodine.

A new two-photon method for the direct determina-
tion of molecular dissociation limits was developed from
the sequential absorption studies described above. The
technique permits selective excitation of rotational band
structure near the convergence limit and is generally ap-
plicable to molecules with vibronic states (E) accessible
by single-photon sequential absorption from an intermediate

state (B). The amount of rotational structure which can be selectively displayed by the method can be adjusted by varying the ratio of the bandwidth of one of the exciting dye lasers to the E state rotational constant. This technique has been applied to analysis of the B←X iodine transition near dissociation and has provided an improved value for the B state dissociation limit. In addition, vibrational and rotational constants for energy levels near D are reported and applied to an investigation of the B state potential function at large internuclear distances.

ACKNOWLEDGEMENT

DEDICATED

to my wife Sandy with gratitude for her encouragement
and support.

TABLE OF CONTENTS

LIST OF TABLES

LIST OF FIGURES

List of Figures, Continued

CHAPTER I

INTRODUCTION

Recently, optical spectroscopy has experienced
a remarkable resurgence in activity. This increased in-
terest stems from a number of far-reaching developments,
foremost among these being the development of the *wave-
length tunable* laser and its application to science and
engineering.

The unique spectral and temporal properties of
tunable laser radiation have done more than enhance the
sensitivity and application range of classical spectroscop-
ic methods. The study of the interaction of intense laser
radiation with matter has, in addition, revealed new
phenomena which have stimulated the development of new and
powerful techniques of modern optical spectroscopy. For
example, ultra-high resolution Doppler-free spectroscopy,
stimulated light scattering and coherent transient effects
have been demonstrated with tunable laser sources (1).

At visible wavelengths tunable laser technology
is based on the broadband fluorescent emission of optical-
ly excited organic dye compounds. Dye lasers, by using
several different compounds as the gain medium, can provide

continuously tunable radiation from approximately 3500 to 7500 Angstroms--a spectral region in which both atomic and molecular electronic transitions are observed. Because of this wide wavelength tunability, dye lasers applied to the study of the electronic structure of matter have been in the forefront of recent spectroscopic advances.

The present study was initiated as the spectroscopic potential of tunable dye laser technology became evident. Some of the experiments reported here were conducted with the prototype to the first commercially marketed nitrogen laser-pumped dye laser, but deficiencies with this device necessitated an instrumentational development program. In addition to modifying the commercial instrument an initial objective of the present study was to design and construct a two-photon spectrometer based on two independently tunable dye lasers.

Historically, optical spectroscopy has been performed in the realm of linear optics where only a single photon interacts with an atomic or molecular system at a time. Now however, laser methods have made the observation of two-photon and higher order nonlinear interactions possible. These multi-photon processes are accompanied by absorption (or emission) or two of more photons from an intense radiation field and induce transitions to quantum states not usually accessible to single photon studies. There is,

therefore, strong academic interest in the study of the unknown eigenstates of matter by multi-photon methods. Keen interest in multi-photon studies has also been sparked by engineering applications such as laser isotope separation (2).

Two-photon spectroscopy (particularly since the advent of the tunable laser) has advanced considerably since the first experimental observation of two-photon transitions in 1961 (3). For example, in 1974 and early 1975, three laboratories (4, 5, 6) independently demonstrated the feasibility of Doppler-free two-photon spectroscopy following the original suggestion of Vasilenko *et al* (7). Yet despite these advances, two-photon spectroscopy is still in its infancy. Although many atomic systems have been investigated by two-photon methods, most notably Hänsch's investigation of the Lamb shift in atomic hydrogen (6), very few *molecular* two-photon studies have been published.

There are two types of two-photon experiment that are relevant to molecular electronic spectroscopy. In one type of experiment, termed double photon absorption spectroscopy, two photons (usually, but not necessarily) of equal frequency interact with the sample to induce transitions to an excited state at twice the photon energy. The light frequency in this case may or may not be "near

resonance" with a single photon transition and experimentally only one laser source is required. The technique has not seen widespread application because the low absorption cross-section of double photon transitions generally requires a tunable laser source of high output power.

The second type of experiment is termed "stepwise excitation" and involves a resonant intermediate energy level. One photon is used to populate an intermediate level while a second photon induces transitions to excited states of higher energy. This technique generally requires two laser sources and has also been termed sequential absorption spectroscopy or optical-optical double resonance spectroscopy by analogy to previous double resonance studies.

Recently, Field *et al* (8) and Danyluk and King (9, 10, 11) demonstrated the high degree of rotational selectivity inherent in high resolution two-photon sequential absorption studies. Unlike double photon spectroscopy (or conventional single photon methods), only a limited number of rotational transitions are observed with the sequential method. This enables the assignment and interpretation of spectroscopic parameters to be determined with comparative ease. In addition, sequential experiments require only modest laser power levels (11) and these requirements can easily be met by the current generation of

tunable dye lasers.

The present study undertook a detailed two-photon sequential absorption study of molecular iodine as a topic for original research for several reasons. It was the objective of the research program not only to demonstrate a new experimental technique but also to provide useful information for a molecule which has attracted spectroscopic attention since the early 1900's (12). Iodine is perhaps the most thoroughly studied diatomic molecule; yet very little is known about its high energy electronic states. In fact, considerable controversy exists with regard to the interpretation of the limited data currently available and the need for further experimental investigation has been recognized (13, 14).

A brief comment on the organizational structure of the remainder of the text concludes this introductory chapter. Chapter II reviews single-photon spectroscopic investigations of the iodine molecule which are relevant to the current study. A more detailed discussion of two-photon optical spectroscopy is presented in Chapter III. Chapter IV discusses the performance evaluation of a high resolution tunable dye laser spectrometer designed and built specifically for two-photon investigations. The application of the spectrometer to two-photon sequential absorption studies of the iodine molecule is discussed in Chapter V. Spec-

troscopic constants for five previously unidentified electronic states are correlated with theoretical predictions and a reassignment of the complex electric discharge emission spectrum of iodine is also suggested in Chapter V.

Chapter VI describes a new two-photon technique for the experimental determination of molecular dissociation limits (9, 15). The method overcomes many of the problems inherent in single-photon methods by selective excitation of individual vibrational and rotational levels. Molecular constants and the form of the long-range potential for iodine near the B state dissociation limit are reported in Chapter VI.

Finally, Chapter VII presents a summary of the more important conclusions derived from a two-photon investigation of molecular iodine.

CHAPTER II

THE SPECTROSCOPY OF IODINE

1. Introduction

Molecular iodine is an ideal candidate for a prototype demonstration of two photon sequential absorption spectroscopy. Both the ground state ($X^1\Sigma_g^+$) and a low energy excited electronic state (B $^3\Pi_{0_u^+}$) have been studied extensively by single photon methods. Yet, for iodine, little is known of the high energy gerade electronic states accessible to two-photon spectroscopy.

In the present sequential study, selected rotational B←X transitions were pumped with a high resolution tunable dye laser. Transitions from B state levels to higher energy electronic states (collectively referred to as "E" states) were simultaneously investigated with a second independently tunable dye laser. This Chapter surveys the published literature pertinent to the X, B and "E" electronic states. No attempt will be made to include topics not relevant to the present two-photon study.

2.   Valence States of Iodine

2.1   Term Manifold

The manifold of electronic states for a diatomic molecule may be deduced from a consideration of the electron configuration assigned to various molecular orbitals (16). Consider, for example, the molecular orbitals illustrated in Figure II-1 which are derived from an LCAO analysis of the 5p electrons of two ground state $(^2P_{\frac{3}{2},\frac{1}{2}})$ iodine atoms (17, 18). The lowest energy arrangement of the ten valence electrons $\sigma^2\pi^4\pi^4\sigma^0$ defines the ground state of the iodine molecule and is shown in Figure II-1. Generally, the electron configurations $\sigma_g^m\pi_u^n\pi_g^o\sigma_u^p$ are abbreviated to the superscripts *mnop* in the following discussion. The ground state for example is given by 2240 while the lowest energy excited electronic configuration is 2431.

The classification of states derived from a given *mnop* configuration must recognize the coupling of electronic and rotational angular momenta (16). For example, the 2431 configuration of iodine is best described as approximately Hund's case (c) because of large spin orbit coupling interactions. In Hund's case (c), Figure II-2, the axial molecular field is not sufficiently strong to break down the atomic coupling and Λ (axial projection of the
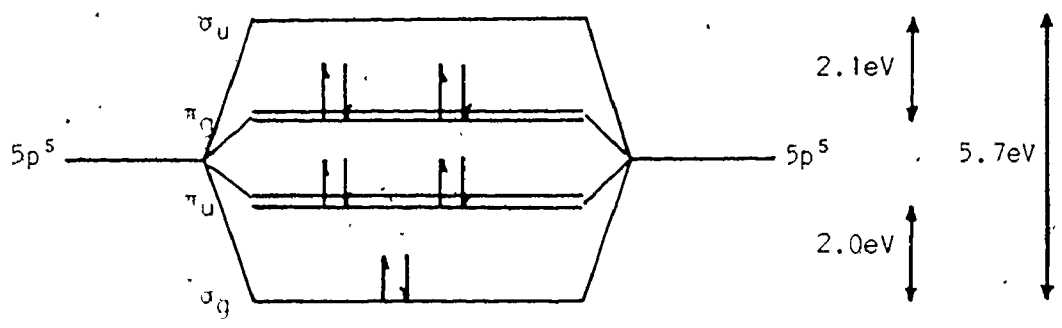
Figure II-1: Molecular Orbitals for the valence shell configurations of I_2. The ground state configuration is illustrated and the energy scale is that estimated by Mulliken (13),
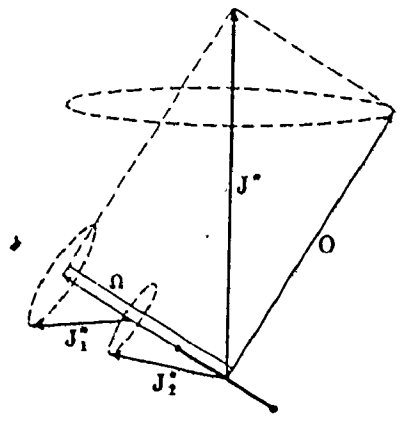
Figure II-2: Hund's coupling case (c).

orbital angular momentum) and Σ (axial spin projection)
are not well defined. Thus molecular states in case (c) ·
must be classified according to Ω, the axial projection of
the total electronic angular momentum. Mulliken (18) has
classified the valence states of iodine according to case
(a) and case (c) notations and derived energy expressions
for the case (c) components ($\Omega = 0$, 1, 2) of the 2431 con-
figuration. His analysis has been successfully applied to
the interpretation of the intensity distribution of the vi-
sible spectrum of I_2 and other halogens (19).

Mulliken (20) has also given correlation rules
which predict the case (c) molecular states obtained from
separate atomic terms. These atomic correlation rules, as
illustrated in Figure II-3, can be used to predict the prob-
able dissociation products of a molecular state. Figure
II-3 shows the 23 molecular states [case (c) Ω notation]
derived from two ^2P ground state iodine atoms and the cor-
relation with terms arising from the four lowest energy
electronic configurations. The correlations are deduced
by rigorous application of the non-crossing rule which
forbids states of the same Ω and g or u symmetry to cross.
Diagrams analogous to Figure II-3 can be constructed for
more energetic states which correlate with excited atoms.

Atomic correlation diagrams are, however, quali-
tative and critically dependent on the relative energy of
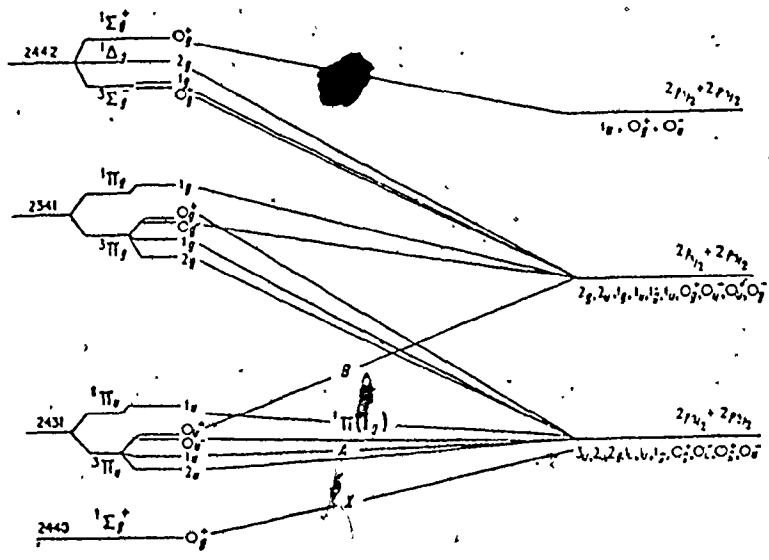
Figure II-3. Schematic correlation diagram for molecular Iodine.

the molecular terms. For larger multiplet splittings the relative positions of 2341 $^3\Pi_{0^+_g}$ and 2422 $^3\Sigma^-_g(0^+_g)$ may be reversed, for example, in Figure II-3. Then 2341 $^3\Pi_{0^+_g}$ would correlate with $^2P_{\frac{3}{2}} + {}^2P_{\frac{1}{2}}$ atoms rather than $^2P_{\frac{3}{2}} + {}^2P_{\frac{3}{2}}$ atoms. It should be noted that 0^+_u derived from $^2P_{\frac{1}{2}} + {}^2P_{\frac{3}{2}}$ atoms is unique, and must correlate with $^3\Pi_{0^+_u}$, defined as the B state in Figure II-3.

Recently Mulliken (13) has reviewed the valence states of iodine. The electron configurations, term assignments, dissociation products and estimated potential curves as discussed by Mulliken (13) are shown in Figure II-4. Only the 2240 $^1\Sigma^+_g(X)$ and 2431 $^3\Pi_{0^+_u}$ (B) potentials are known accurately from experiment. The other potential curves in Figure II-4 were derived from estimates of the vertical energies [at r = $r_e(X)$ = 2.66Å], from the dissociation product energies and by application of the non-crossing rule. Very recently reported pseudopotential calculations (21) have yielded vertical energy values for iodine which are slightly lower than Mulliken's predictions.

As discussed with regard to Figure II-3, when states of the same symmetry species are estimated to be of nearly equivalent energy the relative ordering of molecular terms in Figure II-4 may be in error. Despite its qualitative nature, Figure II-4 does predict which elec-
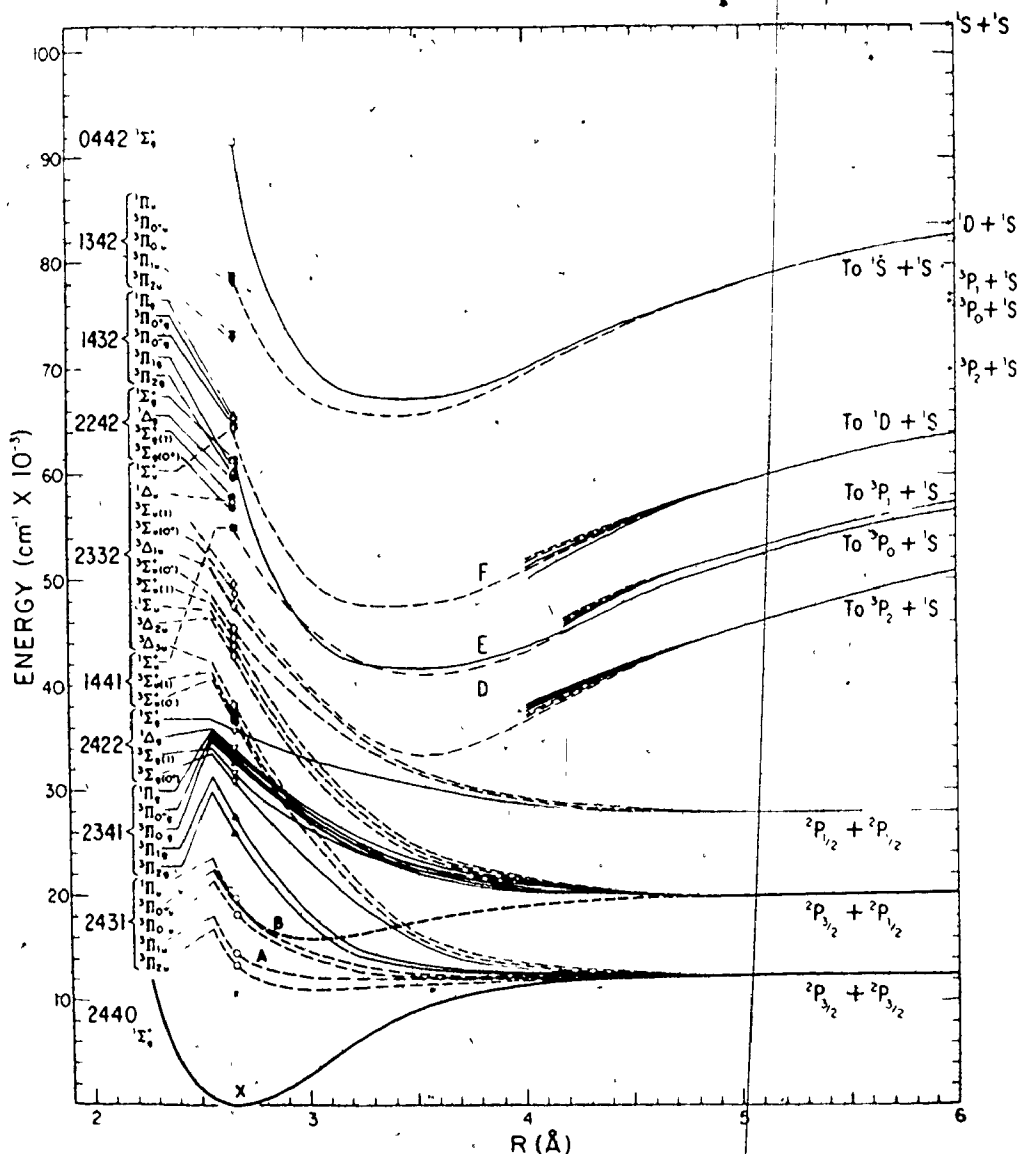
Figure II-4: Estimated potential curves for valence-shell
states of I_2 (13). The curves for gerade
states are shown by full lines, those for
ungerade states by dashed lines. Only B
and X are known quantitatively. Although
the exact position of the D curve is not
known, its approximate position is indi-
cated. Curves E and F are predicted from
the measurements of reference (14).

tronic states are to be expected for iodine and serves as a valuable aid to the assignment of observed transitions.

2.2 Electronic States Accessible by Two-Photon Sequential Absorption

Sequential two-photon transitions originating from the ground state of iodine must terminate in an excited state of gerade symmetry. While this and other considerations are discussed more fully in Chapter III, it is worth while, at the present time, to discuss from a theoretical point of view what is known about the gerade molecular states of iodine.

Table II-1 lists the gerade states of iodine arising from various electronic configurations together with theoretical *estimates* of the vertical energies relative to the ground state (13). There are a large number of stable gerade states theoretically predicted to occur in the 5 to 8.5 eV region. The present study however was limited to energies less than 5.7 eV, primarily due to instrumentational restrictions (see Chapter IV). Nevertheless, several states within the 2242 and 1432 configurations should be amenable to two-photon investigation if the energy estimates of Table II-1 are accurate.

All of the states listed in Table II-1, except those which arise from the 2341 configuration, correlate with the ionic species $I^-(^1S)$ and $I^+(^1S, ^3P_{0,1,2}, ^1D)$. These and similar states in other molecules have been

CONFIGURATION	TERM	T'_E (min)	T'_V
0442	$^1\Sigma_g^+$	8.37	11.3
1432	$^1\Pi_g$	(~5.2)	8.1
	$^3\Pi_{0^+g}$	5.13 or 5.69	8.1
	$^3\Pi_{0^-g}$	(~5.2)	8.0
	$^3\Pi_{1g}$	5.24	7.5
	$^3\Pi_{2g}$	5.0	7.4
2242	$^1\Sigma_g^+$	5.13 or 5.69	7.6
	$^1\Delta_g(2)$		7.4
	$^3\Sigma_g^+(1)$	(~5.0)	7.1
	$^3\Sigma_g(0^+)$		7.0
2422	$^1\Sigma_g^+$	R	4.4
	$^1\Delta_g$	R	4.2
	$^3\Sigma_g^-(1)$	R	3.9
	$^3\Sigma_g(0+)$	R	3.8
2341	$^1\Pi_g$	R	4.1
	$^3\Pi_{0^+g}$	R	4.1
	$^3\Pi_{0^-g}$	R	4.1
	$^3\Pi_{1g}$	R*	3.4
	$^3\Pi_{2g}$	R*	3.2

Table II-1: Approximate Energies (eV) of Excited Electronic Gerade States of I_2 (13).

T'_V is the estimated vertical energy evaluated at the equilibrium internuclear distance of the ground state, X. T'_E(min) is an estimated minimum energy for bound excited states, relative to X. R designates repulsive states. R* may possibly be shallow-bound states.

termed "ion-pair" states because of this correlation.
Ion-pair states are characterized by large equilibrium
internuclear distances and low ω_e values. Not all of the
potential curves for the ion-pair states of Table II-1
are drawn in Figure II-4, in part because it is difficult
to unambiguously predict the dissociation products. For
example, application of the non-crossing rule suggests that
many of the ion-pair states may in practice shortcut to a
neutral atom and one excited atom (in a Rydberg state) at
large r (13).

A review of spectroscopic studies of the gerade
states of iodine is deferred to Section 5 of this chapter.

3. The X $^1\Sigma_g^+$ State of Iodine

For the ground state of most diatomic molecules
spectroscopic constants for only a few low-lying vibration-
al quanta are generally known. The ground state of iodine
however has been studied extensively.

Several resonance fluorescence series (22, 23,
23(a)), in particular those reported by Verma (22), have been
analysed to give rotational and vibrational constants up
to v" = 84. Recently LeRoy (24), in a critical re-analysis
of all available data, has calculated the spectroscopic
parameters given in Table II-2. LeRoy's expansions are
capable of reproducing most of the observed transitions

	range $0 \leq v'' \leq 82$ [a]	range $0 \leq v'' \leq 5$ [b]
$G_v = \sum\limits_{n=1}^{m} C_n (v+\tfrac{1}{2})^n$	$C_1 = 214.5481$ $C_2 = -.616259$ $C_3 = 7.50 \times 10^{-5}$ $C_4 = -1.263643 \times 10^{-4}$ $C_5 = 6.198129 \times 10^{-6}$ [c]	$C_1 = 214.5016$ $C_2 = -.614688$
$B_v = \sum\limits_{n=0}^{m} C_n (v+\tfrac{1}{2})^n$	$C_0 = 3.7395 \times 10^{-2}$ $C_1 = -1.2435 \times 10^{-4}$ $C_2 = 4.498 \times 10^{-7}$ $C_3 = -1.482 \times 10^{-8}$ $C_4 = -3.64 \times 10^{-11}$	$C_0 = 3.73719 \times 10^{-2}$ $C_1 = -1.1376 \times 10^{-4}$
$D_v = \sum\limits_{n=0}^{m} C_n (v+\tfrac{1}{2})^n$	$C_0 = 4.54 \times 10^{-9}$ $C_1 = 1.7 \times 10^{-11}$ $C_2 = 7 \times 10^{-12}$	$C_0 = 4.25 \times 10^{-9}$ $C_1 = 32.1 \times 10^{-11}$
D_0	12440	12440.1

a) Data from LeRoy reference (24).

b) Data from Barrow reference (25).

c) Higher terms up to m=9 are given in reference (24) for G_v.

Table.II-2: Molecular Constants (cm^{-1}) for the Ground State $X^1\Sigma_g^+$ of I_2.

to within $\pm.05\text{cm}^{-1}$ and his molecular constants were used
to calculate the ground state rotational energies, $F_v''(J)$,
for the present study (see Chapter V). Small uncertainties
in the B_v'' values still exist (19), but until measurements
of greater precision are reported it is unlikely that
LeRoy's analysis can be improved. It is also possible, as
observed by Barrow for the B state of iodine (25), that a
low order polynomial expansion may not be capable of fitting
accurately all the bound levels of the ground state.

Also included in Table II-2 are the ground state
constants of iodine determined by Barrow (25) from absorp-
tion experiments. The two parameter expansions given in
Table II-2 were found to adequately represent Barrow's
observations over the limited range $0 \leq v'' \leq 5$ accessible
to his experiments. This data is presented here because the
most extensive rotational analysis of the B state of iodine
(25) makes use of Barrow's ground state parameters.

4.   The $B^3\Pi_{0_u^+}$ State of Iodine

The B state of iodine gives rise to the extensive
visible B←X absorption band system which, because of its
strength and accessibility, is among the most studied of
molecular spectra (26, 17, 28, 29). Nonetheless detailed
analysis of the B state has progressed slowly. For exam-
ple, although the absorption band system has been known

since 1923 (26), the correct vibrational numbering was not established until the I_2^{129} isotope was studied in 1965 (30). Several authors (31, 32, 33) have suggested that the assignments and molecular constants of references (28, 29) be re-evaluated. These difficulties have further led to the erroneous identification and assignment of several resonance fluorescence series (34, 35, 36, 37).

Recently the situation has improved considerably. Barrow (25) has reported a high resolution absorption study of 64 bands with $4 \leq v' \leq 77$ and $0 \leq v'' \leq 5$. Presented in Table II-3, the molecular constants obtained from Barrow's analysis can reproduce some of the observed unblended lines of the B—X band system to within $\pm.02 \text{cm}^{-1}$. However, neither the vibrational levels nor the centrifugal distortion constants can be adequately represented by a single polynomial expansion in $(v' + \frac{1}{2})$ for all bound levels. This behavior is not unique and has also, for example, been observed in H_2 (38). Accurate line positions for B—X transitions are best determined from the term value analysis given in Table 2 of Barrow's paper. The B—X transition energies required for the present study. (see Chapter V) were therefore calculated from the term values specified by Barrow and the molecular constants summarized in Table II-3.

$G_v = \sum_{n=1}^{5} C_n(v+\frac{1}{2})^n$ $0 \leq v' \leq 50$	$C_1 = 125.69708$ $C_2 \cong -.764244$ $C_3 = -1.77598 \times 10^{-3}$ $C_4 = -7.37943 \times 10^{-5}$ $C_5 = 1.03060 \times 10^{-6}$
$B_v = \sum_{n=0}^{4} C_n(v+\frac{1}{2})^n$ $0 \leq v' \leq 77$	$C_0 = 2.90387 \times 10^{-2}$ $C_1 = -1.58190 \times 10^{-4}$ $C_2 = -3.36318 \times 10^{-7}$ $C_3 = -4.77727 \times 10^{-8}$ $C_4 = 3.26287 \times 10^{-10}$
$D_v = \sum_{n=0}^{1} C_n(v+\frac{1}{2})^n$ $0 \leq v' \leq 10$	$C_0 = 5.43 \times 10^{-9}$ $C_1 = 3.0 \times 10^{-10}$
Te	15769.01
D_0	20043.2

Table II-3: Molecular Constants (cm^{-1}) for B $^3\Pi_{0_u}^+$ State of I_2 (25).

The study of energy transfer mechanisms has also been an active area of research which bears relevance to the present two-photon study. For example, collisional deactivation (39, 35), photodissociation (40, 41) and lifetime measurements (43, 43, 44) have been reported for the B state of iodine. Early lifetime measurements were particularly intriguing as the observed radiative lifetime showed large variations with the excitation wavelength. Tellinghuisen has shown (45) that spontaneous predissociation from B to the underlying $^1\Pi_{1_u}$ continuum depends not only on the form of overlap between the respective radial wavefunctions but also on the value of J(J+1). The neglect of the J-dependence appears to be responsible for the apparent discrepancies among the lifetimes reported in the literature. Although the magnitude of the mixing between the B state and $^1\Pi_{1_u}$ is low and no perturbations of the B state levels are readily apparent[†], a significant fraction of the B state population is lost by predissociation because of the long radiative lifetime of this state ($\sim 10^{-6}$s).

Finally it should be noted that $^1\Pi_{1_u} \leftarrow X$ transitions are competitive with the first step of the sequential excitation process (B←X) and will therefore limit the attainable two-photon signal. Hancock and Wilson (46) have

---

[†]Recently, very weak perturbations have been found by Comiland and Ducorse, *Opt. Comm 21*, 199 (1977).

resolved the visible absorption spectrum of iodine into three contributing transitions. Their results, illustrated in Figure II-5, show that the $^1\Pi_{1_u}$ state makes a larger contribution to the continuous absorption above 20,000 cm^{-1} than does the B state. The unexpected strength of the $^1\Pi_{1_u}\leftarrow X$ transition (which dissociates only to ground state atoms) explains why it has not been possible to construct a photodissociation iodine laser operating on the $\left(^2P_{\frac{1}{2}}\rightarrow{}^2P_{\frac{3}{2}}\right)$ atomic iodine transition.

5. Spectroscopic Studies of the Gerade Electronic States of Iodine

As discussed in section 2, a large number of stable gerade electronic states of iodine are expected to occur in the 5 to 8 eV region. Excited gerade states however, are not normally accessible to single photon studies and little experimental data is available. This section surveys the high temperature and emission studies which have provided information, however limited, about the excited gerade states of iodine.

5.1 U.V. Absorption Studies

At low temperature the U.V. absorption spectrum of iodine consists of a broad continuum near 2700Å which blends into an extensive discrete system (Cordes Bands) with maximum intensity at 1825Å. While it has been shown

Figure II-5: Total absorption curve for iodine in the visible region showing the relative contributions of transitions to the A $^3\Pi_{1_u}$, $^1\Pi_{1_u}$ and B $^3\Pi_{0_u^+}$ excited states. (46)
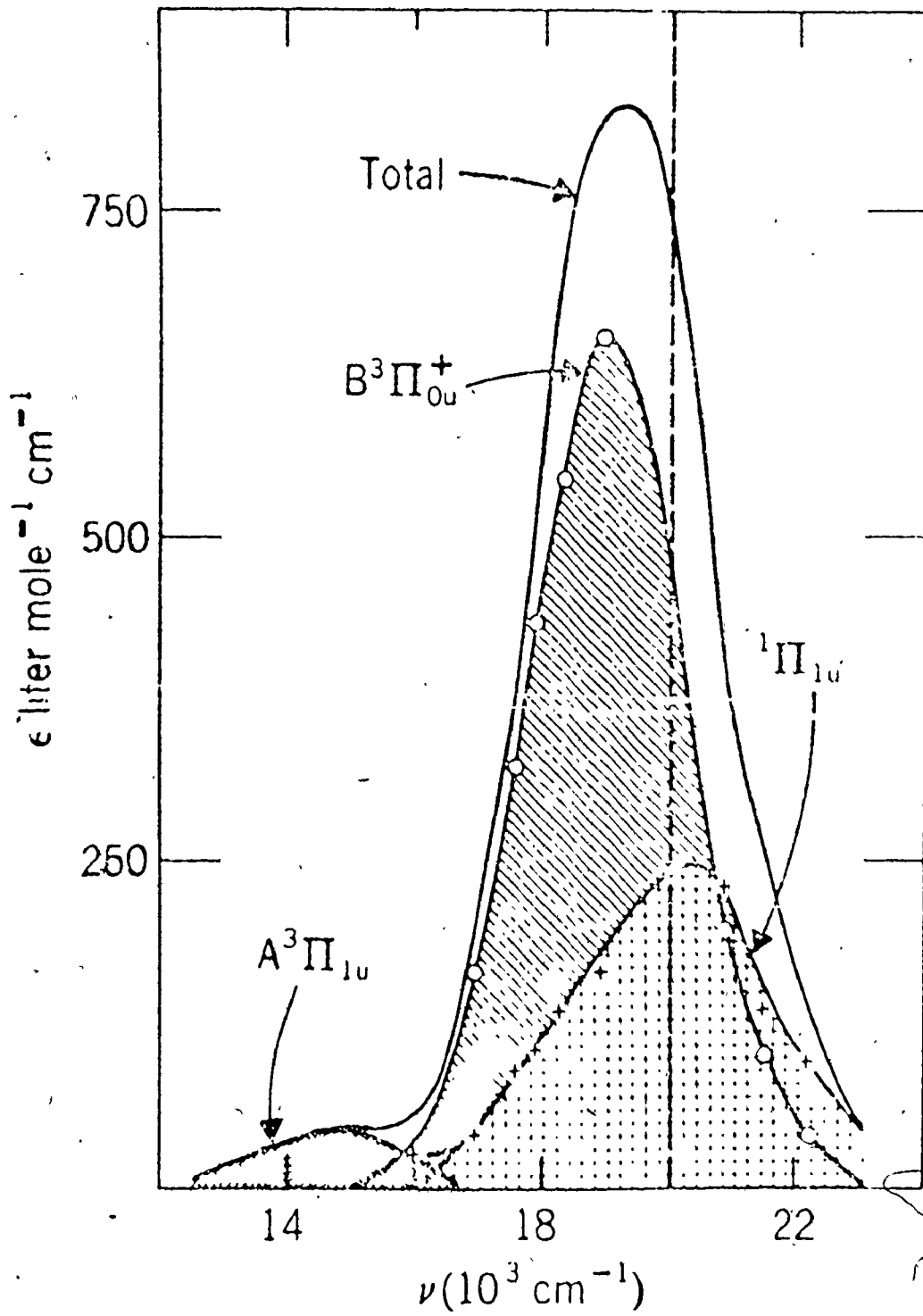
that the 2700Å system arises principly from $^3\Sigma_u^+ \leftarrow {}^1\Sigma_g^+$ transitions (47), the 1825Å system has been subject to many interpretations. For example, Venkateswarlu (48) has assigned the Cordes Bands to two separate transitions, whereas Wieland, in a private communication with Mulliken (13), has obtained a single formula which apparently fits all the U.V. bands. However, Wieland's v' numbering and therefore the electronic origin and molecular constants can not be regarded as reliably established. It is most probable that the Cordes system arises from the strongly allowed 1441 $^1\Sigma_{1u}^+(D) \leftarrow X$ transition (13).

At high temperatures not only the ground state but also vibrational levels of the 2431 $^3\Pi_{2u}$ and $^3\Pi_{1u}$ states must become populated. Thus the so-called Skorko bands which appear at 800 to 1100°C as near continua except for features near 3427Å and 3263Å have been assigned to $^3\Pi_{2g} \leftarrow {}^3\Pi_{2u}$ and $^3\Pi_{1g} \leftarrow {}^3\Pi_{1u}$ transitions respectively. By similar arguments one might also expect that $^3\Pi_{0g}^+ \leftarrow {}^3\Pi_{0u}^+(B)$ would be observed at high temperatures, particularly as the $^3\Pi_{0g}^+ \rightarrow {}^3\Pi_{0u}^+(B)$ emission appears established (14). However, Wieland's 1130°C spectra (13) show no indication of bands in the 3880Å region where this absorption would be anticipated. Mulliken concludes (13), in support of the $^3\Pi_{0g}^+ \rightarrow {}^3\Pi_{0u}^+$ assignment, that the inverse absorption process is probably

present but with weaker transition moment than anticipated.
To some extent this viewpoint is supported by the photolysis
experiments of Briggs and Norris (49) who apparently ob-
served $^3\Pi_{0_g^+} \leftarrow {}^3\Pi_{0_u^+}$ absorption in Cl_2 and Br_2 but *not* in I_2.

Although 1432 $^1\Pi_g$ and $^3\Pi_{g_0^-}$ are expected to have
stable ion-pair potentials, absorption transitions to these
states are not expected because the appropriate lower state
potentials are repulsive. In emission these states are
expected to give rise to continuous emission, however. In
fact most of the information available about the excited
gerade states of I_2 is derived from emission studies.

5.2 Emission Studies

Although the emission spectrum of iodine ranges
from the U.V. to the I.R. only the blue and U.V. bands are
considered relevant to the present study. Until recently
emission spectra of iodine have only been observed with
high energy excitation. Consequently several excited elec-
tronic states are simultaneously populated and the emis-
sion spectra are very complex and difficult to analyse.
Many questions remain unanswered and the need for further
study has been well documented (13).

The U.V. emission spectrum of I_2, excited either
by atomic resonance lines or by autoresonance has been re-
ported by numerous authors (12, 14, 50). The spectra are

typically excited in I_2 vapor alone (50) or at higher pres-
sures in mixtures of I_2 vapor plus an inert gas (14). The
principle excitation in both cases is thought to be to (a)
vibrational-rotational level(s) of the 1441 $^1\Sigma_u^+(D)$ state
giving rise to a resonance fluorescence series on emission
to the ground state. Also observed but less well understood
are groups of diffuse bands extending to longer wavelength
as far as 4800Å (McLennan Bands). At higher pressures
(400mm of Ar plus I_2 vapor), most of the broad McLennan
Bands disappear but some features [see Plate 1 of reference
(14)] increase in intensity and display red degraded dif-
fuse band heads. These bands are thought to originate from
(an) excited electronic state(s) populated by collisional
transfer at high pressure and have recently been assigned
to F$\rightarrow$X and $^3\Pi_{0_g^+}\rightarrow$B transitions in the isotope studies of
Tellinghuisen, Wieland and Nobs (14). Tellinghuisen,
Wieland and Nob's isotopic analysis of a third and stronger
system (D) near 3425Å has indicated that a previously pub-
lished vibrational analysis of the 3425Å system (51) is
likely in error. Although not conclusively established,
it appears that the observed emission has both D$\rightarrow$X and
$^3\Pi_{2_g}\rightarrow{}^3\Pi_{2_u}$ bands present.

Venkateswarlu first suggested (52) that the dif-
fuse series observed in emission might be "fluctuation

bands" arising from discrete-continuum transitions. Very
recently, Rousseau and Williams (53), clearly observed
these internal diffraction bands in the emission following
sequential two-photon absorption in molecular iodine. The
two-photon process was thought to populate either the $^1\Sigma_{0g}^+$
or $^3\Pi_{0g}^+$ state with subsequent discrete and diffuse emission
observed to the $^3\Pi_{0u}^+$ (B) state. Transitions terminating in
the continuum levels of the B state give rise to the dif-
fuse structure. As predicted by Condon in 1928 (54), the
internal diffraction bands arise because of the phase rela-
tionship between the initial and final wavefunctions and
are a direct measure of the frequency variation of the
Franck-Condon factor. The structured continuum because of
an apparent regular interval spacing can be easily mis-
interpreted as an upper state vibrational manifold.
Rousseau and Williams suggest therefore (53) that a re-
analysis of the I_2 emission spectrum is mandatory, parti-
cularly in the 3300-4800Å region.

Rousseau has also measured the radiative lifetime
of the two-photon induced emission discussed above (55).
Of the two most probable assignments Rousseau argued that
the fully allowed $^3\Pi_{0g}^+ \longrightarrow {}^3\Pi_{0u}^+$ transition would have a short
fluorescent lifetime whereas the spin forbidden $^1\Sigma_g^+ \longrightarrow {}^3\Pi_{0u}^+$
transition would have a longer lifetime. From the observed
lifetime of 27±2nsec, Rousseau concluded that the two-photon
excitation was to a $^3\Pi_{0g}^+$ state and that this was probably

the same state (designated E) observed by Tellinghuisen, Wieland and Nobs (14) in emission. In the present author's opinion a single lifetime measurement can not be regarded as conclusive proof that Rousseau observed a $^3\Pi_{0_g^+}$ state in his experiments. In case (c) both $^3\Pi_{0_g^+} \rightarrow {}^3\Pi_{0_u^+}$ and $^1\Sigma_g^+ \rightarrow {}^3\Pi_{0_u^+}$ are formally $0_g^+ \rightarrow 0_u^+$ transitions and the selection rule $\Delta S = 0$ no longer applies. In addition there are several ion-pair states predicted to be of nearly equivalent energy to $^3\Pi_{0_g^+}$ and Rousseau's experiment need not necessarily have populated the same state(s) observed by Tellinghuisen, Wieland and Nobs. Nonetheless Rousseau's papers (53, 55) are important to the present study in that they showed that two-photon sequential absorption studies of molecular iodine were possible.

Finally, it should be noted that there is by no means universal agreement on the analysis of the U.V.-Visible emission of iodine. For example, Verma's analysis of the D system (56) at 3425Å assumes that $^3\Pi_{0_u^+}(B)$ is the lower state; in which case an elaborate explanation is required to interpret the overall emission spectrum (13). As concluded by Mulliken in "Iodine Revisited" (13): "A final answer must await further study."

CHAPTER III

TWO-PHOTON SEQUENTIAL ABSORPTION SPECTROSCOPY

1. Introduction

With the recent advent of high-power wavelength-tunable dye lasers two-photon spectroscopy has emerged as a new and powerful technique for the study of the electronically excited states of atoms and molecules. This chapter reviews some experimental and theoretical aspects of two-photon absorption processes which are relevant to the present study. Emphasis is directed specifically towards sequential absorption studies of the vibronic structure of molecules. More detailed reviews of two-photon processes are presented by Mahr (57), Worlock (58) and McClain (59) while multiphoton processes in general are surveyed by Bonch-Bruevich and Khodovoi (60) and Peticolas (61).

2. Theoretical Considerations

The basic theory of two-photon processes (which includes two-photon absorption, two-photon emission as well

as combined absorption-emission processes) was first

formulated by Goeppert-Mayer in 1931 (62). In time-

dependent second-order perturbation theory the two-photon

transition probability from the ground state g to an ex-

cited state f is expressed in terms of a virtual inter-

mediate state i.[†] The transition probability is then

proportional to the square of composite matrix elements

of the form:

$$A_{fg}^{(2)} = \sum_i \left[\frac{(r_{gi} \cdot \hat{e}_1)(r_{if} \cdot \hat{e}_2)}{(\omega_{ig} - \omega_1)} + \frac{(r_{gi} \cdot \hat{e}_2)(r_{if} \cdot \hat{e}_1)}{(\omega_{ig} - \omega_2)} \right] \quad \dots \quad (3-1)$$

where the transition $g \to f$ (of energy separation ΔE) is in-

duced by photons with angular frequencies ω_1 and ω_2 ($\Delta E =$

$\hbar\omega_1 + \hbar\omega_2$) and polarization vectors $\hat{e}_1$ and $\hat{e}_2$, respectively.

In dipole approximation the r_{gi} and r_{if} variables are

(single-photon) matrix elements like $r_{gi} = <i|r||g>$ between

the combining states g, i and f.

Each term of equation (3-1) can be interpreted

as a probability amplitude for transitions from state g

to f via the virtual intermediate state i and selection

rules for the two-photon process can be derived from an

examination of the non-vanishing matrix elements. This

leads to selection rules for double quantum rovibronic

[†] Virtual states are intermediate in time *not* energy and do not violate energy conservation because of the uncertainty principle. For very short times the uncertainty in the energy ($\Delta E \geq \hbar/\Delta t$) can be very large and the classical concept of energy conservation becomes physically meaningless; see discussion given by Peticolas (61).

transitions in diatomic molecules[†] which are similar to those for the Raman effect ($g \leftrightarrow g$, $u \leftrightarrow u$, $\Delta J = 0, \pm 2$). Unlike single-photon transitions, both the initial and final states have the same parity in two-photon absorption processes. Excited states can therefore be studied by two-photon methods which are not accessible (from the same initial state) by single-photon experiments.

Two-photon transition probabilities in the presence of a nearby (resonant) real intermediate state cannot be evaluated directly from equation (3-1). As resonance is approached ω_1 or $\omega_2 \to \omega_{ig}$ and equation (3-1) diverges because $|\omega_{ig} - \omega_1| \to 0$. To evaluate the perturbation expansion various damping factors must be introduced (57, 60) depending upon the relative values of $|\omega_{ig} - \omega_1|$ and the bandwidths γ_i and γ_f of the intermediate and final state, respectively. Mahr has shown (57) that for the resonant condition $|\omega_{ig} - \omega_1| < \gamma_i$ the two-photon transition probability $\Gamma_{gf}^{(2)}$ is given to good approximation by:

$$\Gamma_{gf}^{(2)} = \Gamma_{gi}^{(1)} (\gamma_i)^{-1} \Gamma_{if}^{(1)} \qquad \ldots (3-2)$$

where $(\gamma_i)^{-1}$ is the natural lifetime of state i, and $\Gamma_{gi}^{(1)}$ and $\Gamma_{if}^{(1)}$ are the normal one-photon transitions probabili-

---

[†]For polyatomic molecules vibronic coupling mechanisms similar to single-photon Herzberg–Teller (16) interactions must also be considered. Honig (63) and more recently Hochstrasser (64) and Metz (65) have approached this problem.

ties. The two-photon transitions g→f can here be regard-
ed as two independent single-photon processes in which the
lifetime of the intermediate state enters dominantly into
the overall two-photon -absorption cross-section. Evalu-
ation of the non-vanishing symmetry products for the matrix
elements in equation (3-2) yields selection rules for
step-wise two-photon absorption which are similar to those
discussed above for double quantum transitions.

For the non-resonant case, a two-photon g→f
process cannot be regarded as two independent single-photon
transitions. However it is useful to consider an effec-
tive lifetime t_{eff} for the virtual intermediate level
which describes the two-photon interaction. t_{eff} is *not*
determined by relaxation phenomena but rather by the re-
quirements of energy conservation within the limits of the
uncertainty principle. For a g→f two-photon transition
with $|\omega_{ig}-\omega_1| \gg \gamma_i$ (non-resonant state i), the absorption
of the first photon $\hbar\omega_1$ must be followed by absorption of
the second photon $\hbar\omega_2$ within the period $t_{eff}=|\omega_{ig}-\omega_1|^{-1}$ to
satisfy energy conservation. The non-resonant transition
probability is then given (57) by:

$$\Gamma_{gf}^{(2)} = \Gamma_{gi}^{(1)}[\gamma_i/(\omega_{ig}-\omega_1)] \times t_{eff} \times \Gamma_{if}^{(1)} \qquad \ldots \text{(3-3)}$$

and t_{eff} can be viewed as the limiting factor which leads
to very low absorption cross-sections for non-resonant
double quantum transitions.

To summarize the foregoing: two-photon absorption studies may or may not involve a resonant intermediate state. In the former case three *real* energy levels are involved and the process is termed sequential or step-wise two-photon absorption. The sample is excited in two steps from an initial level to a final level by way of a real intermediate level. The intermediate level is momentarily populated and its natural lifetime affects the two-photon absorption cross-section. Two independently tunable dye lasers are generally required experimentally to excite the sequential resonances. In the latter case only two real energy levels are involved and the process is called double photon absorption. The sample reaches an excited state through a *virtual* intermediate level by absorption simultaneously of two photons that are normally of equal frequency. Only a single, high-intensity dye laser is therefore usually required for double-photon absorption experiments.[†] As the resonance condition is approached by decreasing $|\omega_{ig} - \omega_1|$ the transition probability for double-photon transitions will increase significantly; see below.

[†]Hochstrasser in Chem. Phys. Lett. *48*,1(1977) has distinguished between two-photon sequential absorption and double photon absorption in terms of incoherent and coherent excitation processes, respectively. In the present application there is no coherence between the two counter-propagating laser beams used to excite the sequential two-photon resonances. The phase relationship between the ground and excited states is not coupled by the incident radiation and a kinetic theoretical model is applicable.

3. <u>Literature Review</u>

Although sequential absorption (49) and emission (66) studies have been attempted with conventional incoherent light sources, these experiments have met with only limited success. Practical two-photon experimentation awaited the superior spectral brightness (intensity per unit bandwidth) of coherent laser sources. With the recent development of high power wavelength-tunable dye lasers, two-photon sequential absorption spectroscopy has become a viable experimental technique for the study of the excited electronic states of both atoms and molecules.

Many different atomic species have been investigated by sequential absorption techniques with lasers (67, 68,69,70) and the progress in this area has been quite remarkable. For example, very high resolution Doppler-free spectra have been obtained with counter-propagating laser beams which excite selectively only those atoms within a small velocity sub-group of the ground state velocity distribution (2). One such experiment (71) has revealed optically-induced level shifts (termed the AC Stark effect) in the two-photon sequential excitation of atomic sodium vapor. Level shifts (which are proportional to the light intensity) up to 1GHz were reported for both the 3S ground state and the 4D excited state of sodium. Optically-induced level shifts must therefore be considered in high resolution two-photon studies employing intense laser radiation. Of particular interest to the present study are the experi-

ments of Liao and Bjorkholm (72) who showed that two-photon sequential absorption in atomic sodium has an absorption cross-section some seven orders of magnitude greater than for non-resonant double quantum transitions. The enhanced signal of the resonant case clearly demonstrated experimentally the sensitivity advantage of stepwise excitation.

Relatively few sequential absorption studies of the excited electronic states of molecules have been reported previously and in large part this motivated the present study of iodine. Sequential absorption experiments on ICl (73), I_2(53,55) and BaO (8) are the only prior reports to those of Danyluk and King (9,10,11,15) which are detailed in subsequent chapters.

The iodine experiments of Rousseau and Williams (53,55) have been described in Chapter II, section 5.2, and need not be further discussed here. However it is of interest to discuss both the ICl and BaO experiments as well as very recently published multiphoton ionization studies of molecular iodine.

In 1974 Barnes et al (73) employed two independently tunable lasers (each with approximately 1Å bandwidth) to excite by a two-step process fluorescence from the E vibronic state of iodine monochloride. A commercial parametric oscillator laser was used to excite A←X transitions while a nitrogen-laser pumped dye laser was used to excite simultaneously E←A transitions. It was only possible for

the authors to excite unambiguously a few A←X transitions of iodine monochloride because of molecular iodine impurities in the ICl sample (I_2 exists in equilibrium with ICl). The report did not provide accurate molecular constants for any of the electronic states involved but. it did successfully demonstrate the feasibility of two-photon sequential excitation of molecular fluorescence.

In 1975 Field *et al* (8) published the first detailed sequential absorption study of the vibronic structure of a molecular system.. The authors used a fixed wavelength (4380 or 4965Å) argon ion laser to pump optically single-photon rotational transitions of the A←X absorption of BaO and a CW tunable dye laser to excite transitions from the optically pumped level to (a) higher energy electronic state(s) of $^1\Sigma$ symmetry. Nineteen sequential absorption bands which exhibited irregular vibrational intervals and rotational constants were observed between $36490 cm^{-1}$ and $38620 cm^{-1}$ (relative to $X_{v''=0, J''=0}$). The rotational selectivity of the sequential technique was clearly demonstrated: each band consisted of only two rotational lines arising from $\Delta J = \pm 1$ transitions from the pumped intermediate level. The experiment also showed that vibronic states not observable from the ground state because of prohibitive selection rules or small Franck-Condon factors could be investigated

---

†A preliminary report of this work was given somewhat earlier at the Twenty-ninth Sumposium on Molecular Structure and Spectroscopy, Columbus, Ohio, June 1974.

by two-photon methods.

The BaO sequential absorption bands observed by Field *et al* arose most probably from transitions to two or more perturbed electronic states. The authors could not investigate the apparent perturbations by a systematic study of many different A←X pump lines with different J values because only two pump frequencies were available from the argon ion laser. Thus, neither the magnitude of the perturbations nor the accuracy of the calculated rotational constants and band origins could be concluded. This diffi- culty is likely to be encountered in most two-photon sequen- tial absorption studies (in which closely-spaced excited states perturb one another) and underlines the need experi- mentally for two independently tunable lasers to excite sys- tematically the two-photon resonances.

Dalby *et al* (74) have recently observed double- photon absorption transitions from the ground state of mole- cular iodine to a Rydberg state of 1g symmetry. Intense laser pulses near $26500cm^{-1}$ were employed to excite the two- photon resonances which were detected by observation of the photoionization signal produced by the subsequent sequential absorption of a third photon (the ionization potential of $I_2 \rightarrow I^+ + e$ is $75814cm^{-1}$) from the same laser beam. Photoioni- zation was detected with a proportional counter which pro- vided very high sensitivity because the produced ions could be collected with 100 percent efficiency. The $2cm^{-1}$ band-

width of the .tunable dye laser used by Dalby did not permit
resolution of individual rotational transitions so that the
symmetry assignment of the excited state was concluded from
analysis of vibrational band contours and relative band in-
tensities.   The observed term values of the excited state
were fit by least squares to

$$T_R^1(cm^{-1}) = (53562.8\pm1.0) + (241.41\pm.04)(v+\tfrac{1}{2}) - $$
$$(0.58\pm.36)(v+\tfrac{1}{2})^2$$

to provide values for T_e^1, ω_e^1 and $\omega_e x_e^1$. As expected for
Rydberg states, ω_e^1 was about thirteen percent higher than
that of the ground electronic state. It should be noted
that the present study has undertaken to investigate the
valence states of iodine at somewhat lower energies.

For intense laser irradiation of molecular iodine
in the range $\omega_L = 25300$ to $22200 cm^{-1}$ Dalby and Tai (75) also
observed UV fluorescence and photoionization of *atomic*
iodine. The authors invoke a four-step, five-photon pro-
cess which depends quadratically on the laser power:

$$\overset{(1)}{X\xrightarrow[2\omega_L]{}}\overset{(2)}{E\xrightarrow[\omega_L]{}}E \xrightarrow{radiationless} I*\overset{(3)}{\xrightarrow[\omega_L]{}}I**\overset{(4)}{\xrightarrow[\omega_L]{}}I^+ +e$$

The steps include:

(1)   double-photon absorption from the ground state of the mole-
cular iodine to an excited E_g state (Rydberg or possibly
a valence state);

(2)   sequential absorption by single-photon absorption from E_g to a high energy molecular state E_u which predissociates into one excited iodine atom I* and one ground-state atom I.

(3)   single-photon atomic transitions from I* to highly excited atomic states I**.

(4)   ionization of atomic iodine by sequential absorption from I** to the continuum.

It is of interest to the present study that the atomic fluorescence I*→I observed by Dalby was continuous as the laser frequency was scanned below 4500Å. This suggests a very dense level structure for the E_g state(s) in this region since the laser bandwidth was approximately $2cm^{-1}$. Moreover, the E_g levels involved in Dalby's studies must have energies above $44715cm^{-1}$ ($\frac{2}{3} \times 67072$) because the minimum energy required to photodissociate I_2 into I* is $67072cm^{-1}$. [If Dalby's E_g levels correspond to any of the states identified in Chapter V, they must have very high ($v_E \sim 30$ to 50) v_E values.]

CHAPTER IV

EXPERIMENTAL CONSIDERATIONS

1. Introduction

Dye lasers have undergone a remarkable trans-
formation since the first observation of stimulated light
emission from solutions of organic dye compounds (76, 77).
From these initial observations have evolved sophisticated
sources of tunable laser radiation which have revolution-
ized modern optical spectroscopy. The discussion of this
chapter is restricted to a brief survey of the nitrogen
laser-pumped dye laser and its application to two-photon
spectroscopy. For more detailed information, including an
account of continuous-wave (CW) and flashlamp-pumped dye
lasers the reader is referred to several recently published
reviews (78, 79).

2. Nitrogen Laser-Pumped Dye Lasers

Tunable dye lasers vary widely in their perform-
ance and operating parameters. For example, bandwidth,

tuning range and output power are determined not only by resonator design but also by the optical source used to excite the gain medium. Both pulsed and CW lasers as well as flashlamps have been used to stimulate dye laser emission, but nitrogen laser-pumped dye lasers offer several important advantages for high-resolution spectroscopy.

The 3371Å output of the nitrogen laser is well matched to the $S_1 \leftarrow S_0$ absorption of most organic dyes. In addition, triplet state quenching is minimized by the short pulse length (typically ≤ 10nsec) and fast rise time of nitrogen lasers. High conversion efficiency and high peak output power can therefore be achieved. The low threshold and high gain of nitrogen laser-pumped dye lasers also provides the largest tuning range (~3600 to 9000Å) realized for a single excitation source.

The advantages of nitrogen laser-pumped dye lasers are particularly important for two-photon spectroscopy. Since the transition probability for two-photon transitions is small, high peak power is generally required to render two-photon interactions observable. The large tuning range of these devices and the pulsed nature of the laser output can be used to advantage (10, 11).

The present study employed two independently tunable nitrogen laser-pumped dye lasers based on a design originally proposed by Hänsch (80) and illustrated in Fi-

gure IV-1. As shown, a flowing dye solution is transverse-
ly excited by a repetitively pulsed nitrogen laser and
stimulated broadband fluorescence is collected and col-
limated by an intercavity telescope. A Littrow-mounted
diffraction grating and an optional Fabry-Perot etalon are
used as wavelength selectors in a long optical cavity. For
short pulse excitation no discrete axial mode structure is
expected (80) and the output bandwidth of the dye laser is
then not much smaller than the bandpass of the inter-
cavity dispersive elements. In principle therefore, con-
tinuous tuning without mode hopping can be achieved without
the difficult synchronous tracking of cavity length re-
quired to scan the resonator modes of CW laser- and
flashlamp-pumped dye lasers (81). In practice, high reso-
lution scanning of nitrogen-laser pumped dye lasers still
requires the simultaneous tuning of the grating and inter-
cavity etalon. This can be a difficult problem particular-
ly as the grating and the etalon exhibit different non-
linear mechanical scanning characteristics. For limited
wavelength intervals (~4 to 5Å) Klauminzer (82) has de-
scribed a computer-controlled stepper motor system for the
simultaneous tracking of grating and etalon dispersive
elements in Hänsch-type dye lasers.

NITROGEN LASER PUMP BEAM

ASPHERIC FOCUSING LENS

VISIBLE OUTPUT

POLARIZER

OUTPUT MIRROR (80).

DYE CELL

BEAM EXPANDER

ETALON

GRATING

43
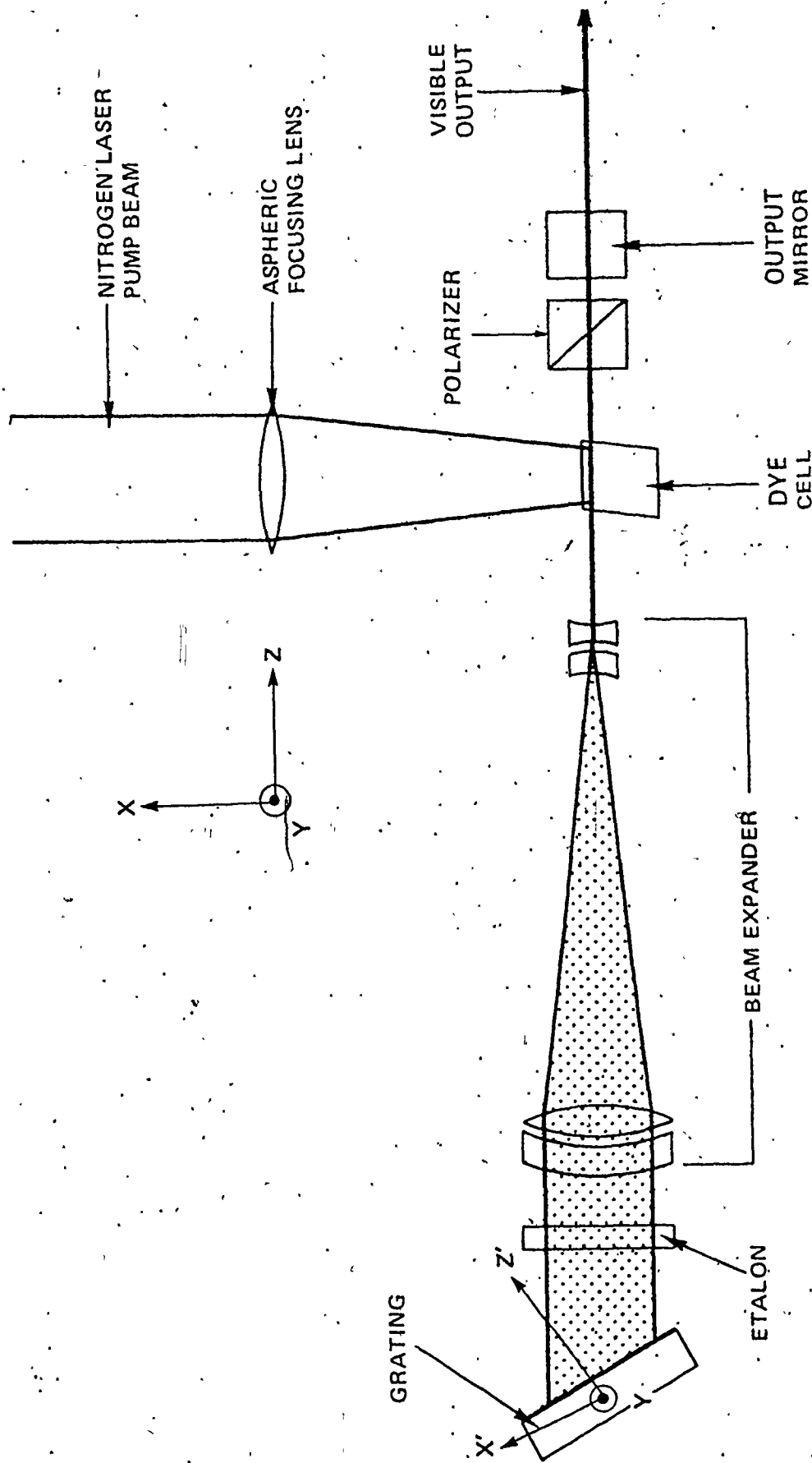
Figure IV-1: Hänsch resonator design for a nitrogen laser-pumped dye laser (80).

3. Design and Construction of a Pressure-scanned Nitrogen
    Laser-pumped Dye Laser

     An alternative approach to the synchronous tun-
ing of multiple dispersive elements in nitrogen laser-
pumped dye lasers was suggested by Wallenstein and Hänsch
(83) and by Flach, Shahin and Yen (84). Synchronous scan-
ning was accomplished without mechanically moving parts by
varying the gas pressure in a chamber which enclosed the
grating and Fabry-Perot interferometer. Although pressure
tuning of multiple interferometers is well established in
conventional high-resolution spectroscopy (55), it has
been less widely recognized that it is also possible to
tune diffraction gratings in a similar manner.

     For a medium of refractive index $n(p)$, the
vacuum wavelength $\lambda(p)$ for a diffraction grating and a
Fabry-Perot etalon is given by

$$(2D \sin\theta)/k = \lambda(p)/n(p) \qquad \ldots \ldots \quad (4\text{-}1)$$

$$(2L \cos\phi)/l = \lambda(p)/n(p) \qquad \ldots \quad (4\text{-}2)$$

respectively. Here k and l are integer values, D is the
grating groove spacing and L is the etalon plate separa-
tion. θ and ϕ define the angle of incidence for the grat-
ing and the etalon respectively. Equations (4-1) and (4-2)

both have the same functional dependence on the refractive index which, in turn, is pressure dependent. Therefore, if at some pressure P_0 both the grating and etalon are tuned to resonance at λ_0, then synchronous tuning may be achieved by varying the pressure, P.

The pressure scanning technique has two major advantages over alternative methods of frequency scanning Hänsch-type dye lasers. First, *linear* frequency scanning over large wavelength intervals can be achieved fairly simply without the sophisticated computer control required of mechanical tuning methods. Secondly, good beam quality with *constant output power* can be maintained throughout the wavelength scan, in contrast to other methods. Mechanically tilting the intracavity etalon, for example, leads to large "walk-off" losses which seriously degrades output power during the wavelength scan. These considerations encouraged the design and construction of a high-resolution pressure scanned dye laser system suitable for two-photon investigations.

The pressure scanned dye laser built for the present study was based on the optical configuration indicated in Figure IV-1 with the addition of a windowed pressure chamber to enclose the grating and Fabry-Perot etalon. The pressure chamber window was a $\lambda/20$ quartz plate 50mm in diameter with broadband antireflection coatings and 30-

minute wedge angle. An 1800 1/mm diffraction grating, a 3mm invar spaced etalon with broadband coatings on 25mm plates (reflectivity finesse of 30) and a 20X achromatic telescope produced a bandwidth less than .07cm^{-1}. Narrower bandwidths could easily be achieved (but at reduced output power) with the use of larger etalon spacers (L = 4, 5 or 6mm) and a 600 1/mm grating used in high order.[†] The dye cell windows were fabricated from plane and parallel quartz flats, that were inclined at approximately 2 degrees to the laser axis to eliminate unwanted etalon effects. For high-gain dyes the output mirror was simply an uncoated quartz flat ($\lambda/20$, 4% reflector) while a 50% broadband reflector was used for low gain dyes. The outer surfaces of both output mirrors had a 30-minute wedge angle and were broadband antireflection coated.

All optical components were mounted on a massive invar stabilized frame with multi-axis translation or rotation stages. The 40cm stabilized cavity consisted of four 25mm diameter invar rods. The pressure chamber was also supported by the invar rod, but in a manner such that deformation of the walls of the pressure chamber (expected

---

[†]Although not used in the present study, a pressure scanned confocal interferometer (2Ghz FSR, 200 finese) was also constructed from invar material. The confocal interferometer may be used as an extracavity filter to the laser described in the main text. Bandwidths of less than 25MHz have been achieved, but at greatly reduced peak power.

during pressure scanning) would not affect the optical alignment of the cavity. The pressure chamber was fabricated from 25cm diameter aluminum pipe and was equipped with calibrated feedthroughs for the angular adjustment of the grating and intercavity etalon. Thus both the grating and the etalon could be conveniently aligned to any wavelength without the need to open the pressure chamber (83, 84).

The laser was scanned by first adjusting the grating and etalon to resonance at a selected wavelength, then leaking gas into the evacuated pressure chamber through a calibrated needle valve. A large pressure drop was maintained across the needle valve to assure a nearly-linear pressure increase as a function of time in the pressure chamber (86). Although designed to accommodate pressures as high as 5 atmospheres, the pressure chamber was only usually charged to 1-2 atmospheres pressure. Propane was used as the scanning gas and the laser could be continuously scanned over 6 Angstroms with less than .3% nonlinearity by changing the pressure from 0 to 760torr.

Figures IV-2 to IV-4 illustrate the operating characteristics and performance capabilities of the pressure scanned laser built for the present study. The figures are representative of test data obtained with a Rhodamine B-Cresyl Violet mixture of dyes in ethanol and

Figure IV-2: Transmitted light intensity of a thermally stabilized confocal interferometer (2GHz, FSR) for a pressure-tuned (a) and mechanically-scanned (b) dye laser. Additional details are provided in the main text.

(a)

Pressure (torr)

(b)

Angular Displacement (mrad)

ABSORBANCE

σ (cm^{-1})

→ .557 ←
cm^{-1}

15802

15871
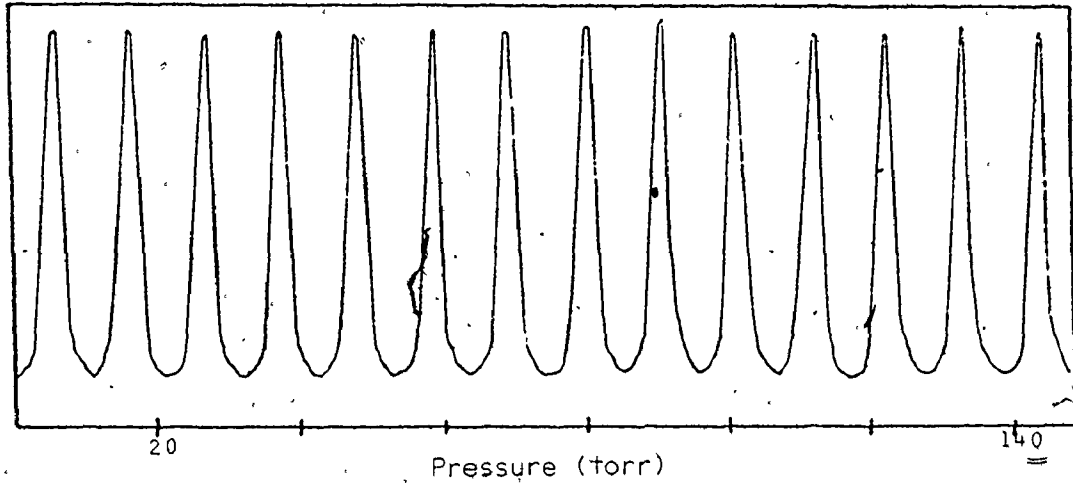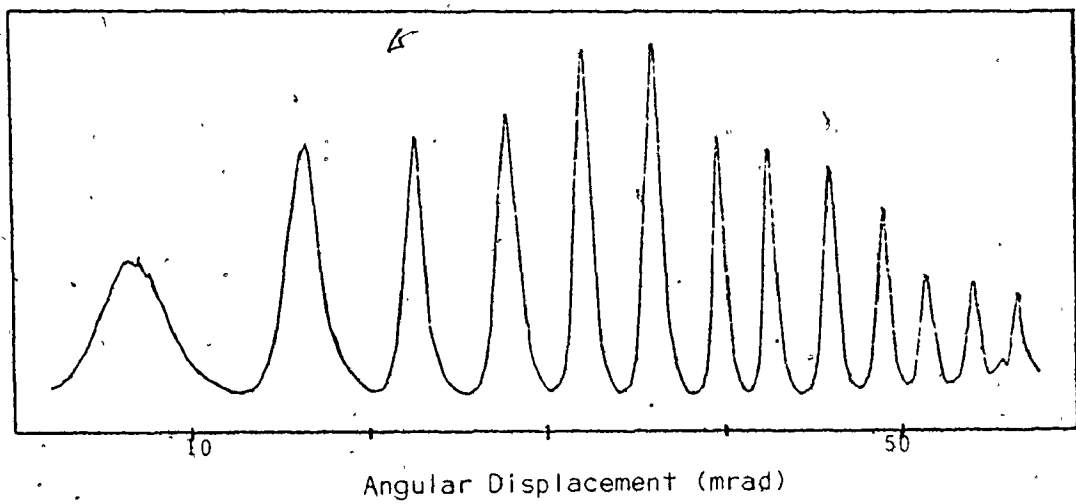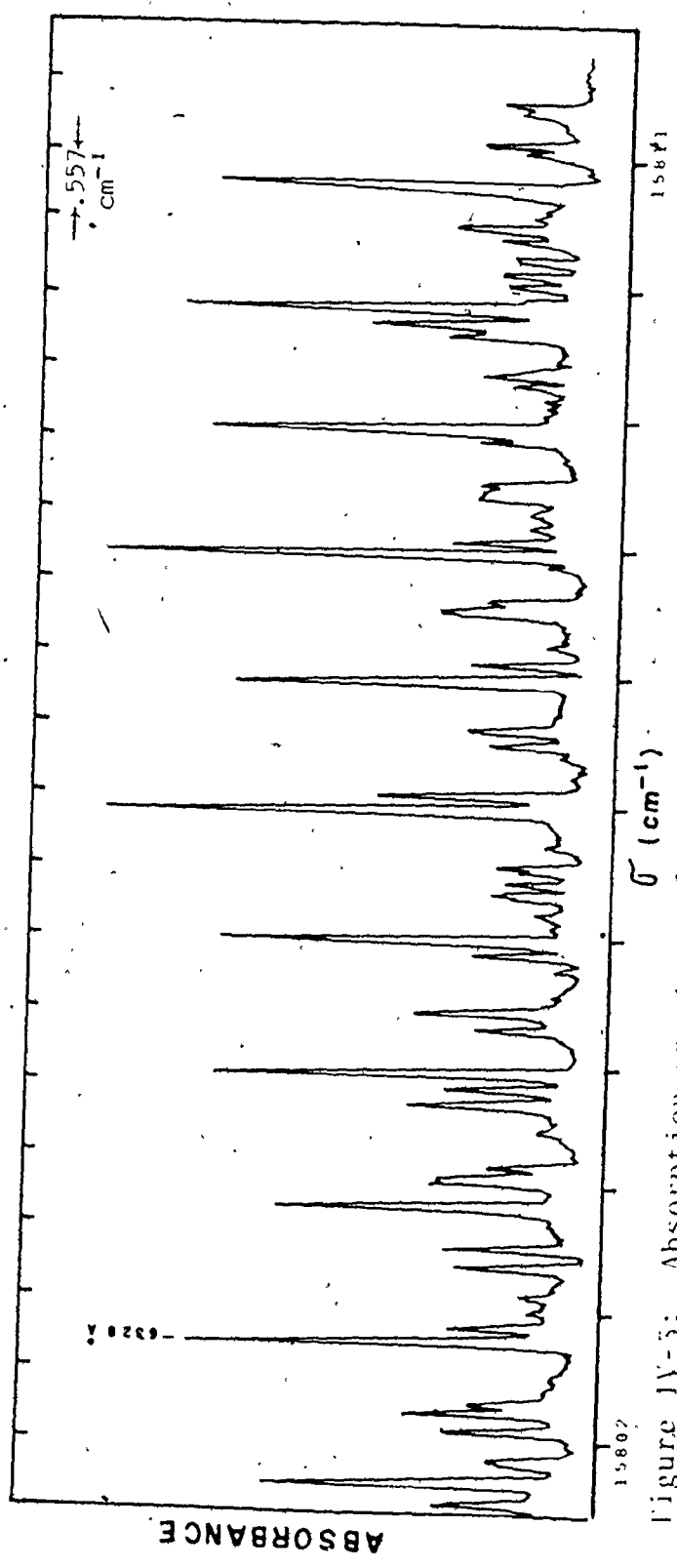
6328 Å

Figure IV-5: Absorption spectrum of iodine near 6328Å obtained with the pressure-tuned dye laser. Frequency markers each .557cm^{-1} were provided by a solid quartz monitor etalon.
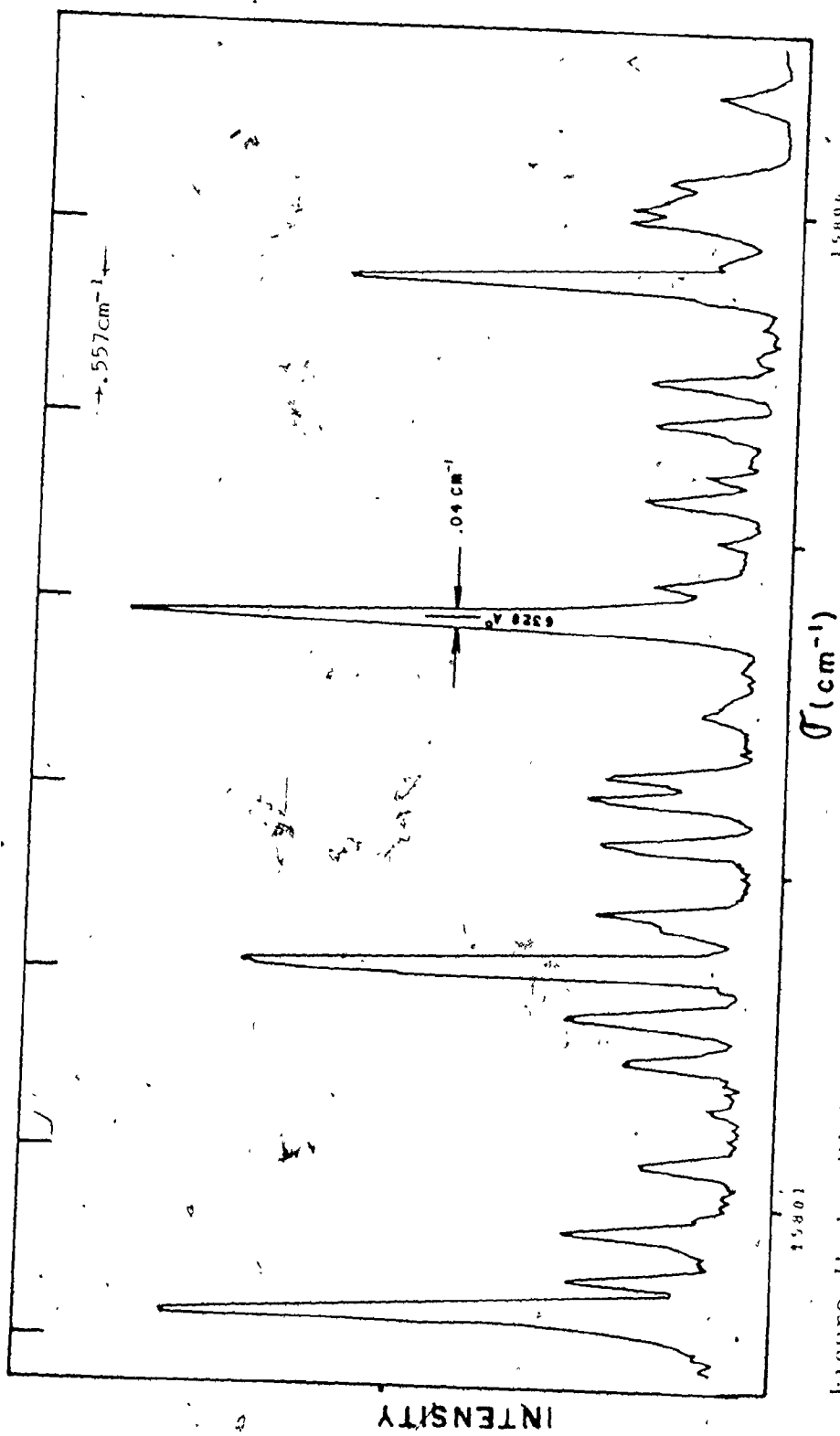
Figure IV-1: High dispersion fluorescence excitation spectrum of iodine near 6328Å.

50

the dye laser operating with the 600 1/mm diffraction grating and 4mm etalon spacer.

Figure IV-2 clearly illustrates the two major advantages of pressure scanned nitrogen laser-pumped dye lasers. Figure IV-2 shows the transmitted light intensity of a thermally stabilized confocal interferometer with a Free Spectral Range (FSR) of 2GHz for both a pressure-scanned and a mechanically tuned dye laser. The trans-mitted light pulses were detected with a photo-diode and averaged with a 1sec time constant in a single-channel Molectron LSDS box car averager. In Figure IV-2(a) the dye laser frequency was pressure scanned through several transmission maxima of the confocal interferometer. Ex-cellent scan linearity is demonstrated (nonlinearity $\sim 3\%$) at constant output power for a bandwidth of approximately $600MHz$ ($.02cm^{-1}$) FWHM. For comparison, Figure IV-2(b) shows the output of the same confocal interferometer, for the same laser bandwidth, as the intercavity etalon is mechanically tilted (at constant rate) through a small angle. The scanning nonlinearity of mechanically tilting the etalon is demonstrated by the convergence of the trans-mission peaks, each equally spaced by 2GHz. Note also in Figure IV-2(b) that the output power during the scan is modulated by the grating gain profile of about 12GHz ($.4cm^{-1}$) FWHM.

Figure IV-3 illustrates a 12cm^{-1} interval of the absorption spectrum of iodine near 6328Å obtained with the pressure-scanned dye laser as the pressure was varied from 0 to 760torr. The *absorbance* of a 75cm cell containing iodine vapor at .25torr is plotted as a function of the laser output frequency. Sample and reference laser pulses were normalized and processed by a dual channel Molectron LSDS box car signal averager. The spectrogram clearly displays the complex rotational structure of iodine and illustrates a convenient means for determining absolute intensity data. The observed line-widths in Figure IV-3 arise from Doppler broadening of unresolved hyperfine splitting (87) and are *not* limited by instrumental resolution, see below.

An application of the pressure-scanned dye laser to a detailed lineshape study of the iodine spectrum near 6328Å is illustrated in Figure IV-4. Figure IV-4 was obtained as a fluorescence excitation spectrum as the dye laser was slowly pressure scanned through approximately 3cm^{-1}. It is interesting to note that the Doppler broadened line of iodine near 6328Å (FWHM of .04cm^{-1}) has been resolved into 21 hyperfine components by saturated absorption experiments with helium-neon lasers (88).

4. Two-Photon Laser Spectrometer

'The pressure scanned dye laser described above
was an integral element of a high-resolution two-photon
spectrometer constructed for the present study. A simpli-
fied schematic of the two-photon spectrometer is presented
in Figure IV-5 and will be discussed in the following sec-
tion.

Two independently tunable dye lasers, labelled
MDL and PDL in Figure IV-5, were simultaneously pumped by
a 300kW nitrogen laser (Molectron UV 300). The nitrogen
laser produced 12nsec pulses at 3371Å and was usually oper-
ated at a repetition rate of 15Hz. 5nsec light pulses[†]
from the two dye lasers were directed in opposite directions
through a sample cell and sequential two-photon transi-
tions were monitored by the fluorescence output detected
by a cooled photomultiplier tube.

MDL was a 40cm mechanically tuned dye laser
(modified prototype Molectron DL200) operated without an
intercavity etalon. MDL was operated in the 6th order of
a 600 I/mm replica grating and provided pulses of approxi-
mately 1.5cm^{-1} bandwidth throughout the visible region.

[†]The organic dyes used as the gain media are excited above
threshold for a period of time somewhat less than the duration of the
pump pulse. Only for this reduced time period (~5nsec) is sufficient
pump power available for laser oscillation.
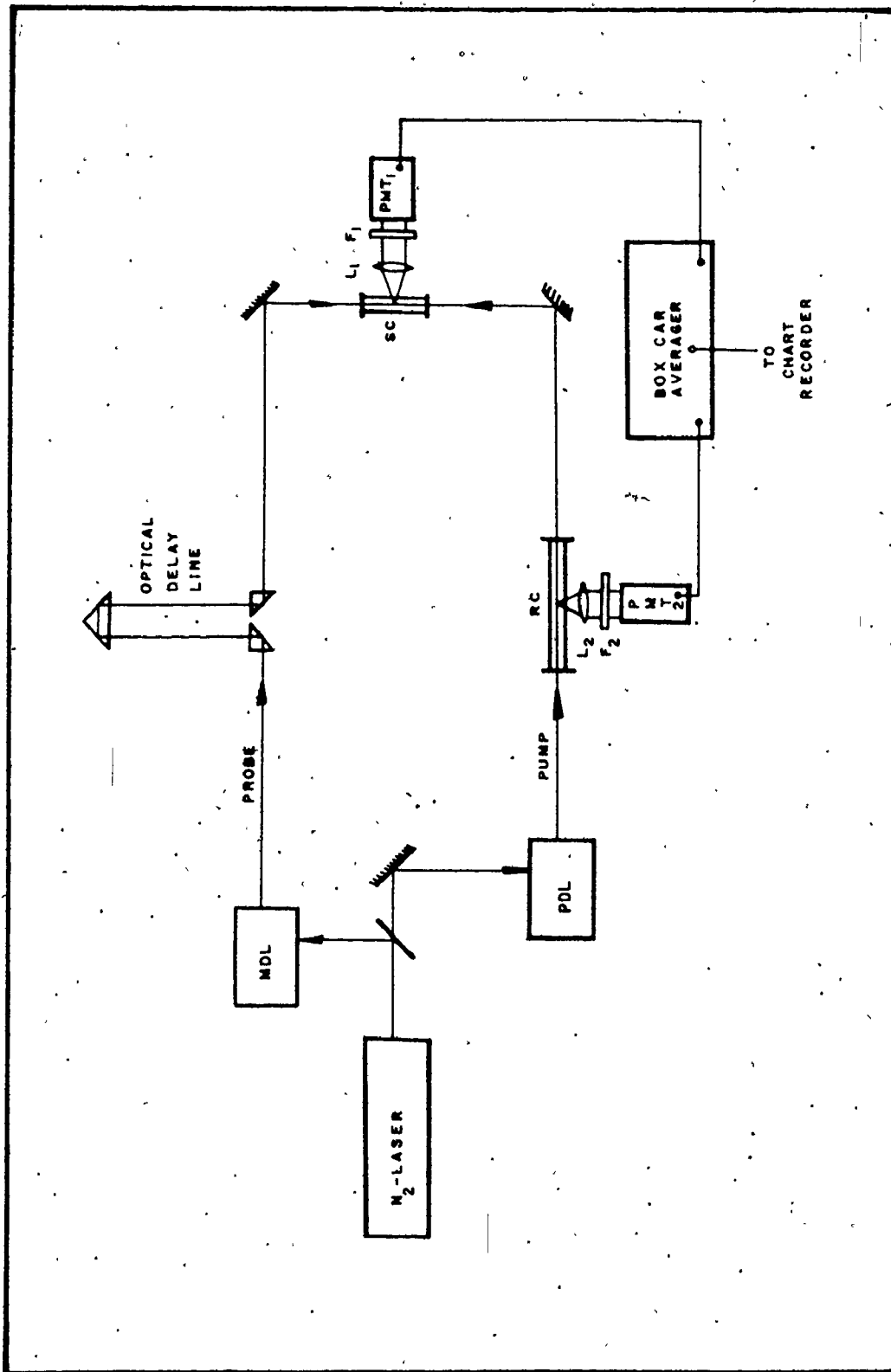
Figure IV-5: Schematic diagram of the two-photon laser spectrometer.

PDL was the pressure-scanned dye laser described in the previous section and was operated with an 1800 l/mm grating and an intercavity etalon with 3mm invar spacer. In this configuration the output bandwidth of PDL was less than $.07 \text{cm}^{-1}$.

The output beams from MDL and PDL were directed along a collinear counter-propagating path and focused to a 300 micron spot in the center of the sample cell containing iodine vapor at .25torr. This value for the beam cross-section was found to give adequate two-photon signal levels without the beam overlap instability problems which resulted from tighter focusing.

PDL was used to pump selected rovibronic transitions of the iodine B←X absorption system which were identified by monitoring the B→X broadband fluorescence from an iodine reference cell with collector lens L_2, filter F_2 (Corning 3-71, transmission ≥ 4800Å) and photomultiplier PMT_2 (RCA type 1P28). MDL was used to probe for transitions from the intermediate B state to electronic states of higher energy, herein collectively referred to as "E" states. Two-photon sequential absorption was detected with a thermoelectrically cooled phototube PMT_1 (EMI type 9816QB) by monitoring the "E"→B broadband fluorescence through an f/4 collector lens L_1 and filter assembly (Corning 7-54

plus Schott BG-12, transmission ≤ 4000Å).[†]

Double photon absorption induced by either the probe or pump beams could not be observed under the experimental conditions described above. By alternately blocking each beam it was established that only sequential absorption signals were discernable above the background noise. The signal output of both photomultipliers was processed by a Molectron LSDS box-car averager and plotted on a two-pen chart recorder. Signal-to-noise ratios of 300:1 were typically achieved with an effective time constant of .3sec.

Optimal signal levels were observed when the optical paths from each laser to the center of the sample cell were of equal length. This assured that the 5nsec laser pulses were coincident in time in the sample cell. To facilitate an examination of relaxation processes in the intermediate B state an optical delay line was inserted into the probe beam path. The delay line consisted of a 1.86m multiple reflection White cell and allowed the delay of the probe beam by integral multiples of 12.4nsec by the adjustment of only one mirror. However, scattering

---

[†]Two-photon resonances could also be detected by monitoring the decrease in the B→X fluorescence (typically 5 to 10%) when "E"→B transitions were excited by the probe laser. However, better signal-to-noise ratios were obtained by measuring the E→B emission with PMT$_1$.

and absorption losses of the White cell aluminized mirrors limited the maximum practical delay to 37.2nsec. It was also necessary to position the two dye lasers MDL and PDL so as to avoid optical feedback. For laser dyes with overlapping gain profiles it was possible for one laser to induce multifrequency oscillation in the other. In order to decouple the two lasers the total optical path separating them was kept greater than 2 meters.

To make most efficient use of the limited laser power available, the beamsplitter (see Figure IV-5) was chosen so that PDL pumped B—X transitions at slightly below saturation. Saturation conditions were determined with the aid of neutral density filters by measuring the B→X fluorescence intensity as a function of the pump laser intensity. For most of the experiments reported here a beamsplitter with a reflectivity of 60% proved satisfactory. The beamsplitter was fabricated from a 7.5cm diameter quartz plate and partially coated with aluminum in an Edwards High Vacuum aluminizer.

In sequential absorption experiments it is critical that the pump laser exhibit good long-term frequency stability. The frequency stability of PDL was determined by monitoring the B→X fluorescence from the reference cell during all two-photon experiments. These tests confirmed a frequency stability, in the absence of large ambient tem-

perature fluctuations, of ±200MHz for periods of several hours.

5. Wavelength Calibration of the Two-photon Spectra

A precise knowledge of both the pump and probe laser wavelength is required for the accurate wavelength calibration of two-photon sequential absorption spectra. In the present study the probe laser wavelength was determined spectroscopically, while the pump laser wavelength was inferred from the iodine fluorescence excitation spectra obtained by pressure scanning PDL. The details of these calibration procedures are outlined below.

For the probe laser (MDL) a switch actuated by the grating sine drive mechanism provided a wavelength marker at approximately 4.2 Angstrom intervals. The wavelength corresponding to each marker was determined photographically on a 1.5 meter B/L spectrograph by comparing the laser output with the emission lines of an Fe/Ne hollow cathode lamp. These calibration spectra were taken immediately before and after each two-photon experiment to assure reproducible results. A least squares fit of the calibration data provided a polynomial equation which was used to calculate the laser wavelength between markers by interpolation. The procedure allowed frequency calibration of the probe laser to within ±.2cm^{-1}. This uncertainty arose

primarily from mechanical limitations of the grating drive mechanism.

An absolute frequency calibration for the pump laser PDL was determined from high-resolution spectra of the B—X transition in iodine. B→X fluorescence excitation spectra were obtained from the reference cell by pressure scanning PDL. Relative frequency shifts during the scan were determined to within $\pm.005 \text{cm}^{-1}$ by photoelectrically monitoring the output of PDL through a 6mm (nominal) solid quartz etalon. Transmission fringes were thereby produced every $.557 \text{cm}^{-1}$ and were simultaneously plotted with the excitation spectra on a two-pen chart recorder. B—X rotational transitions in the iodine spectra were identified from the molecular constants of Barrow and Yee (25) and the absolute frequency of PDL determined to within $\pm.05 \text{cm}^{-1}$ by interpolation between unblended rotational lines. This indirect procedure for the absolute calibration of PDL provided the accuracy required for the present study and eliminated the need for additional calibration instrumentation.

CHAPTER V

TWO-PHOTON SEQUENTIAL ABSORPTION SPECTROSCOPY OF THE IODINE MOLECULE

1. Introduction

Figure V-1 shows schematically the application of two-photon sequential absorption spectroscopy to the excited electronic states of molecular iodine. The frequency of the pump laser PDL (see Chapter IV) was chosen to selectively populate a single (v_B, J_B) rovibronic level of the B state manifold by one-photon absorption. The frequency of the probe laser MDL was then scanned to excite the molecule from the (v_B, J_B) level to other highly excited electronic states, herein collectively referred to as "E" states. As detailed in Chapter IV, E→B fluorescence was used to detect the two-photon resonances, while B→X emission was used to monitor the pumped intermediate level. Throughout this chapter the ground state level, the intermediate level and the level structure probed by two-photon absorption are specified by (v'',J''), (v_B,J_B) and (v',J'), respectively.

Figure V-1: Two-photon sequential absorption spectroscopy
as applied to the excited electronic states
of iodine.
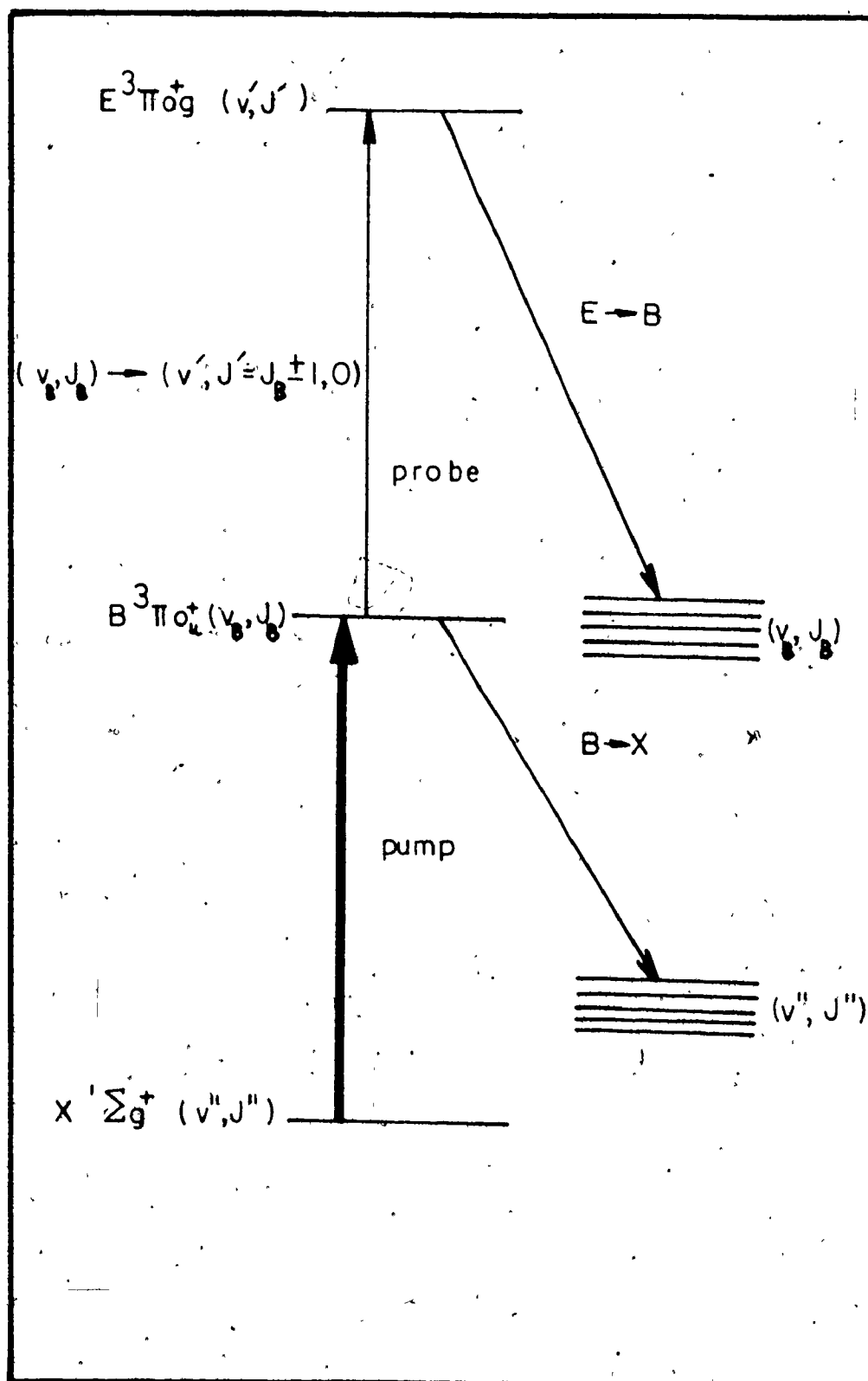
It is advantageous if the pump laser excites only a single (v_B,J_B) intermediate level. This generally requires a pump laser with narrow bandwidth, but greatly simplifies the analysis of the two-photon spectra since then only a limited number of rotational transitions (ΔJ=0,±1) can be excited by the probe laser. In the present study the pump laser PDL was operated with a bandwidth of .07cm^{-1}. Although somewhat greater than the Doppler broadened linewidth of B←X rotational transitions, this value for the pump laser bandwidth provided an optimum compromise between peak power and resolution which gave adequate two-photon signal levels. The probe laser MDL was operated without an inter-cavity etalon and provided light pulses of approximately 1.5cm^{-1} bandwidth. For all but very low J values this bandwidth was sufficient to resolve the rotational structure observed in the two-photon spectra of the iodine molecule.

2. Selection and Identification of B←X Pump Lines

The assignment of two-photon sequential absorption spectra requires the accurate identification of the intermediate pump level(s). It was therefore necessary to spectrally isolate and identify selected B←X rovibronic transitions prior to detailed two-photon studies of molecular iodine.

Barrow and Yee's (25) recent high resolution investigation of the B←X absorption system has provided accurate molecular constants which were applied to the present study. The single-photon B←X absorption spectrum of iodine was excited by scanning the pump laser across the absorption and recording fluorescence emission from the reference cell (Chapter IV). The iodine fluorescence excitation spectrum was then assigned using the spectroscopic constants and term values published by Barrow and Yee (25).

A computer program was used to calculate line frequencies in an attempt to predict which lines in the iodine excitation spectra should be unblended and free from overlap. It was hoped that the calculation would successfully identify potential pump lines which would yield two-photon spectra with only limited and readily assigned rotational structure. Unfortunately, the procedure was not very successful and relatively few lines identified in this manner gave acceptable two-photon spectra.

Many more transitions than reported in Barrow and Yee's analysis were revealed by the high resolution and sensitivity of the laser excitation technique. Most B←X "lines" consisted of many blended and overlapped components. Pumping on these lines gave rise to two-photon spectra which were complex and unresolved because several

B state levels were populated simultaneously. It is also possible that re-absorption of B→X emission may have populated several B state levels in addition to the pumped level, thereby adding to the complexity of the sequential two-photon spectra. However, it is not likely that energy transfer within the B state manifold through collisional deactivation contributed to the complexity of the two-photon spectra.[†]

Pump lines which provided strong, rotationally resolved two-photon spectra were best found empirically by the procedure illustrated in Figure V-2. The probe laser MDL was first tuned approximately to an E←B resonance, identified by the procedure outlined above. The wavelength of the pump laser PDL was then scanned across a portion of the B←X absorption and the single-photon excitation spectrum recorded [line (b), Figure V-2] from the reference cell. Simultaneously the E→B emission was also recorded [line (c), Figure V-2] from the sample cell as the pump laser was tuned across the B←X spectrum. A strong two-photon resonance was indicated by a sharp increase in the

---

[†]At 300mtorr simple kinetic theory predicts approximately 5×10^6 collisions per molecule per second for I_2 at 300°K. However, the probe and pump beams only had a temporal overlap of 5nsec during which time fewer than 2.5×10^{-2} collisions were possible. For experiments in which the probe pulse is delayed with respect to the pump pulse or for CW laser experiments collisional energy transfer may be significant.

Figure V-2: Location and identification of B←X pump
lines--

(a) Monitor etalon fringes used for fre-
quency calibration;

(b) B←X fluorescence signal recorded from
the reference cell as the pump laser
frequency was scanned;

(c) E→B fluorescence signal recorded from
the reference cell simultaneously to
(b) above. Two strong E←B resonances
are shown coincident with B←X pump
lines.
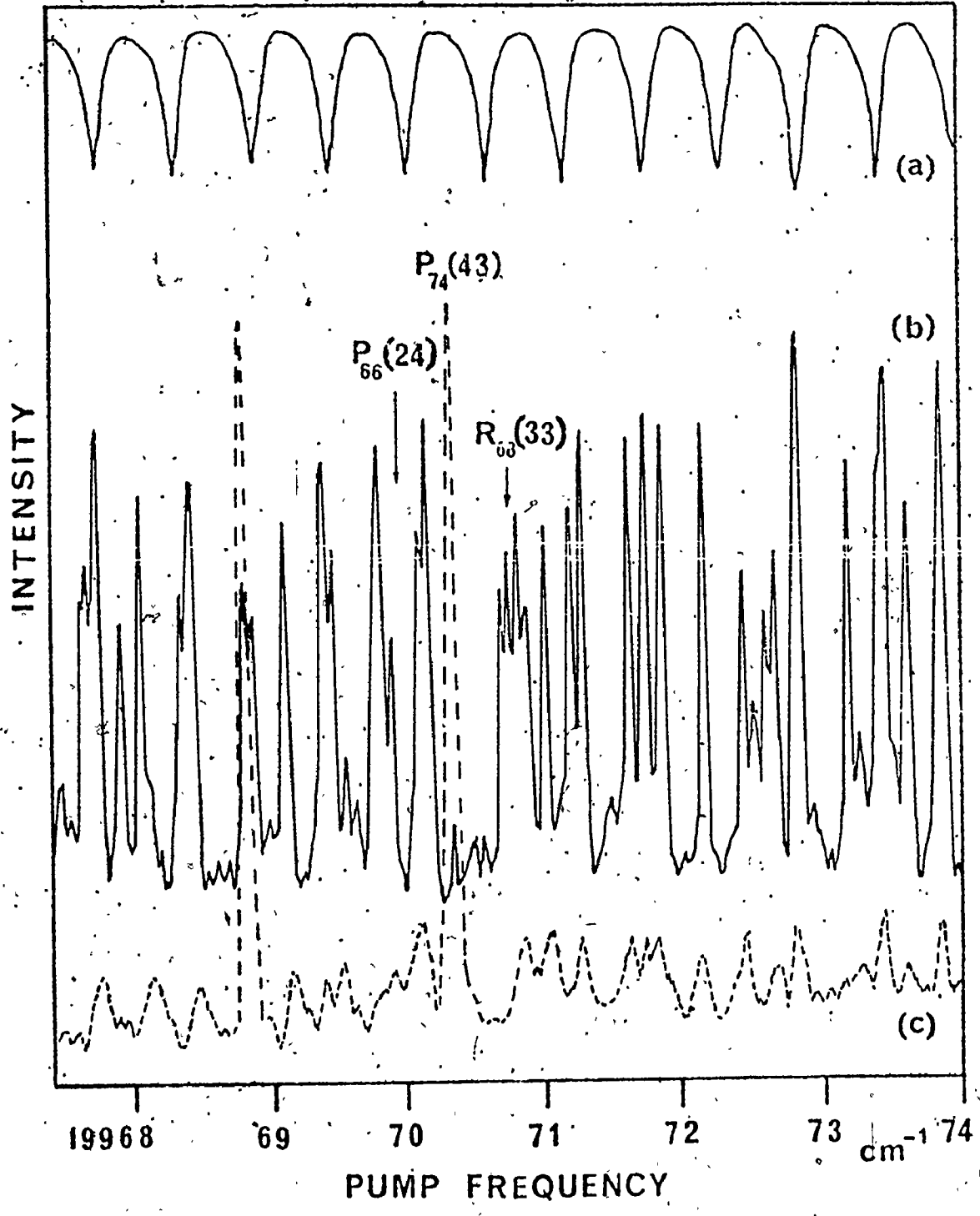
E→B signal level at the corresponding pump laser frequency. Calibration of the pump laser frequency for spectra like that illustrated in Figure V-2 was discussed in Chapter. IV.

At resonance the two-photon signal was maximized by making slight wavelength adjustments alternately to the probe and pump lasers. Although the method was tedious many pump lines so discovered yielded clean rotationally resolved two-photon spectra.

The pump lines were assigned with the aid of a computer program which calculated all possible transitions from the known molecular constants within $\pm.2cm^{-1}$ of the pump line frequency. The accuracy of the programs written to evaluate these transitions was determined by comparison with published assignments (25, 33) and was found to reproduce reported frequencies within $\pm.05cm^{-1}$. In most cases the pump line could be assigned by simply choosing the calculated transition whose frequency most closely matched that of the pump line. However, as discussed below the assignments were also verified by other means.

Table V-1 lists the assignment and frequency of each pump line chosen for intensive study. A suitably wide range of J values was selected to enable an accurate determination of the E state(s) rotational constants (see Section 4).

Transition $X_{v_B}(J)$	Transition Energy σ_1 (cm^{-1})	Pumped Level J_{v_B}	Level Energy $T(v_B, J_B)$ (cm^{-1})
$R_{78}(7)$	20037.77	$J_{78}(8)$	20039.86
$R_{59}(21)$	19888.43	$J_{59}(22)$	19905.66
$R_{74}(41)$	19976.68	$J_{74}(42)$	20040.92
$P_{74}(43)$	19970.37	$J_{74}(42)$	20040.92
$P_{76}(66)$	19888.43	$J_{76}(65)$	20054.24
$P_{63}(104)$	19654.44	$J_{63}(103)$	20061.57

Table V-1.: B←X Transitions Used as Pump Lines in the Two-photon Sequential Absorption Studies. The energies of the B state levels populated by the pumped transitions are relative to $v''=0$, $J''=0$ in the ground X state and are equal to the transition energies in column 2 plus $F_v''(J)$.

The pump lines $R_{74}(41)$ and $P_{74}(43)$ each pumped the same B state level and produced identical two-photon spectra. This provided a useful confirmation of the (v_B,J_B) assignment for this level. The pump level $J_{78}(8)$ was within 4cm^{-1} of the B state dissociation limit and could not be assigned using Barrow's molecular constants since his analysis is restricted to $v_B \leq 77$. A technique was developed which enabled not only this pump level to be identified, but also resulted in the assignment of much of the rotational level structure from $v_B = 77$ to the dissociation limit, D. The technique is discussed in greater detail in Chapter VL.

As illustrated in Table V-1 both the $J_{76}(65)$ and $J_{63}(103)$ levels have energies above the 20043.2cm^{-1} B state dissociation limit. The successful use of these quasibound levels for two-photon studies represents experimental evidence for an effective rotational potential barrier (16) to dissociation for these levels. It is of interest to note that the lifetimes of such energy levels have, in the past, only been deduced indirectly from scattering experiments (89). Using the equations derived by LeRoy and Bernstein (90) and Barrow's (25) RKR potential, the lifetime of the $J_{63}(103)$ level was calculated to be approximately 100nsec. Experiments in which the probe pulse was delayed with respect to the pump pulse confirmed that the $J_{63}(103)$ level lifetime was greater than 36nsec.,

but could not provide an accurate lifetime determination. Unfortunately, optical scattering and absorption losses limited the maximum practical delay to 36nsec. However, the experimental technique could in principle be refined to enable the direct determination of lifetimes of such quasibound energy levels.

Both the probe and the pump lasers were pumped by a relatively low power nitrogen laser (300kW peak) which limited their simultaneous operation to efficient high-gain laser dyes. The best two-photon spectra were therefore obtained with coumarin-type dyes which emit at wavelengths near the short wavelength end of the B←X absorption system. Most of the B state levels pumped in the present study therefore have high v_B values because of this instrumental limitation.

3. The Two-Photon Sequential Absorption Spectra

This section presents a qualitative introduction to the two-photon sequential absorption spectra obtained in the present investigation. A more detailed quantitative analysis of the spectra follows in Section 4.

All of the two-photon spectra were obtained with a constant probe beam bandwidth of about $1.5cm^{-1}$. Therefore the two-photon spectra discussed here do not differ in effective resolution, but may differ in dispersion depending on the wavelength interval illustrated. Unless

. explicitly stated otherwise the two-photon spectra were
obtained with no time delay between the probe and the pump
laser pulses. That is, both laser pulses were coincident
in time in the region of the absorption cell viewed by
the detection system.

When more than one probe laser dye was required
to scan a specified wavelength interval, a continuous re-
cord of the two-photon spectrum was always obtained by
overlapping the wavelength coverage of each laser dye.
The spectra were not normalized to constant laser power so
that the intensity profile of the two-photon spectra tended
to map the gain profile of each probe laser dye(s).

B$\rightarrow$X fluorescence induced by the pump laser was
continuously monitored at the reference cell during all
two-photon studies. The fluorescence signal provided a
measure of the frequency stability of the pump laser. Any
drift of the pump laser off resonance with the selected pump
line could be detected by a change in the B$\rightarrow$X fluores-
cence intensity.

A typical two-photon sequential absorption spec-
trum is presented in Figure V-3. The spectrum was obtained
by scanning the probe laser frequency while pumping the
$J_{74}(42)$ level in the B state with the $R_{74}(41)$ pump line.
An identical spectrum to that illustrated was also obtained
with the $P_{74}(43)$ pump line which populated the same inter-
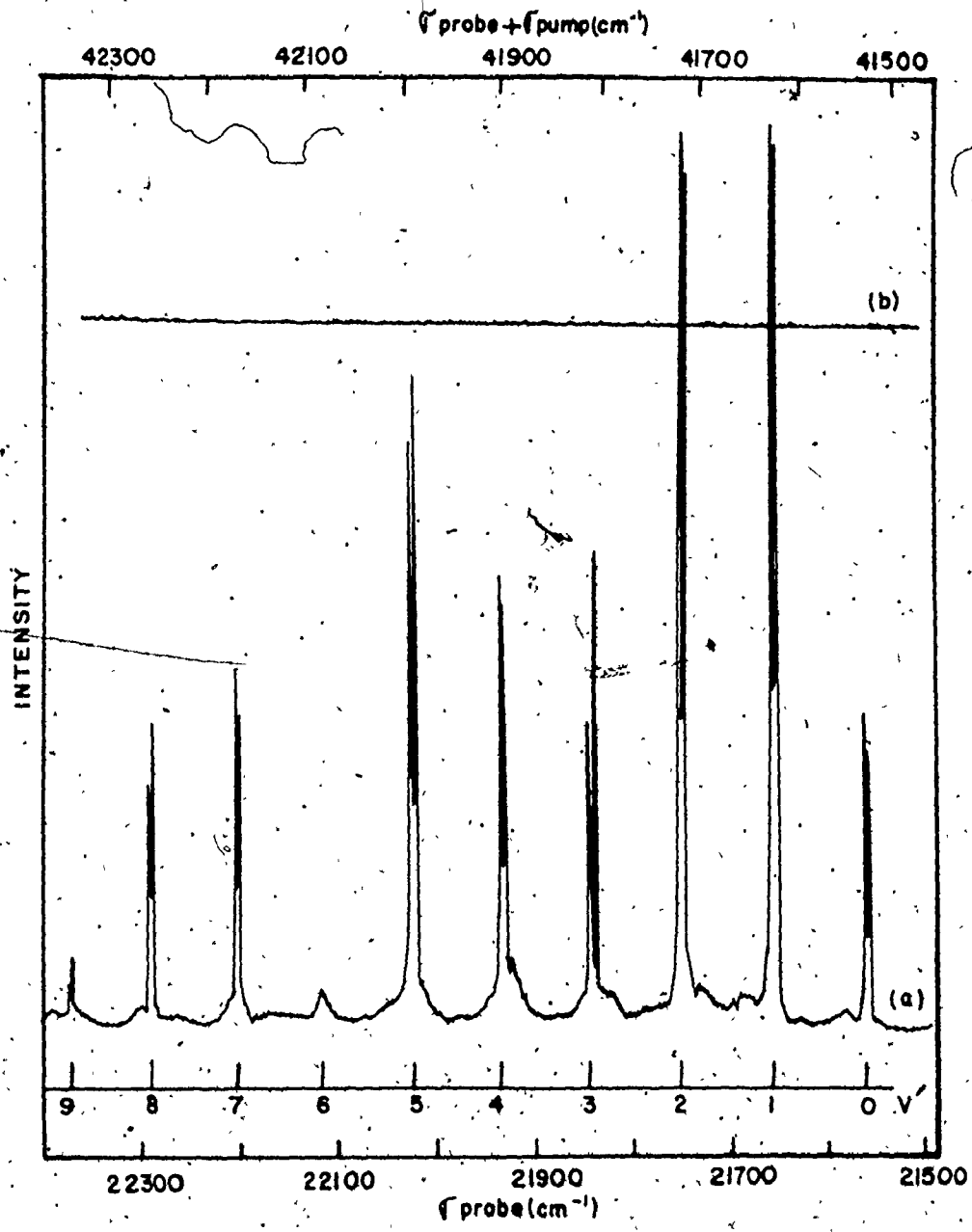
Figure V-3: A portion of the two-photon sequential absorption spectrum for the $R_{74}(41)$ pumped B←X transition--

(a) the first nine members of the γ progression;

(b) simultaneous B→X fluorescence intensity monitored from the reference cell.

mediate level.

Figure V-3(b) is a record of the B$\rightarrow$X emission during the two-photon experiment. Its constant amplitude indicates that the frequency of the pump laser was stable and that the pump laser did not drift off resonance with the pump line. Figure V-3(a) depicts nine vibrational quanta of an E state reached by two-photon absorption. The vibrational progression is made up of bands which have only two rotational lines because of the $\Delta J = \pm 1$ selection rule. So, in this example, only E state levels with J=41 and 43 are observed.

As discussed previously the two-photon spectra reflect the gain profile of the probe laser dye. In the example of Figure V-3, 7-diethylamino-4-methyl-coumarin was the laser dye used in the probe laser and the anomalously low intensity of the $v''=9$ band is instrumental in origin. On the other hand intensity variations between adjacent bands are genuine. The $v'=6$ member of the progression in Figure V-3 has a relatively low intensity and was so observed for all two-photon experiments.

Figure V-4 presents under high dispersion the first four members of the progression illustrated in Figure V-3 and more clearly illustrates the rotational selectivity of the two-photon method. The relative intensities of the P and R branches vary slightly in the bands of

Figure V-4:   The first four members of the γ progression
under high dispersion. Like Figure V-3 the
pumped B state level was $J_{74}(42)$. Each vi-
brational band consists of only two rota-
tional lines which correspond to $\Delta J=\pm 1$
transitions from the $J_{74}(42)$ B state level
to the upper γ state.
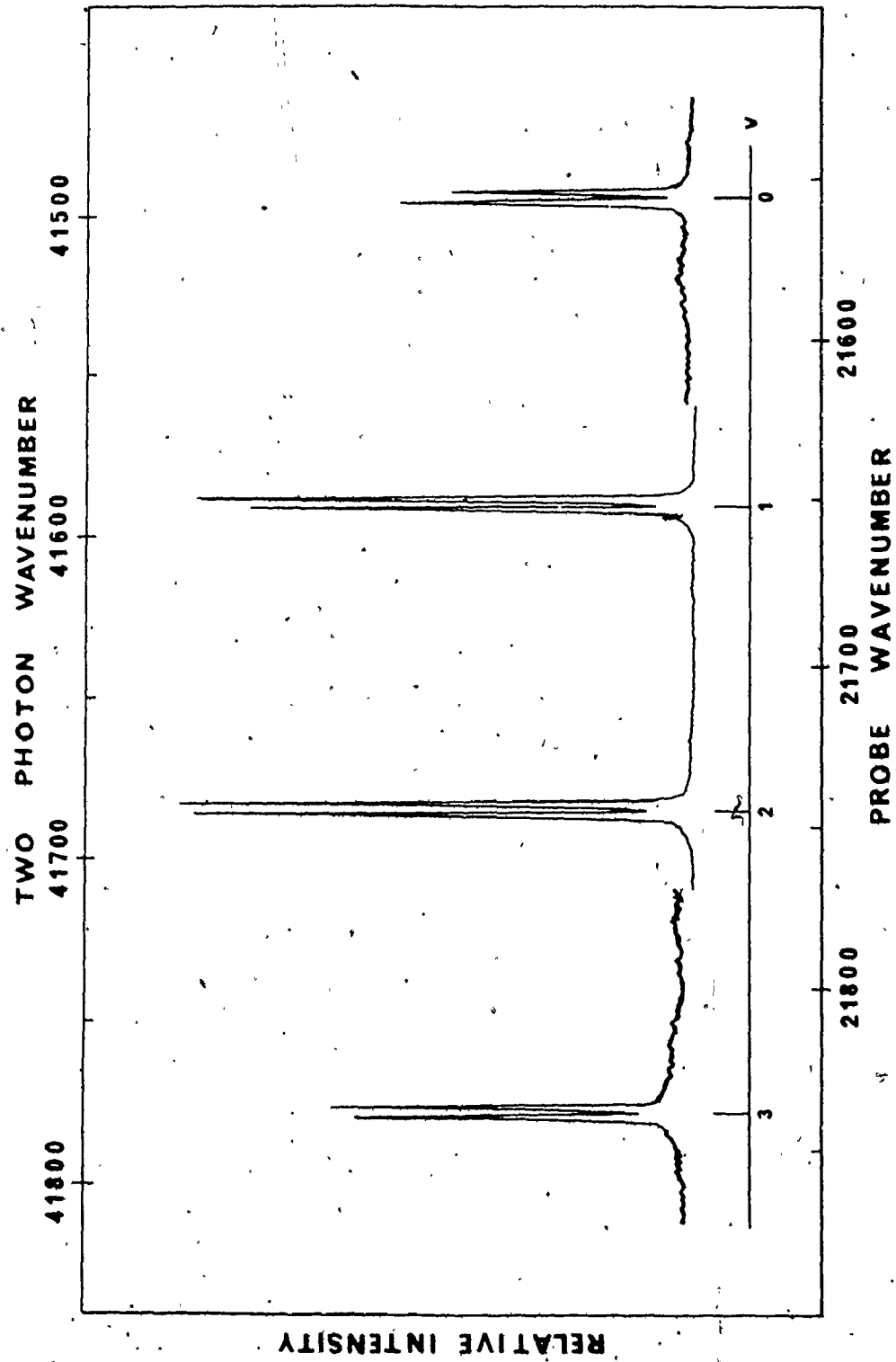
Figure V-4.   This arises from random amplitude fluctuations
in the output of the nitrogen laser used to pump the tun-
able dye lasers, but does not seriously affect the two-
photon spectra.   As illustrated the rotational structure
was clearly resolved and excellent signal levels were typi-
cally obtained.

For iodine several electronic states are theore-
tically predicted to occur in the 5eV energy region (13).
In accord with these theoretical energy estimates, the
two-photon spectra have revealed five separate vibrational
progressions, each representative of a different electronic
state, in the 5 to 5.5eV region.   The five vibrational pro-
gressions have been labelled α, β, γ, δ and ε according to
the frequency of the first observed member of each progres-
sion.   α denotes the lowest frequency progression, β the
next higher frequency progression, and so on in order of
increasing frequency.

While the previous examples have illustrated only
the γ bands, the α, β, γ, and δ bands are illustrated col-
lectively in Figure V-5.   This two-photon spectrum was
obtained with the $R_{78}(7)$ pump line.   For pump levels with
low J values, E←B rotational transitions were too closely
spaced to be resolved with the probe laser used in the pre-
sent study (1.5cm^{-1} bandwidth).   Thus the rotational struc-
ture is not resolved in Figure V-5 and each vibrational .

Figure V-5: The α, β, δ and γ progressions under low dispersion. The B state level pumped was $J_{78}(8)$. Each vibrational band appears only as a single peak because the $\Delta J = \pm 1$ rotational transitions are not resolved for this low J_B value.
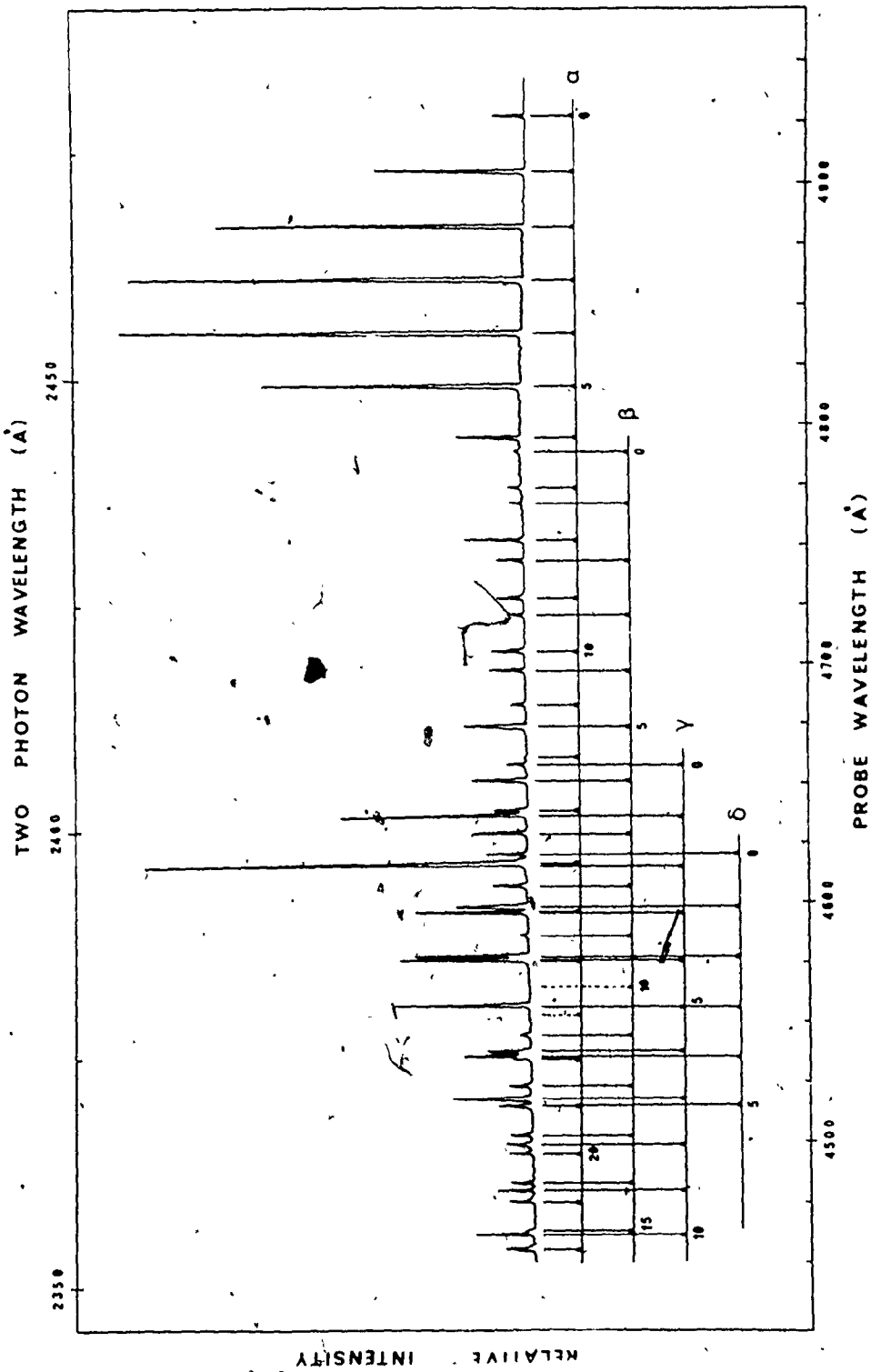
band appears only as a single line. The two intensity maxima observed in the spectrum reflect the gain profiles of the two probe laser dyes required to scan the illustrated wavelength region.

To shorter wavelengths the higher members of the α, β and γ progressions are joined by the ϵ bands. This is illustrated in Figure V-6 which, like Figure V-5, was also obtained with the $R_{78}(7)$ pump line. Here too the rotational structure is not resolved and each vibrational band consists of simply one line. Figure V-6 illustrates in a single spectrum all of the vibrational progressions observed in the present study.

All five of the vibrational progressions observed by two-photon sequential absorption had a vibrational interval spacing of approximately 95 to $105cm^{-1}$. The series of α and β bands, each with over twenty observed members, formed extensive progressions. The δ bands were very weak and only six members were observed for this progression. The γ and ϵ bands were the strongest, with the intensity of the ϵ bands increasing rapidly to higher frequencies.

Although the strong γ and ϵ bands were observed for all pump lines (see Table V-1), the α, β and δ progressions were only observed for pump lines of low J value within approximately $5cm^{-1}$ of the B state dissociation limit. Figures V-5 and V-6 are typical of such spectra, with

Figure V-6: A portion of the two-photon spectrum to the
blue of Figure V-5. All five identified pro-
gressions are visible in the spectrum for which
the B state pump level was $J_{78}(8)$. Each vibra-
tional band appears only as a single line since
the $\Delta J=\pm 1$ rotational structure is not resolved.
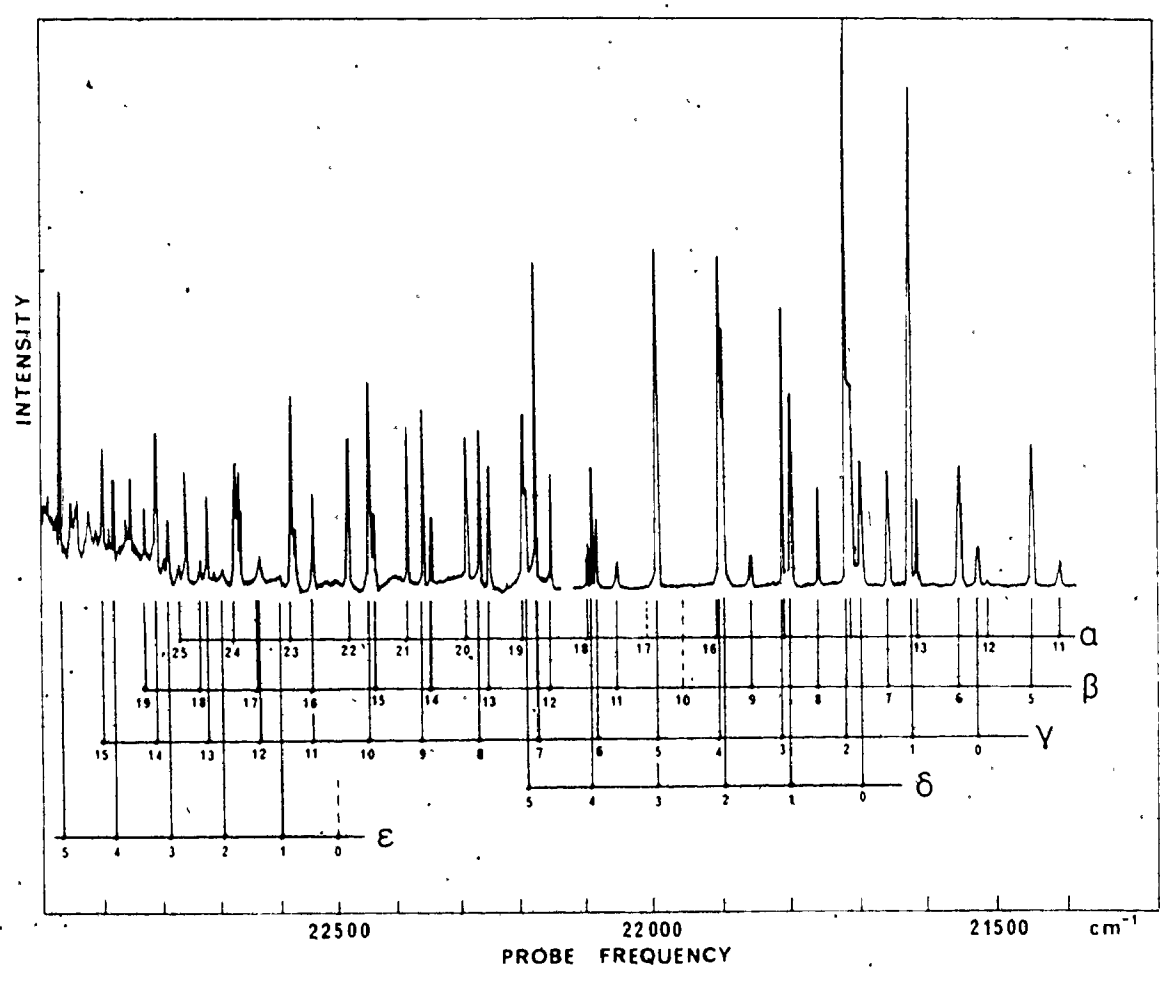
the $J_{78}(8)$ pump level just 3.26cm^{-1} below D. B←X transitions to levels near D, although very weak, when successfully pumped yielded exceptionally sharp and clear two-photon spectra. This observation supports the contention given earlier that reabsorption of B→X fluorescence can populate levels other than the pumped level and so degrade the sequential absorption spectra. Near D, Franck-Condon factors restrict the intensity of the B→X emission and levels other than the pump level are not significantly populated by reabsorption.

It is also probable that Franck-Condon factors favored transitions from pump levels near D to the ionic E states which have large equilibrium internuclear distances (see Chapter II). For example, the outer turning point of the $J_{78}(8)$ level is about 11Å as determined from the B state RKR potential (25). (This is probably the main reason that the α, β and δ progressions could only be observed using pump levels near D.)

Since only low J values could be used to excite the α, β and δ bands, individual rotational transitions could not be resolved and a detailed rotational analysis for these progressions was not possible. However, the vibrational molecular constants were deduced and are reported in Section 4.

Rotational analysis of the γ and ε bands was

possible and revealed several interesting features for these progressions. Only the first 13 members of the γ progression were observed for all pump levels. Higher members of the series were only observed for pump levels of low J value, like $J_{78}(8)$. For pump levels of higher J value, there was an apparent discontinuity in the regular vibrational interval spacing of the γ bands. Above $v'=12$ the γ bands were apparently perturbed or at least weakened so that the progression seemed to break off with only the strong ε bands observed to higher frequencies. This is illustrated in Figure V-7.

Also shown in Figure V-7 is the complex multi-lined structure usually observed for the ε bands. Figure V-7 was recorded with the same pump level, $J_{74}(42)$, as Figures V-3 and V-4. Even though the γ bands display a simple two-line rotational structure (and despite very careful control of the pump laser's frequency stability) the ε bands in the same spectrum revealed a complex multi-lined structure in which successive bands differed in both intensity and rotational pattern. The complex structure was observed for all two-photon spectra of the ε bands.

Initially, it was thought that two interleaved progressions were responsible for the observed spectra. However following more detailed analysis, it was concluded that only one progression was in fact present. The strong

Figure V-7: Two-photon spectrum showing the apparent break-off of the γ progression and the appearance of the multilined ε bands. Transitions are identified according to $J_X - (J_B)_v - J_\varepsilon$. The B state pumped level was $J_{74}(42)$. ε_4 was recorded at lower gain, the actual relative intensity was approximately $100\times$ that of the γ_{12} band.
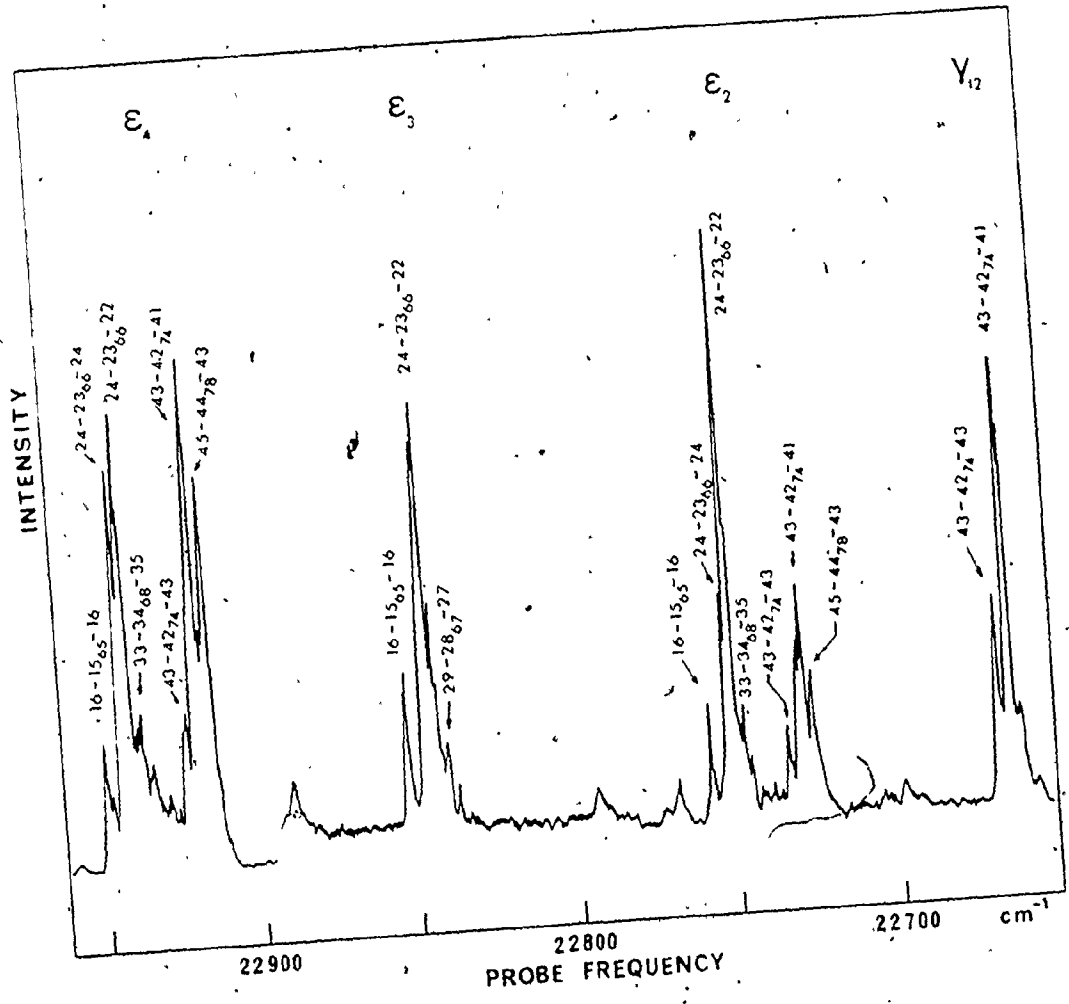
multi-lined ε bands have been assigned to sequential absorption transitions following multi-frequency pumping of several (v_B, J_B) levels. These considerations are discussed more fully in Section 4.

Every attempt was made to establish conclusively the origin bands and verify the vibrational numbering for each of the five progressions observed in the present study. Different pump lines and probe laser dyes revealed no additional bands to the red of those reported herein. The vibrational assignments have therefore assumed that the first observed member in each series is the origin band. For the γ series in which the $v'=0$ band is relatively strong the assignment is probably not in error. For the weaker progressions, especially the δ series, it is possible that the actual 0-0 band lies to the red of the first observed member.

4. Analysis and Assignment of the Two-Photon Spectra

Conventional spectroscopic studies (13,14) of the E states of molecular iodine have provided very complex spectra which have precluded detailed analysis. However, the present two-photon investigation of iodine has revealed five separate electronic states in the 5 to 5.5eV region for which spectroscopic constants may now be determined.

In general the term value for a specified ro-

vibronic level in an excited electronic state is given by:

$$T_{(v',J')} = T'_e + G'(v) + F'_v(J) \quad \ldots (5-1)$$

where T'_e, $G'(v)$ and $F'_v(J)$ are the electronic, vibrational and rotational energies, respectively (16). In the present study the term values T' relative to the $(v''=0, J''=0)$ level of the ground state are given by:

$$T(v',J') = \sigma_1 + \sigma_2 + F''_0(J) \quad \ldots (5-2)$$

where σ_1 is the pump frequency, σ_2 is the probe frequency and $F''_0(J)$ is the rotational term for the $(v''=0, J'')$ level from which the pumped B←X transition(s) originate(s). $F''_0(J)$ was calculated from LeRoy's molecular constants which are tabulated in Table II-2. For low J values Barrow's simpler equations, also given in Table II-2, gave nearly identical results. σ_1, the frequency of the pumped B←X transition, was determined as described in Section 2 of this chapter. σ_2 for each observed E←B transition was determined by the probe calibration procedure reported in Chapter IV.

The term values determined in this manner were used to calculate the molecular constants for the E states of molecular iodine. For example, the vibrational constants were determined from a least squares fit of equations of the form (16):

$$T_0(v',J'=0) = T_e' + \omega_e'(v+\tfrac{1}{2}) + \omega_e x_e'(v+\tfrac{1}{2})^2$$

$$+ \omega_e y_e'(v+\tfrac{1}{2})^3 + \ldots \quad \ldots \quad (5\text{-}3)$$

A third order polynomial fit of the observed band origin $T_0(v',J'=0)$ to $(v'+\tfrac{1}{2})$ yielded the electronic energy T_e', the vibrational frequency ω_e', and the anharmonicity constants $\omega_e x_e'$ and $\omega_e y_e'$.

Similarly, linear regression of the observed term values to $J'(J'+1)$ according to:

$$T(v',J') = T_0(v',J'=0) + B_v' \, J'(J'+1) \quad \ldots \quad (5\text{-}4)$$

provided the E state(s) band origins (relative to $v''=J''=0$) and the rotational constant B_v'. Higher order distortion terms in equation (5-4) were not considered because the probe laser frequency calibration limited the accuracy of T' to $\pm .2\text{cm}^{-1}$. Trial fits to a quadratic in $J'(J'+1)$ were attempted but the uncertainty in T' was too large to provide reliable centrifugal distortion constants.

Finally, the vibrationless rotational constant B_e' was obtained from the observed B_v' by linear regression of equations of the form:

$$B_v' = B_e' + \alpha_e(v+\tfrac{1}{2}) + \ldots \quad \ldots \quad (5\text{-}5)$$

Note that the analyses outlined above made use
of all the available spectroscopic data. For example, B_v'
was not determined from a single combination difference
(16). Instead, all of the observed E←B rotational transi-
tions for each B state pump level were included in the cal-
culated fit of equation (5-4). For the $R_{78}(7)$ pump line
the E state rotational structure could not be resolved and
it was necessary to use the mean line frequency as an ap-
proximate value for the P and R branch components. This
assumption however did not contribute a significant error to
the rotational analyses (see Sections 4.2 and 4.3).

Sections 4.1 to 4.3 present the molecular con-
stants deduced from the two-photon spectra by the proce-
dures outlined above for the α, β, δ, γ and ε excited
states. A discussion of the electronic state assignment
of all five excited states is presented in Section 4.4.

4.1 The α, β and δ Band Systems

As mentioned above it was not possible to rota-
tionally resolve the α, β and δ bands because these pro-
gressions could only be excited from pump levels near D
with low J_B value. Although rotational analysis of these
three systems was not possible, the vibrational constants
were determined and are reported herein.

Tables V-2 to V-4 summarize the vibrational ana-
lysis of the α, β and δ band systems. The vibrational

	T_e'	40281.8	
	ω_e'	104..83	
	$\omega_e x_e'$	.320	
	$\omega_e y_e'$	3.9×10^{-3}	

$v' + \frac{1}{2}$	T_{obs}' (cm^{-1})	T_{calc}' (cm^{-1})	$T_{obs}' - T_{calc}'$ (cm^{-1})
.5	40334.5	40334.1	+.39
1.5	438.7	438.3	+.39
2.5	541.4	541.9	-.49
3.5	644.4	644.9	-.50
4.5	747.3	747.4	-.07
5.5	848.9	849.3	-.27
6.5	950.5	950.7	-.18
7.5	41051.9	41051.6	+.39
8.5	152.1	152.1	+.04
9.5	251.5	252.1	-.56
10.5	352.3	351.7	+.64
11.5	451.2	450.8	+.35
12.5	549.9	549.7	+.22
13.5	649.3†	648.2	+(1.1)
14.5	~ 748.3	--	--
15.5	~ 845.8	--	--
16.5	~ 943.4	--	--
17.5	--	--	--
18.5	42136.5	42136.1	+.39
19.5	232.7	232.9	-.26
20.5	329.3	329.7	-.37
21.5	425.2†	(426.2)	(+1.0)
22.5	523.7†	(522.7)	(-1.0)
23.5	619.1	518.9	+.23
24.5	715.3	715.1	+.24
25.5	811.1	811.2	+.10

Standard Error for $T_{calc}' = \pm .44$cm^{-1}

Table V-2: Vibrational Constants for the α Excited State. T' values are expressed relative to $X_{v''=0, J''=0}$. The B state level pumped was $J_{78}(8)$. T_{obs}' values labelled with an ~ sign are not accurately known from experiment. T_{obs}' values labelled

with a $\dagger$ symbol could not be accurately fit to a single polynomial expansion and were also excluded from the least squares calculation of the vibrational constants.

		40925.1
T'_e		40925.1
ω'_e		104.07
$\omega_e x'_e$		.219
$\omega_e y'_e$		8.6×10^{-5}

$v'+\frac{1}{2}$	T'_{obs} (cm^{-1})	T'_{calc} (cm^{-1})	$T'_{obs}-T'_{calc}$ (cm^{-1})
.5	40976.9	40977.1	−.15
1.5	41080.9	41081.1	+.21
2.5	41184.1	41184.3	+.22
3.5	41286.7	41286.7	−.07
4.5	41388.6	41388.3	−.35
5.5	41490.4	41489.9	−.44
6.5	41592.4	41592.5	+.11
7.5	41693.3	41693.3	−.01
8.5	41793.9	41793.9	+.01
9.5	41894.5	41894.9	+.46
10.5	~41995	--	--
11.5	42093.5	42093.9	+.43
12.5	42191.9	42191.9	0.0
13.5	42289.8	42289.2	−.53
14.5	~42387	--	--
15.5	42485.5	42485.1	−.37
16.5	~42582	--	--
17.5	42679.9	42680.2	+.29
18.5	42775.6	42775.2	−.39
19.5	42871.9	42871.9	+.05
20.5	42967.9	42968.5	+.63
21.5	43062.4	43062.5	+.14
22.5	43156.4	43155.9	−.42

Standard Error for T'_{calc} = ±.36cm^{-1}

Table V-3: Vibrational Constants for the β Excited State. T' values are expressed relative to $\ddot{X}_{v''=0,J''=0}$. The B state pump level was $J_{78}(8)$. T'_{obs} values labelled with an ~ symbol could not be accuratly determined from experiment and were excluded from the numerical analysis.

T_e'	41682.9
ω_e'	100.41
$\omega_e x_e'$	.180

$v'+\frac{1}{2}$	T_{obs}' (cm^{-1})	T_{calc}' (cm^{-1})	$T_{obs}'-T_{calc}'$ (cm^{-1})
.5	41733.0	41732.0	$-.11$
1.5	41833.2	41833.2	$+.04$
2.5	41933.2	41933.5	$+.35$
3.5	42031.9	42931.6	$-.28$
4.5	42131.0	42130.8	$-.15$
5.5	·42229.9	42230.0	$+.13$

Standard Error for $T_{calc}' = \pm.24$cm^{-1}

Table V-4: Vibrational Constants for the δ Excited State. T' values are expressed relative to $X_{v''=0,J''=0}$. The B state pump level was $J_{78}(8)$.

constants for the excited state determined from a least
squares fit of the observed terms, T'_{obs}, to equation (5-3)
is presented in each table.[†] The term values calculated
from the derived vibrational constants, T'_{calc}, are also
given for comparative purposes. The derived vibrational
constants were found to represent adequately the α, β and δ
band systems (see Tables V-2 to V-4) although irregulari-
ties apparently due to perturbations were noted between
T'_{obs} and T'_{calc} (experimental uncertainty $\pm.2cm^{-1}$). This
is not unexpected as the upper states of all five of the
progressions observed in this study are closely interleaved
and may perturb each other.

The vibrational constants for the α and β progres-
sions were remarkably similar, and each β band was approxi-
mately $642cm^{-1}$ to higher frequency than the corresponding
α band with identical v' numbering. It might be suggested
on the basis of these observations that both the α and β
series represent transitions to a single E state. The β
bands might then be assigned to E←B transitions from (a)
B state level(s) $642cm^{-1}$ lower in energy than the pump level

---

[†]It was necessary to use $T(v',J'=8)$ rather than $T_0(v',J'=0)$
in evaluating equation (5-3) for the α, β and δ bands. This procedure
does not significantly affect ω'_e, $\omega_e x'_e$ or $\omega_e y'_e$ but may yield a T'_e value
slightly in error. Since B'_v for these excited states is less than
$.02cm^{-1}$, the error in the calculated T'_e is probably less than $1cm^{-1}$.

and populated by vibrational relaxation within the B state manifold. This contention however is improbable for several reasons.

First, the relaxation mechanism would have to be remarkably selective because only limited and constant J' values are observed for both the α and β bands. Secondly, the relaxation process would have to take place in less than 5nsec, the overlap period of the probe and the pump laser pulses. Fewer than 2×10^{-2} intermolecular collisions are possible in this period (see footnote page 64).

Experiments in which the probe pulse was delayed optically by up to 24nsec with respect to the pump pulse did not reveal any change in the relative intensities of the α and β bands. The intensity of both progressions was reduced but only by the same relative amount for each band. Moreover, for the time delays investigated, no additional bands were observed in the two-photon spectra.

In addition it should be noted that use of either the α, β or γ bands in the two-photon experiments described in Chapter VI gave identical results. That is either the α, β or γ bands (at least in the 21200 to $21700cm^{-1}$ region) yielded identical rotational structure for the B state near dissociation and gave the same value of D for all three series.

These observations are not consistent with a

proposed B state vibrational relaxation mechanism which must, therefore, be considered an unlikely explanation for the β series. It is most probable on both experimental and theoretical grounds, that the α and β progressions arise simply from transitions to similar but separate electronic E states of iodine.

4.2 The γ Band System

The γ bands could be excited from pump levels of sufficiently high J_B value to permit resolution of individual rotational transitions. Therefore, it was possible to determine not only the vibrational constants but also the rotational parameters for the excited state.

In the two-photon spectra the first observed member of the γ progression was probably the origin band. No additional γ transitions were observed to the red of the apparent origin band for all the pump levels investigated. The intensity distribution of the progression changed markedly with different pump levels, but no additional γ bands were observed even at very high detection sensitivity. It is unlikely that unfavorable Franck-Condon factors would obscure the origin band for all pump levels.

Table V-5 illustrates some of the experimental two-photon data and the assignments concluded for the γ

$X_{VB}(J)^1$	$R_{78}(7)$	$R_{59}(21)$	$R_{59}(21)$	$R_{74}(41)^2$	$R_{74}(41)^2$	$P_{76}(66)$	$P_{76}(66)$	$P_{63}(104)$	$P_{63}(104)$
σ_1	20037.77	19888.43	19888.43	19976.68	19976.68	19888.43	19888.43	19654.44	19654.44
$F_0''(J)$	2.0906	15.6790	15.6790	64.2738	64.2738	164.99	164.99	407.1331	407.1331
$\sigma_1 + F_0''(J)$	20039.86	19905.66	19905.66	20040.92	20040.92	20054.24	20054.24	20061.57	20061.57
J'	8	21	23	41	43	64	66	102	104
$J'(J'+1)$	72	462	552	1722	1892	4160	4422	10506	10920
γ_0	41562.86	41568.07	41571.53	41595.57	41599.09	41643.16	41648.52	41768.74	41776.74
γ_1	41657.96	41665.44	41667.26	41690.09	41693.15	41738.34	41743.15	41862.69	41870.88
γ_2	41752.66	41760.27	41761.87	41784.12	41787.42	41832.16	41837.60	41956.38	41964.48
γ_3	41845.86	41853.47	41855.64	41877.42	41881.02	41926.39	41931.26	42050.38	42058.10
γ_4	41939.06	41947.16	41949.44	41971.32	41974.82	--	--	42142.80	42150.99
γ_5	42031.86	42040.81[3]	42040.81[3]	42064.52	42068.02	(42110.57)[4]	42116.74	42235.80	42243.84
γ_6	42124.66	--	--	(42157.12)[4]	(42160.22)[4]	42209.50	42214.69	42328.15	42336.29
γ_7	42216.56	42224.97	42226.02	42248.92	42252.22	--	--	--	--
γ_8	42308.06	42316.69	42318.54	42341.22	42344.72	42388.64	42393.40	--	--
γ_9	42399.86	42408.64	42410.56	42432.52	42435.82	42480.21	42485.19	--	--
γ_{10}	42491.66	--	--	42524.12	42527.42	--	--	--	--
γ_{11}	42582.76	42591.35	42592.90	42615.52	42619.32	--	--	--	--
γ_{12}	42673.36	42681.91	42683.46	42705.12	42708.52	--	--	--	--

[1]All pumped transitions originate from v"=0.
[2]Equivalent spectra obtained with $P_{74}(43)$.
[3]Unresolved line center, assigned to $J'=22$.
[4]Values in brackets are uncertain.

Table V-5: Rotational Analysis of the γ Bands. The table presents T'_{obs} for each γ_v band. The J' values follow directly from the assignment of the pumped transition $X_{VB}(J)$.

progression.[+] For a given pump line Table V-5 lists the T'_{obs} values deduced from the two-photon spectra according to equation (5-2). The data presented in Table V-5 represents the first successful rotational analysis of an excited gerade state of iodine. Note that the $R_{78}(7)$ pump line did not provide rotationally resolved spectra and that an average value $J'=8$ was assigned to these T'_{obs} values. This treatment introduces only a nominal uncertainty in T' ($<.05cm^{-1}$) because of the small rotational constant of the excited state.

Other than $R_{78}(7)$, all pump lines illustrated in Table V-5 yielded rotationally resolved two-photon spectra. In principle, the excited state rotational constants could have been estimated from the combination differences (16) of the transitions listed in the table. However, optimal use of the available data, including unresolved transitions, was achieved by a simultaneous least squares fit of the T' values to $J'(J'+1)$ according to equation (5-4). This is illustrated graphically in Figure V-8 which displays T'_{obs} versus $J'(J'+1)$ for the first four vibrational quanta of Table V-5. The slope and intercept of the lines

---

[+] In the detailed analysis of the two-photon spectra, data in addition to that illustrated in Table V-5 was considered. For example in addition to the $R_{74}(41)$ pump line, the $P_{74}(43)$ pump line was used to populate the same B state level, $J_{74}(42)$. This provided an independent determination of $T'(v', J'=41$ or $43)$ for each v' level.
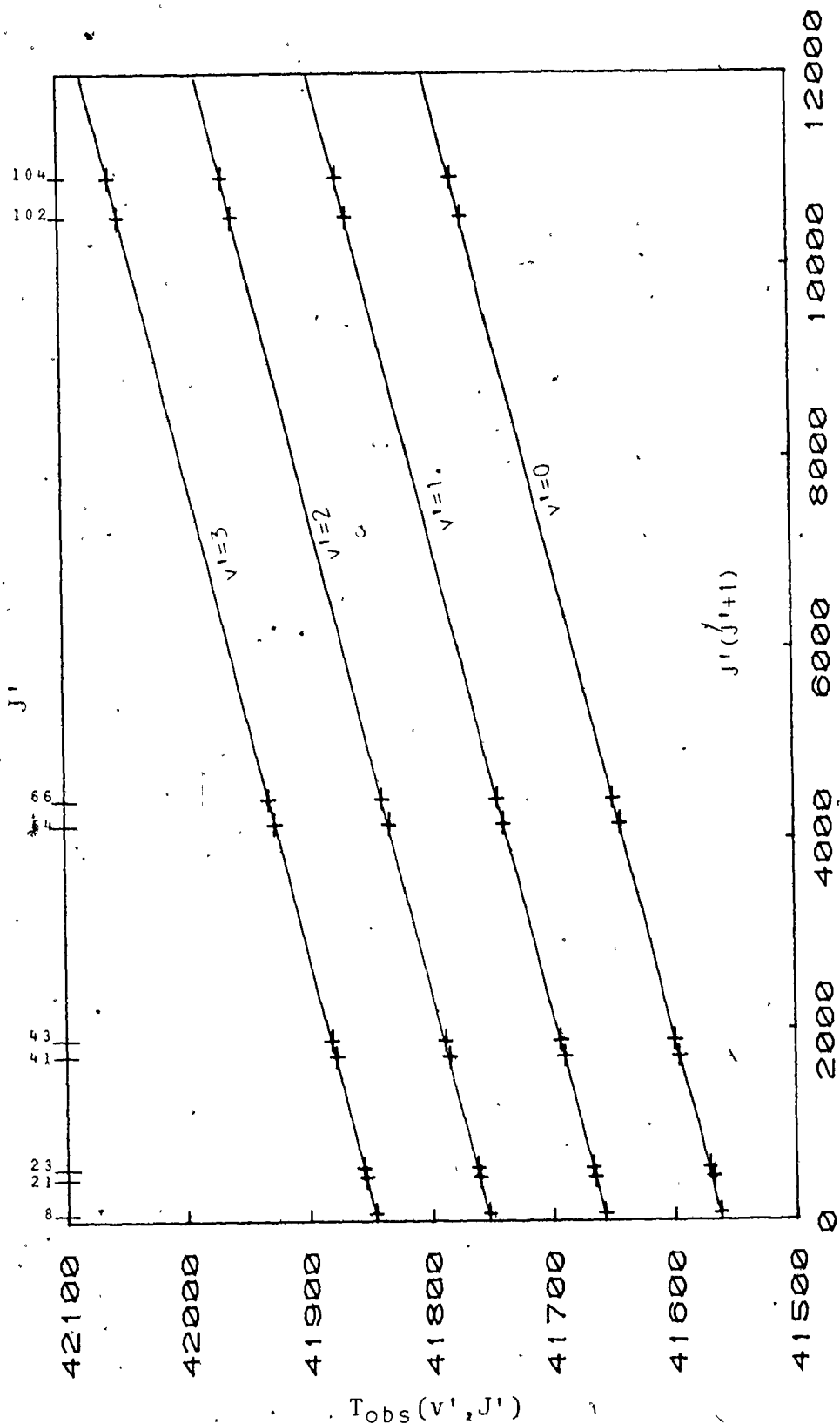
Figure V-8: Graphical representation of the rotational analysis of the γ bands. T_{obs} values are shown versus $J'(J'+1)$ for a given J' assignment. Only the first four vibrational quanta are shown. The rotational constants B'_v and the band origins $T_0(v',J'=0)$ are given by the slope and intercept of the lines, respectively.

in Figure V-8 yield the rotational constants B_v' and the band origins $T_0(v', J'=0)$, respectively. B_e' and the molecular vibrational constants (ω_e', $\omega_e x_e'$, etc.) then follow directly from application of equations (5-5) and (5-3).

The rotational constants and band origins for the γ excited state of iodine are given in Table V-6, while the vibrational constants are collected in Table V-7. The molecular constants in Tables V-6 and V-7 are average quantities which can reproduce the observed two-photon transition energies to within experimental uncertainty in most cases. However some of the γ excited state levels are apparently perturbed and transitions to these levels cannot be calculated exactly.

For example, the $v'=6$ band has anomalously low intensity and is displaced from its anticipated frequency in all two-photon spectra. The $v'=6$ band was therefore excluded from the fit for B_e' and T_e' for the γ excited state. In view of the many electronic states observed in the same spectral region, perturbations are expected. But nothing more can be conclusively stated with regard to perturbations, until more detailed investigations are undertaken.

Finally, Table V-8 presents an approximate RKR potential curve (91) for the γ excited state. The potential function was calculated from the spectroscopic constants given previously (in Tables V-6 and V-7) with a

v'	$T_0(v',J'=0)$ (cm^{-1})	B_v' $(10^2 \ cm^{-1})$
0	41561.23 ± 49	1.9764 ± 73
1	41656.33 ± 13	1.9645 ± 19
2	41750.82 ± 17	1.9561 ± 26
3	41844.23 ± 23	1.9608 ± 34
4	41937.86 ± 27	1.9506 ± 33
5	42030.97 ± 26	1.9493 ± 37
*) 6	42124.47 ± 133	1.9506 ± 172
7	42215.40 ± 21	1.9579 ± 24
8	42307.55 ± 21	1.9502 ± 29
9	42399.10 ± 25	1.9459 ± 35
10	42490.25 ± 10	1.9582 ± 10
11	42581.82 ± 34	1.9664 ± 41
12	42672.53 ± 28	1.9250 ± 35
$B_e' = 1.9664 \times 10^{-2} \quad \alpha_e = 1.79 \times 10^{-5}$		

*) The $v'=6$ level is perturbed and was
   excluded from the fit for B_e'.

Table V-6: Band Origins and Rotational Constants for the
γ Excited State of Iodine.

$v' + \frac{1}{2}$	$T_{0}^{'}{}_{obs}(v',J'=0)$ (cm^{-1})	$T_{0}^{'}{}_{calc}(v',J'=0)$ (cm^{-1})	$T_{obs}^{'} - T_{calc}^{'}$
	$T_{e}^{'}$	41513.6	
	$\omega_{e}^{'}$	95.53	
	$\omega_{e}x_{e}^{'}$	.3091	
	$\omega_{e}y_{e}^{'}$	.0067	
.5	41561.2	41561.3	-.10
1.5	41656.3	41656.3	.06
2.5	41750.8	41750.6	.18
3.5	41844.2	41844.5	-.27
4.5	41937.9	41937.9	-.02
5.5	42031.0	42030.8	.14
6.5	42124.6	42123.3	(1.32)[1]
7.5	42215.4	42215.6	-.14
8.5	42307.5	42307.5	.09
9.5	42399.1	42399.1	.04
10.5	42490.2	42490.4	-.17
11.5	42581.8	42581.6	.22
12.5	42672.5	42672.6	-.09

Standard Error for $T_{calc}^{'} = \pm.18$cm^{-1} [1]

[1] Y_6 is perturbed and was excluded from the fitting procedure.

Table V-7: Vibrational Molecular Constants for the γ Excited State of Iodine. T' values are expressed relative to $X_{v''=0,J''=0}$.

v'	G_v (cm^{-1})	ΔG_v (cm^{-1})	R_{min} $(\AA)$	R_{max} $(\AA)$
0	47.5642	94.9346	3.6024	3.7516
1	142.4987	94.3770	3.5500	3.8093
2	236.8757	93.8598	3.5145	3.8501
3	330.7355	93.3829	3.4860	3.8840
4	424.1184	92.9464	3.4616	3.9138
5	517.0648	92.5503	3.4399	3.9409
6	609.6151	92.1945	3.4203	3.9659
7	701.8095	91.8790	3.4023	3.9893
8	793.6885	91.6039	3.3856	4.0115
9	885.2925	91.3692	3.3699	4.0325
10	976.6617	91.1748	3.3552	4.0527
11	1067.8365	91.0208	3.3414	4.0720
12	1158.8574	90.9072	3.3282	4.0906
Equilibrium Internuclear Distance r_e=3.6757				

Table V-8: RKR Potential Curve for the γ Excited State of Iodine. The molecular constants given in Tables V-6 and V-7 were used to evaluate the potential function.

computer program similar to that described by Tellinghuisen (92). Both the low vibrational interval ($\omega_e \sim 95 cm^{-1}$) and the large equilibrium internuclear distance ($r_e \sim 3.7 \text{Å}$) shown in Table V-8 are typical of an ion-pair excited state (13).

4.3   The ε Band System

The complex multi-lined ε bands (see Figure V-7) were perhaps the most intriguing feature of the two-photon spectra. Even for spectra in which the γ bands displayed a simple two-lined P and R branch rotational structure, the ε bands exhibited a complex multi-lined rotational pattern. Even-numbered members of the ε progression showed a different rotational pattern from the odd-numbered members and the intensity of each band also appeared to alternate in similar fashion (even-numbered members strongest).

At first these observations appeared to indicate that two interleaved progressions were responsible for the two-photon spectra. However a detailed rotational analysis has strongly suggested that only one progression is in fact active, and that the observed transitions share a common upper electronic state.

Most of the ε bands were very ·intense, even relative to the strong γ bands. For example in Figure V-7, ε_4 was about 100 times the intensity of γ_{12}. The intrinsic intensity of the ε progression suggests that these multi-lined bands arise from sequential absorption processes

rather than, for example, double quantum transitions or higher order three-photon interactions. The rotational structure in each ε band was limited so that double-photon transitions were excluded on this basis also. (For iodine double quantum transitions would yield very complex rotationally unresolved spectra since rotational levels up to $J''=100$ are thermally populated at room temperature.)

It was therefore considered most probable that the multilined ε bands could be assigned to transitions which originate from several intermediate B state levels. A computer search of all possible B←X rotational transitions produced a list of approximately 10 to 20 additional transitions within $\pm.5cm^{-1}$ of each pump line listed in Table V-1. Most of the calculated transitions were not separately included in Barrow's analysis of the B—X absorption system (25) and because of overlap could not be easily recognized in the single-photon laser excitation spectra of the present study. The exact frequency of the calculated transitions could not therefore be determined experimentally, but there is certainly a very high density of potential pump lines throughout the visible absorption system of iodine. Given the finite bandwidth of the pump laser, multifrequency pumping of several B state levels can readily occur.

The ε bands were therefore considered to result from multifrequency pumping of various B←X transitions

calculated to lie within $\pm.5\text{cm}^{-1}$ of each of the pump lines.
presented in Table V-1. In all cases the two-photon rotational structure could be successfully assigned to $E\leftarrow B$ transitions from several B state levels populated by multifrequency pumping of $B\leftarrow X$ transitions identified in this manner.

For example, Tables V-9 and V-10 illustrate the rotational analysis of the ε bands observed for pumping the $R_{74}(41)$ transition at 19976.68cm^{-1}. Table V-9 lists several additional transitions which were calculated to lie near 19976cm^{-1} and that, following rotational analysis of the ε bands, account for the multilined nature of the two-photon spectrum. Table V-10 details the rotational analysis for pumping at 19976cm^{-1}. The transitions $R_{65}(7)$, $R_{66}(19)$, $P_{68}(29)$, and $P_{76}(35)$ as well as $R_{74}(41)$ are shown in the table to contribute to the sequential absorption spectrum of the ε bands for pumping at 19976cm^{-1}. Table V-10 also includes data for multifrequency pumping of transitions near 19888.4cm^{-1}.

Linear regression of the T'_{obs} values to $J'(J'+1)$ according to equation (5-4) provided the rotational constants and band origins for the ε excited state. Figure V-9 displays graphically T'_{obs} versus $J'(J'+1)$ for the first five vibrational quanta of the example discussed above. The excellent fit illustrated in the figure serves to confirm the assignments given in Table V-10.

$X_v(J)$	σ [1] (cm^{-1})	$\Delta\sigma$ [2] (cm^{-1})	E [3] (cm^{-1})	ΔE [4] (cm^{-1})	Relative Intensity [5]	
					ϵ_2	ϵ_3
$R_{65}(7)$	19976.44	+.235	19978.53	62.39	10	10
$R_{66}(19)$	19976.82	−.135	19991.00	49.92	9	5
$P_{68}(29)$	19977.11	−.432	20009.59	31.33	2	3
$P_{76}(35)$	19976.86	−.180	20023.89	17.03	3	3
$R_{74}(41)$	19976.68	0.0	20040.92	0.0	1	10

[1] σ = calculated transition frequency.

[2] $\Delta\sigma = \sigma_{pump} - \sigma$. Note that $\Delta\sigma$ is larger than the pump bandwidth of .07cm⁻¹(FWHM).

[3] E = B-state level energy with respect to $X_{v''=0,J''=0} = \sigma + F_v''(J)$.

[4] $\Delta E = E_{pump} - E$.

[5] Estimated relative intensity of observed two-photon transitions ($\Delta J''=0,2$) in ϵ_2 and ϵ_3 bands.

Table V-9: B←X Transitions Nearly Coincident with $R_{74}(41)$ observed to be active in the two-photon sequential absorption spectra of the ϵ bands.
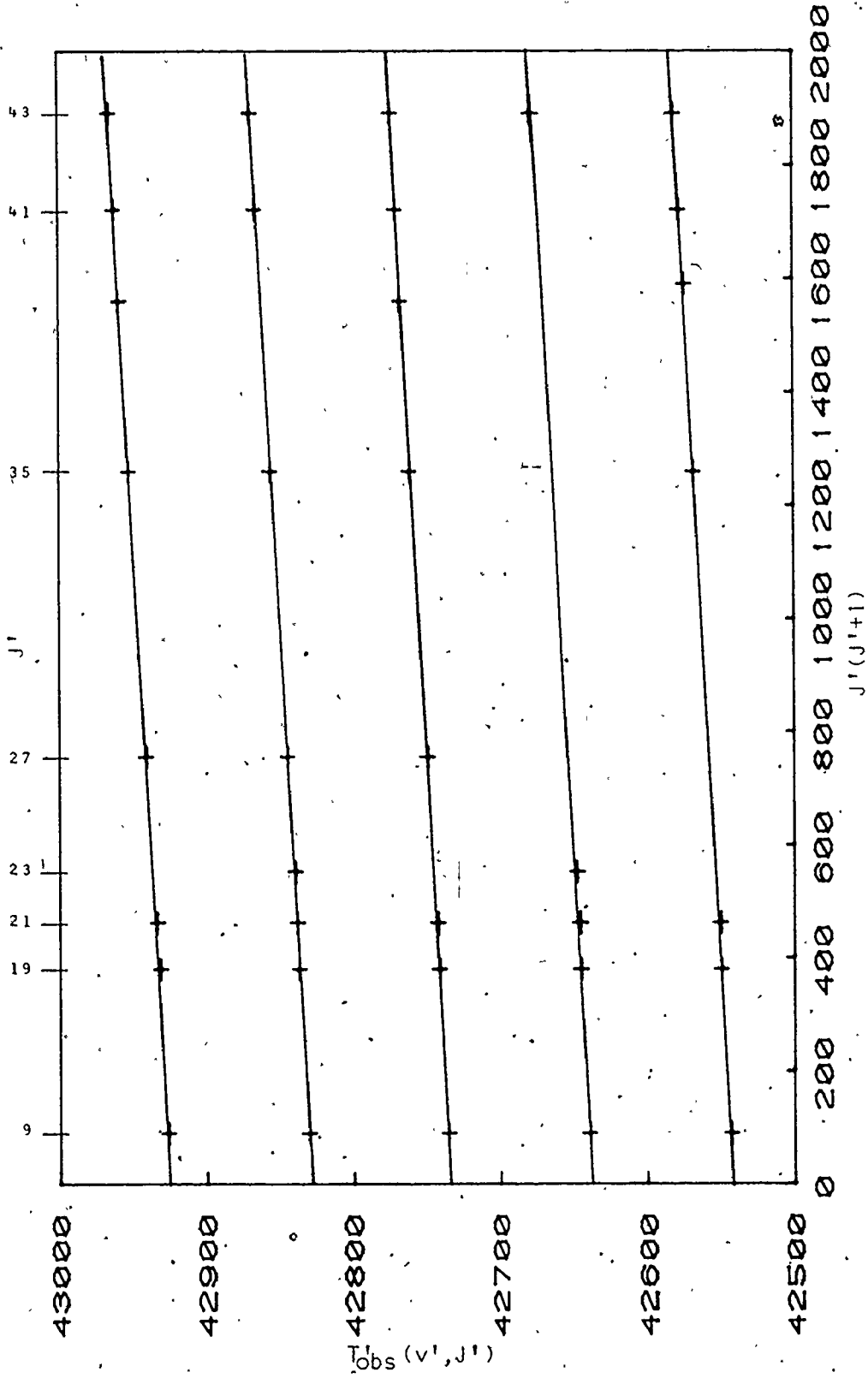
Figure V-9: Graphical Representation of the Rotational Analysis of the ε Bands. T'_{obs} values are shown versus $T'(J'+1)$ for a given J' assignment. Only the first five vibrational quanta are shown, see Table V-10.

	$R_{65}(7)$	$R_{66}(19)$	$R_{59}(21)$	$R_{59}(21)$	$P_{68}(29)$	$P_{76}(35)$	$R_{74}(41)$	$R_{74}(41)$	$P_{63}(45)$
$X_{v_B}(J)$ / σ_1	19976.65	19976.65	19888.43	19888.43	19976.65	19976.65	19976.65	19976.65	19888.43
$F_\delta''(J)$	2.091	14.186	17.247	17.247	32.476	47.032	64.274	64.274	77.260
$\sigma_1+F_\delta''(J)$	19978.74	19990.84	19905.68	19905.68	20009.13	20023.68	20040.92	20040.92	19965.69
J'	9	19	21	23	27	35	41	43	43
$J'(J'+1)$	90	380	462	552	756	1260	1722	1892	1892
ε_0	42543.84	42550.04	42550.63	--	--	42568.38	42577.62	42580.92	--
ε_1	42639.54	42645.04	42645.81	42647.72	--	--	--	--	42677.45
ε_2	42735.44	42741.34	42742.49	--	42749.13	42760.58	42770.12	42773.12	42773.14
ε_3	42830.14	42836.54	42837.78	42839.21	42844.03	42855.78	42865.72	42868.72	42868.69
ε_4	42925.84	42931.24	42933.42	--	42940.13	42951.58	42961.12	42964.22	42964.31
ε_5	43020.84	43026.98	43026.84	--	43033.93	--	--	--	43059.06
ε_6	43115.74	43121.54	43122.47	--	43128.43	43140.78	43149.72	43152.92	43153.56
ε_7	43209.34	43215.44	43217.61	--	43222.33	43234.18	--	--	43247.99
ε_8	43303.14	43308.94	43309.91	--	43315.63	43327.68	43336.52	43340.12	43340.95
ε_9	43397.14	43404.34	--	--	43416.83	--	--	--	--
ε_{10}	43489.44	43495.64	43497.1	--	43501.63	43513.68	43522.72	43526.22	--

Table V-10: Typical Rotational Analysis of the ε Bands. Most of the illustrated two-photon transitions arise from B-state levels populated by B←X transitions nearly coincident with the main pump line $R_{74}(41)$, but data from pump line $R_{59}(21)$ is also included. T'_{obs} values from other two-photon spectra were analysed in similar fashion, see Figure V-9.

The ε bands from pumping at other frequencies (see Table V-1) were analysed in similar fashion and the molecular constants were then derived from the line frequencies obtained from all two-photon spectra. The rotational constants and band origins for the ε excited state are presented in Table V-11, while the vibrational constants are tabulated in Table V-12.

In general the standard error for the molecular constants of the ε excited state are greater than the uncertainty reported for the γ state constants. This is partly due to the uncertainty introduced by overlap of individual rotational lines in the ε bands, but also likely arises from perturbations between levels of the γ and ε excited states, see below.

For the ε excited state Table V-13 presents an approximate RKR potential function calculated from the spectroscopic constants given previously. The ε state has a low vibrational interval ($\omega_e \sim 95 \text{cm}^{-1}$) and large internuclear equilibrium distance ($r_e = 3.5 \text{Å}$) and, like the γ state, is typical of an ion-pair excited state as described by Mulliken (13).

The lower portion of the ε and γ potential functions are schematically illustrated in Figure V-10, together with the vibrational levels observed by two-photon sequential absorption. To higher energies the potential functions are not accurately known; this is indicated by

v'	$T_0(v',J'=0)$ (cm^{-1})	B'_v (10^2 cm^{-1})
0	42541.80 ± 30	2.076 ± 24
1	42636.89 ± 45	2.123 ± 53
2	42732.63 ± 22	2.196 ± 18
3	42828.36 ± 36	2.183 ± 27
4	42923.63 ± 16	2.161 ± 13
5	43017.93 ± 45	2.176 ± 50
6	43113.11 ± 25	2.132 ± 19
7	43207.54 ± 28	2.114 ± 32
8	43300.33 ± 29	2.134 ± 22
9	43394.78 ± 71	2.077 ± 102
10	43487.55 ± 46	2.053 ± 35
$B'_e = 2.153 \times 10^{-2}$		$\alpha_e = 5.07 \times 10^{-5}$

Table V-11: Band Origins and Rotational Constants for the ε Excited State of Iodine.

	T_e'	42493.7	
	ω_e'	95.75	
	$\omega_e x_e'$	.0265	
	$\omega_e y_e'$	-7.4×10^{-3}	
$v' + \frac{1}{2}$	$T_0'_{obs}(v', J'=0)$	$T_{0\ calc}(v', J'=0)$	$T_{obs}' - T_{calc}'$
.5	42541.80	42541.57	+.24
1.5	42636.89	42637.24	-.35
2.5	42732.63	42732.79	-.16
3.5	42828.36	42828.18	+.18
4.5	42923.63	42923.36	+.27
5.5	43017.93	43018.29	-.36
6.5	43113.11	43112.92	+.19
7.5	43207.54	43207.21	+.33
8.5	43300.33	43302.12	-.78
9.5	43394.78	43394.59	+.19
10.5	43487.55	43487.59	-.03
Standard Error for T_{calc}' = ±.44cm^{-1}			

Table V-12: Vibrational Constants for the ε Excited
State of Iodine. T' values are expressed
relative to the ground state $X_{v''=0, J''=0}$.

v'	G_v (cm^{-1})	ΔG_v (cm^{-1})	R_{min} (Å)	R_{max} (Å)
0	47.8657	95.6695	3.4403	3.5893
1	143.5352	95.5495	3.3900	3.6482
2	239.0847	95.3849	3.3567	3.6903
3	334.4696	95.1756	3.3304	3.7253
4	429.6452	94.9216	3.3081	3.7563
5	524.5668	94.6229	3.2886	3.7846
6	619.1897	94.2796	3.2710	3.8109
7	713.4693	93.8916	3.2550	3.8358
8	807.3609	93.4589	3.2402	3.8595
9	900.8198	92.9815	3.2263	3.8823
10	993.8013	92.4595	3.2133	3.9043

Equilibrium Internuclear Distance = 3.5126Å

Table V-13: RKR Potential Curve for the ε Excited State of Iodine. The molecular constants given in Tables V-11 and V-12 were used to evaluate the potential function.

R (10†2 ANGSTROMS)

T_e'(cm-1)

ε–Excited State
(0⁺_g)
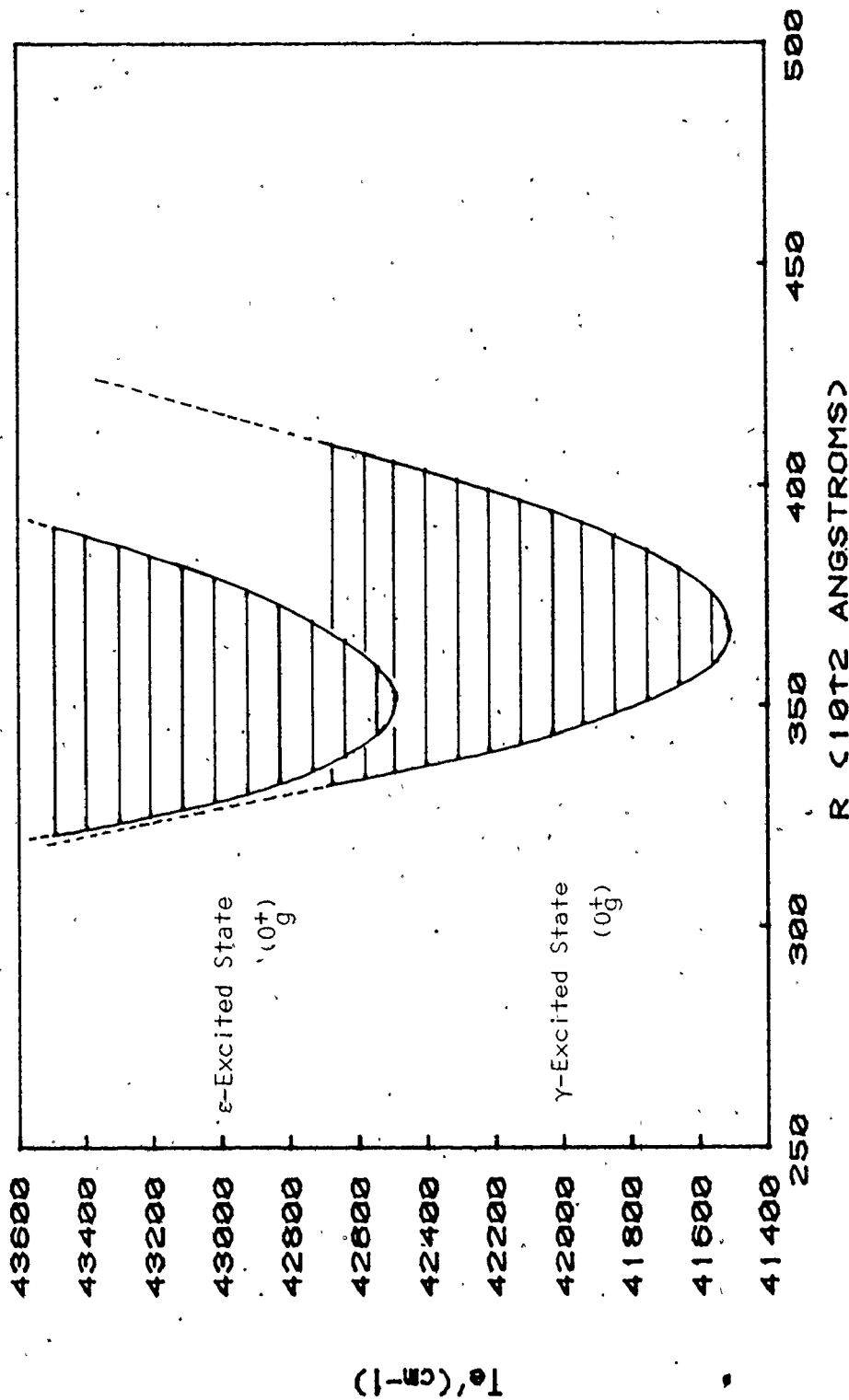
γ–Excited State
(0⁺_g)

Figure·V-10: Schematic Representation of the RKR Potential Functions
for the γ and ε Excited States of Iodine. The energy
levels observed by two-photon sequential absorption are
illustrated.

the dashed lines in the figure. Since both excited states are likely of O_g^+ symmetry (see section 4.4) an avoided crossing of the respective potential functions is anticipated at higher energies. Perturbations are also expected as the energy levels of the γ state at higher energies phase into those of the ε state, see Figure V-10.

Multifrequency pumping of several B state levels was firmly established as the origin of the complex rotational structure of the ε bands by the rotational analysis discussed above. Multifrequency pumping can readily occur because of the extreme density of the B state level structure. The fact that simple two-photon spectra could be obtained at all for the α, β, δ and γ states is perhaps the more surprising observation. The Franck-Condon factors to these excited states from the assigned single pump levels must be very selective.

It might be argued that level shifts (AC Stark Effect) induced by the strong pump laser radiation might shift several B state levels into simultaneous resonance with the pumping frequency. Such level shifts have been observed in very high resolution two-photon studies (72) but would only be of the order of a few GHz ($<.1 cm^{-1}$) under the present experimental conditions. Note in the example of Table V-7, that although several B—X transition frequencies are nearly coincident, the corresponding B state energy levels are not degenerate. Thus it is unlikely that

level shifts within the B state contribute significantly to the complexity of the two-photon spectra reported herein.

It is also improbable that the multilined structure of the ε bands arises from near resonant intensity enhancement of double photon processes (see Chapter III). From equation 3-2, absorption of the second photon in a non-resonant two-photon process must occur within a period $t_e = |\omega_{ig} - \omega_1|^{-1}$ to satisfy energy conservation. For non resonant excitation within $\pm.5cm^{-1}$ of an intermediate state this time corresponds to an extremely short period of approximately 10^{-11} sec. The two-photon transition rate would then be given by:

$$\Gamma_{gf}^{(2)} = \Gamma_{gi}^{(1)}(10^{-11})\Gamma_{if}^{(1)}$$

for the nonresonant process. Since the radiative lifetime of individual rotational levels in the B state are approximately 10^{-6} sec. (93, 44), Γ_{gf}^2 for two-photon excitation involving a resonant intermediate B state level is given by:

$$\Gamma_{gf}^2 = \Gamma_{gi}^{(1)}(10^{-6})\Gamma_{if}^{(1)}$$

The transition rate for near resonant pumping ($\pm.5cm^{-1}$) is

about a factor of 10^5 smaller than that for resonant pumping. Thus near resonant intensity enhancement can not account for the strong multifrequency two-photon transitions observed for the ε bands.

It is most likely that all the ε bands arise from sequential transitions pumped not only by frequencies within the .07cm^{-1} FWHM bandwidth of the pump laser, but also by frequencies within the tails of the pump laser output profile. The marked variation of intensity of individual rotational lines in the ε bands (see Figure V-7 and Table V-9) arises most probably from a superposition of several factors. The most significant factor is likely the Franck-Condon integrals for the B—X and E—B transitions, because these integrals have been shown to have a strong J dependence (94). But the pump energy available at different frequencies, the lifetime of the pumped intermediate level and the magnitude of the dipole matrix elements connecting all three combining states may also play an important role.

4.4 Symmetry Assignments for the Electronic States Observed in Two-Photon Absorption

It is of interest to correlate the upper electronic states of the five progressions observed in the current two-photon experiments with the theoretically predicted valence states of iodine, see Table II-1.

For the strong γ and ε bands only ΔJ=±1 rotational transitions were observed. Assuming that only formally allowed electronic transitions (g↔u, ΔΩ=0,±1, etc.) were active in the two-photon spectra, then under case (c) coupling conditions both the γ and ε excited states would be of 0_g^+ symmetry (16). Mulliken's theoretical arguments (25) support this conclusion. A number of ion-pair type E states [e.g. $1432\,^3\Pi_{0_g^+}$ and $2242\,^1\Sigma_g^+(0_g^+)$] with 0_g^+ symmetry are predicted for iodine in the 5 to 8eV energy region and are expected to yield intense E——B bands.

For the weaker α, β and δ bands the assignment of the upper state is not so clear. The rotational structure was not resolved and it was not possible to establish whether or not Q branches (ΔJ=0) were present in the observed bands. Strict application of selection rules [case (c)] require that the upper state for the α, β and δ bands be either 0_g^+ or 1_g^+. However it is difficult to unambiguously correlate this assignment with the valence states of iodine predicted by Mulliken (Table II-1). As discussed below it is also possible that one or more of the weak progressions involve transitions to an excited state in violation of strict selection rules.

Consider, for example, Tellinghuisen's very recent reassignment of the 3400Å emission spectrum of iodine (95). Tellinghuisen attributes the emission (electric dis-

charge with .5atm of Ar gas) to $1432\,^3\Pi_{2_g} \rightarrow 2431\,^3\Pi_{2_u}$ transitions in which $^3\Pi_{2_g}$ is most probably the lowest energy ion-pair excited state of iodine. The vibrational frequency ($\omega_e'=103.97$) and anharmonicity constant ($\omega_e x_e'=.205$) for the $^3\Pi_{2_g}$ state bear a striking similarity to those deduced for both the α and β excited states in the present investigation. Moreover, Tellinghuisen's estimate of 40500cm^{-1} for the electronic term T_e' is very near the 40281.8cm^{-1} value for the α state and the 40925.1 value for the β state.

If as an example Tellinghuisen's vibrational constants are used together with the electronic term of the α excited state, then the calculated term values for the α progression reproduce the first 13 members observed in the two-photon spectra within a standard deviation of ±1.13cm^{-1}. The close agreement is quite remarkable.[†] It is therefore possible, if not likely, that either the α or β (perhaps even δ) excited states could have 2_g symmetry,[††] and that the high sensitivity of the two-photon technique renders transitions to 2_g states observable in violation of strict selection rules.

[†]If α is indeed the lowest energy ion-pair excited state of iodine then the lower $^3\Pi_{2_u}$ state of the 3400Å emission has an electronic term very near to 9940cm^{-1}.

[††]Tellinghuisen's analysis could not exclude the possibility of a second electronic transition contributing to the emission below 3250Å.

5. Correlation of the Two-Photon Spectra with Previous
   Emission Studies

Wieland, Tellinghuisen and Nobs (WTN) have re-
cently assigned the 4000 to 4380Å emission spectrum of
iodine (14) to E→B transitions originating from levels
of a *single* ion-pair E state. The E state was assigned
$^3\Pi_{0_g^+}$ symmetry and the electronic term (T_e') and the vibra-
tional constants (ω_e', $\omega_e x_e'$) were reported to be 41411.8cm^{-1},
101.59cm^{-1} and .2380cm^{-1}, respectively. Using these mole-
cular constants Rousseau and Williams (53) assigned the
energy level(s) reached by two-photon stepwise excitation
and also reported (55) the radiative lifetime of what was
thought to be the $^3\Pi_{0_g^+}$ E state. Tellinghuisen subsequently
(95) employed Rousseau's fluorescence data (53) to calcu-
late an approximate potential curve for the $^3\Pi_{0_g^+}$ excited
state of iodine.

The present study has revealed five separate E
states for iodine in the 5eV energy region. This raises
questions about the validity of WTN's interpretation of the
iodine emission spectrum (assigned to only one excited E
state) and a re-examination of their spectral data was
therefore undertaken.

Unfortunately, the emission spectra reported by
WTN are very complex in the 4000 to 4380Å region and much
of the vibrational structure is either diffuse or severely

overlapped. Numerous N_2 and CN impurity bands are also apparent. The authors do not report the precision of their bandhead (red degraded) measurements but the uncertainty is probably large (± 2 to $3 cm^{-1}$) in view of the nature of the spectra.

New assignments for the emission bands were determined with the aid of a computer program[†] which calculated all possible E–B transitions arising from the E state levels observed in the present two-photon study. Although all five excited E states were considered, only calculated E–B transitions originating from the γ, δ and ε excited states appeared compatible with the observations of WTN. For these states it was possible to identify E→B transitions whose calculated frequency and isotope shift were in satisfactory agreement with most of the reported emission bands.

Table V-14 presents several prominent progressions observed by WTN but reassigned in accord with the present study. The table includes most of the strong lines reported by WTN and accounts for greater than 70 percent of all the observed emission bands in this region. The average difference between the calculated frequency of the assignments

---

[†]The transitions were calculated from the E state (α, β, γ, δ and ε) molecular constants presented in Section 4 and the B state term values given by Barrow (25). Note that the assignments proposed by WTN are based on the less precise B state parameters given by Steinfeld *et al* (28).

Table V-14: Reassignment of the 4000 – 4360Å Emission Spectrum of Iodine.

EMISSION BANDS[1]			REASSIGNMENT[2]		$v'_E - v_B$		
σ_{obs} (cm⁻¹)	Δ^3_{obs} (cm⁻¹)	Assignment $v' - v_B$	$\sigma_{obs} - \sigma_{calc}$ (cm⁻¹)	Δ^3_{calc}	γ-State	δ-State	ε-State
24840.5	--	7–13	1.3	7.1	3–11		
			2.0	8.5		0–10	
827.5	8.5	11–17	1.5	7.0	4–12		
			3.0	8.4		1–11	
746.5	6.5	5–12	1.5	7.8	2–11		
642.0	--	5–13	.1	8.4	2–12		
544.0	8.0	4–13	3.4	9.1	1–12		
			2.2	13.9			2–24
496.0	--	19–30	1.0	9.8	1 13		
442.0	6.5	4–14	.10	10.4	1–14		
340.5	9.0	4–15	3.6	10.3		5–20	
240.5	10.0	3–15	.93	10.9	1–15		
			2.3	11.0		4–20	
159.5	--	7–20	.3	11.0		5–22	
140.5	11.5	2–15	.1	11.5	1–16		
			1.3	11.7		3–20	
047.0	--	4–18	2.7	12.1		3–21	
041.0	--	2–16	2.4	12.0	1–17		
			1.1	12.5		2–20	
23963.0	--	5–20	.8	12.5		3–22	
950.0	--	3–18	1.8	12.5	1–18		
			.41	12.92		2–21	
940.5	11.5	1–16	.27	13.3		1–20	
866.5	--	4–20	3.5	13.3	1–19		
855.5	11.0	3–19	.74	12.9		2–22	
			4.7	13.7		(1–21)	

(Table V-14, Continued)

840.0	--	0-16	.18	14.1	8-27	0-20	2-33
830.5	--	8-25	.8	10.4		5-26	2-34
814.0	--	7-24	.9	12.0	7-26		
773.0	--	4-21	3.5	14.9			
23763.0	--	3-20	1.3	10.8	1-20	1-22	
755.0	--	2-19	1.8	14.8	8-28		2-36
748.0	12.5	1-18	.3	13.4	7-27	0-21	
742.5	13.0	0-17	.2	14.0	7-28		
664.0	12.5	2-20	.7	10.5		0-22	
654.5	13.5	1-19	2.0	14.5	6-27	4-27	
647.5	13.0	0-18	4.6	11.1	1-22		
587.0	13.0	3-22	1.6	11.2	6-28		
573.0	12.5	2-21	.9	14.8	5-27	5-30	
554.0	14.0	0-19	1.0	13.0	4-26	3-27	
534.0	--	5-25	2.7	14.6	7-30	(5-30)	
518.0	9	4-24	1.8	11.8	1-23		2-39
501.0	12	2-22	.7	14.1	5-28		
489.0	11	1-21	3.2	11.9	4-27	5-31	
473.5	13.5	0-20	1.9	12.5	1-24		2-40
462.5	14.0	4-25	.91	12.5	4-28		
437.0	--	3-24	.49	13.7			
422.1	11	1-22	3.6	12.9			
386.0	15		1.9	12.5			
			.2	11.4			
			.3	14.4			
			.6	14.1			
			4.2	12.6			
			2.3	13.2			
			.4	12.6			
			1.0	13.8			
			4.9	14.7			
			1.26	13.3			

Table V-14, Continued

			Δ_{obs}	Δ_{calc}			E→B
336.0	11.5	3-25	3.7	13.5	1-25		2-41
			.5	14.9	11-39		
318.0	13	2-24	1.0	7.8		3-30	
301.0	14.5	1-23	1.5	14.0	7-33		2-43
286.0	8	0-22	1.3	11.4	11-40		
257.0	13.5	3-26	1.8	13.0	7-34		
			.6	7.5		0-27	2-44
			.2	11.3			
254.0	--	6-30	1.5	16.0	1-26		
235.5	6	2-25	.1	12.5	11-41		
			1.0	15.1		2-30	2-45
217	(14)	1-24	2.8	7.2	11-42		
23189.0	--	6-31	.3	14.8	7-35		
			.5	12.2	1-27		
			3.0	6.9			
179.5	13.0	3-27	4.0	11.2			
			.9	15.2		0-28	2-46
			.5	16.2			
137.0	12.5	1-25	1.4	11.8	7-36		
			.3	11.1		1-30	2-47
			1.5	15.5			
132.0	10.5	4-29	4.4	11.4	5-33		
104.5	13.0	3-28	.1	12.7	1-28		
			1.3	15.4			
			2.2	11.1			2-48
079.0	--	2-27	1.2	11.0	7-37		
069.0	--	--	.1	12.7	5-34		
22973.5	--	--	2.5	10.5	7-39		

[1] Assignments as reported by Wieland *et al.* (14). The authors attribute the emission to E→B transitions from a single ion-pair E state.

[2] New assignments were calculated from the spectroscopic constants deduced from analysis of the two-photon spectra. The emission bands are reassigned to E→B transitions originating from levels of the γ, δ and ε excited states.

[3] Δ_{obs} is the observed isotopic shift between I_2^{129} and I_2^{127} spectral data. Δ_{calc} is the calculated isotopic shift for the proposed reassignments.

given in Table V-14 and the bandhead measurements of WTN
is ±1.56cm^{-1}.

In many cases the new assignments avoid the com-
plexity of WTN's original interpretation. For example, in
the 4100 to 4200Å region, WTN assigned a vibrational series
to four different v_B progressions (i.e. $v'=2$, 3 or 4 with
$v_B=13,14,15$ or 16). By comparison, the reassignment pro-
posed here accounts for the same series as a single v_B pro-
gression ($v'=1$ with $v_B=12$ to 20) arising from the γ excited
state.

It was also possible to use to advantage the
emission data reported for the I_2^{129} isotope. Consider,
for example, the strong band at 24140.5cm^{-1} assigned to
(2-15) for I_2^{127} by WTN. For the γ excited state this band
is reassigned (1-16) for which an isotope shift of 11.52cm^{-1}
is anticipated. In the I_2^{129} emission spectrum an analogous
band is indeed observed at 24152cm^{-1} [but assigned as
(3-26) by WTN] in good agreement with the calculated iso-
tope shift. In general, the calculated isotope displace-
ments for the new assignments were within ±2cm^{-1} of the
values tabulated by WTN. Without access to the original
emission spectra it is difficult to derive more precise
comparisons.

Finally, in support of the assignments presented
in Table V-14 consider the relative intensities of the
emission bands reported by WTN. Classically the Franck-

Condon principle states that the most intense transitions

between two electronic states may be represented schemati-

cally by vertical lines joining the respective potential

energy curves (17). The more intense transitions occur at

constant internuclear separation and will therefore likely

have classical turning points (R_{min} or R_{max}) which are ap-

proximately equal for each combining state. For iodine

the turning points for the B state potential are well

known (25) and an approximate potential function for the

γ state is presented in Table V-8.

Consider one of the strongest bands observed in

emission [see Figure 1 of reference (14)] which is ascribed

to (7-34) in Table V-14 and originates in the γ excited

state. The outer turning points for v_γ' and v_B are 3.898Å

and 4.068Å, respectively. Similarly for another intense

emission band, reassigned to (1-17), the inner turning

point of v_γ' is 3.550Å and the outer turning point for v_B

is 3.582Å. Thus the relative intensity of these transi-

tions (as well as others in Table V-14) is consistent with

Franck-Condon expectations and further supports the pro-

posed reassignment of the emission bands.

CHAPTER VI

ENERGY LEVELS OF IODINE NEAR THE
B STATE DISSOCIATION LIMIT

1. Introduction

During the course of the experiments described
in Chapter V, it was observed that energy levels near the
B state dissociation limit D could be successfully pumped
to yield two-photon sequential absorption spectra of the
E states of molecular iodine. The pumped B state level
$J_{78}(8)$, for example, was just $3.2 cm^{-1}$ below D. The $J_{78}(8)$
level was typical of other pumped levels near D which gave
strong two-photon resonances despite the fact that the
single-photon B$\rightarrow$X emission was relatively weak.

The interpretation of these sequential absorp-
tion experiments required the assignment of individual
B$\leftarrow$X transitions to rovibronic energy levels near D. Un-
fortunately, the single-photon B$\leftarrow$X absorption spectrum
of iodine, even at high-resolution, appears nearly con-
tinuous within about $10 cm^{-1}$ of D because of the very high
density of rovibrational states close to the dissociation
energy. For example, in the high-resolution B$\leftarrow$X absorp-

tion spectra of Steinfeld *et al* (28) the last discrete line which could be observed was some 11cm^{-1} below D.

This behaviour is typical of other heavy molecules in which the generally weak (for Franck-Condon reasons) transitions to rovibronic states near D are essentially indistinguishable from the adjoining continuum. The convergence limit in such cases can only be deduced by extrapolation from the observed discrete bands and the level structure near D is not known from experiment.

A two-photon technique is reported in this chapter which enables the dissociation limit of molecules to be determined directly without recourse to extrapolation procedures. The method permits selective excitation to rovibronic levels near D and has led to the assignment of much of the rotational level structure of iodine from $v_B=77$ to $v_B=83$. The origin for $v_B=83$ is just 0.36cm^{-1} below the B state dissociation limit. The highest level analysed previously (25) by conventional absorption spectroscopy was $v_B=77$, approximately 5cm^{-1} below D.

The vibrational and rotational constants determined for the energy levels near D were applied not only to the identification of B state pump levels, but also to an investigation of the B state potential function at large inter-nuclear distances (9, 15).

2.   The Two-Photon Method

The two-photon technique for the determination of molecular dissociation limits evolved from the pump line calibration procedures described previously in Chapter V, section 2.   The experimental set-up was the same as that illustrated in Figure IV-5 in which B→X fluorescence was continously monitored at the reference cell and E→B emission following sequential two-photon absorption was detected at the sample cell.   The pump and probe laser band-widths were respectively .07cm^{-1} and 1.5cm^{-1}, as for the previously reported experiments.

In the sequential absorption experiments of Chapter V, the pump laser frequency (σ_{pump}) was fixed in resonance with a selected B←X pump line(s) while the probe laser frequency (σ_{probe}) was scanned through various E←B resonances, see Figure V-1.   In the present application σ_{probe} was fixed in resonance with a E←B transition while σ_{pump} was scanned through the spectral region near the B state dissociation limit.   This technique has enabled transitions to rovibronic levels near D to be selectively excited and analysed and has permitted the direct experimental observation of the convergence limit for the B state of iodine.

Figure VI-1 illustrates schematically how the

Figure VI-1:   Successive stages in the convergence of the
pump laser frequency upon the dissociation
limit D.

Stages (a) to (b) result from steps (iii)
and (iv) as described in the main text.
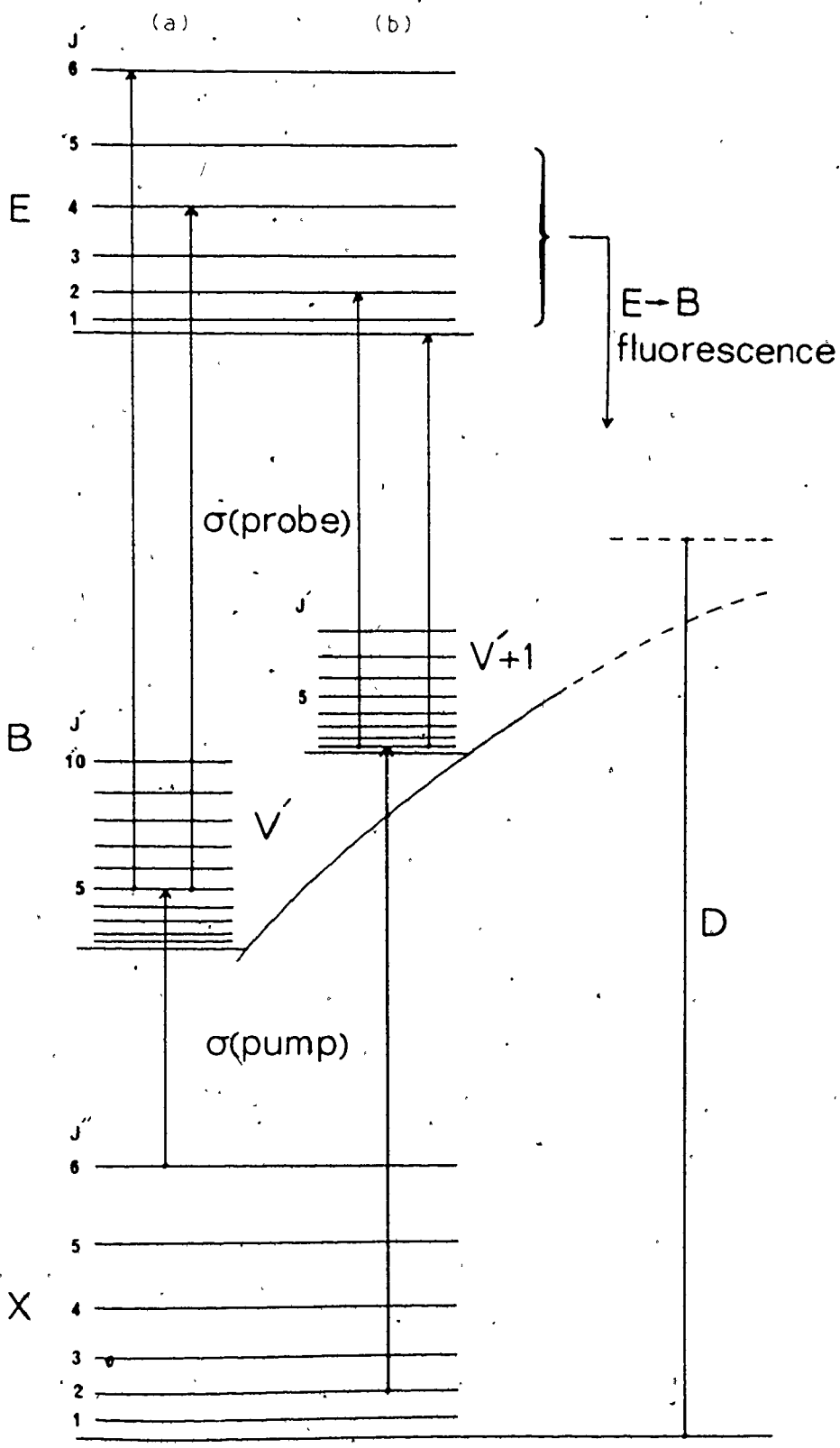
frequency of the pump laser was successively adjusted to converge upon the dissociation energy D. The procedure is outlined below:

i) σ_{pump} was adjusted to a B←X absorption near D (~5000Å). σ_{pump} was positioned by monitoring B→X fluorescence from the reference cell and served to excite iodine molecules from the $v_x=0$ ground state to a (v_B,J_B) level(s) near the convergence limit.

ii) σ_{probe} was then tuned to an E←B resonance by monitoring the E→B emission from the sample cell.

iii) with σ_{probe} held fixed, σ_{pump} was increased to the highest frequency for which an E←B resonance could still be observed. The 1.5cm^{-1} bandwidth of the probe laser encompassed several J_E levels (B_V for the E states is typically ≤.02cm^{-1}) so that several E←B resonances could be excited as σ_{pump} was tuned. However, rotational selection rules limited the observed E←B resonances to $\Delta J=\pm1$ transitions.

iv) σ_{probe} was decreased by a small incremental amount (~.5cm^{-1}) and step (iii) repeated.

The above procedure results in the convergence of σ_{pump} upon transitions to eigenstates with low J_B and high v_B value because of the restriction imposed by the $\Delta J=\pm1$ rotational selection rule. That is, σ_{pump} tended towards the B state dissociation limit as steps (iii) and (iv) were applied alternately. For single-photon excitation near D, B→X fluorescence was very weak, but E→B emission following two-photon sequential absorption was generally strong and enabled D to be experimentally determined to be 20043 ±.5cm^{-1}. The finite bandwidth of the

probe laser determined the precision with which D could
be determined experimentally.

E→B fluorescence from the sample cell was re-
corded as a function of the frequency of the pump laser as
steps (iii) and (iv) were alternately repeated. For each
different (but fixed) probe laser frequency the recorded
spectra exhibited selective rotational structure for a
B←X band of high v_B value near D. A spectrum obtained in
this fashion is illustrated in Figure VI-2. In this exam-
ple rotational transitions up to $J=15$ are selectively en-
hanced for the $v_B=78$ band. For comparative purposes the
single-photon B←X absorption spectrum (obtained from a
fluorescent excitation experiment) is also illustrated in
Figure VI-2. The rotational selectivity of the method
described above is readily apparent from comparison of the
complex single-photon spectrum (practical resolving power
~800,000) with the much simpler two-photon recording. In
contrast to the two-photon spectrum also note that for
Franck-Condon reasons the single-photon spectrum is not
discernible above the signal background in the immediate
vicinity of the dissociation limit.

Different frequency settings for σ_{probe} while
σ_{pump} was scanned through the spectral region near D yield-
ed enhanced rotational lines for different v_B bands in a
manner similar to Figure VI-2. Figures VI-3 to VI-5 il-
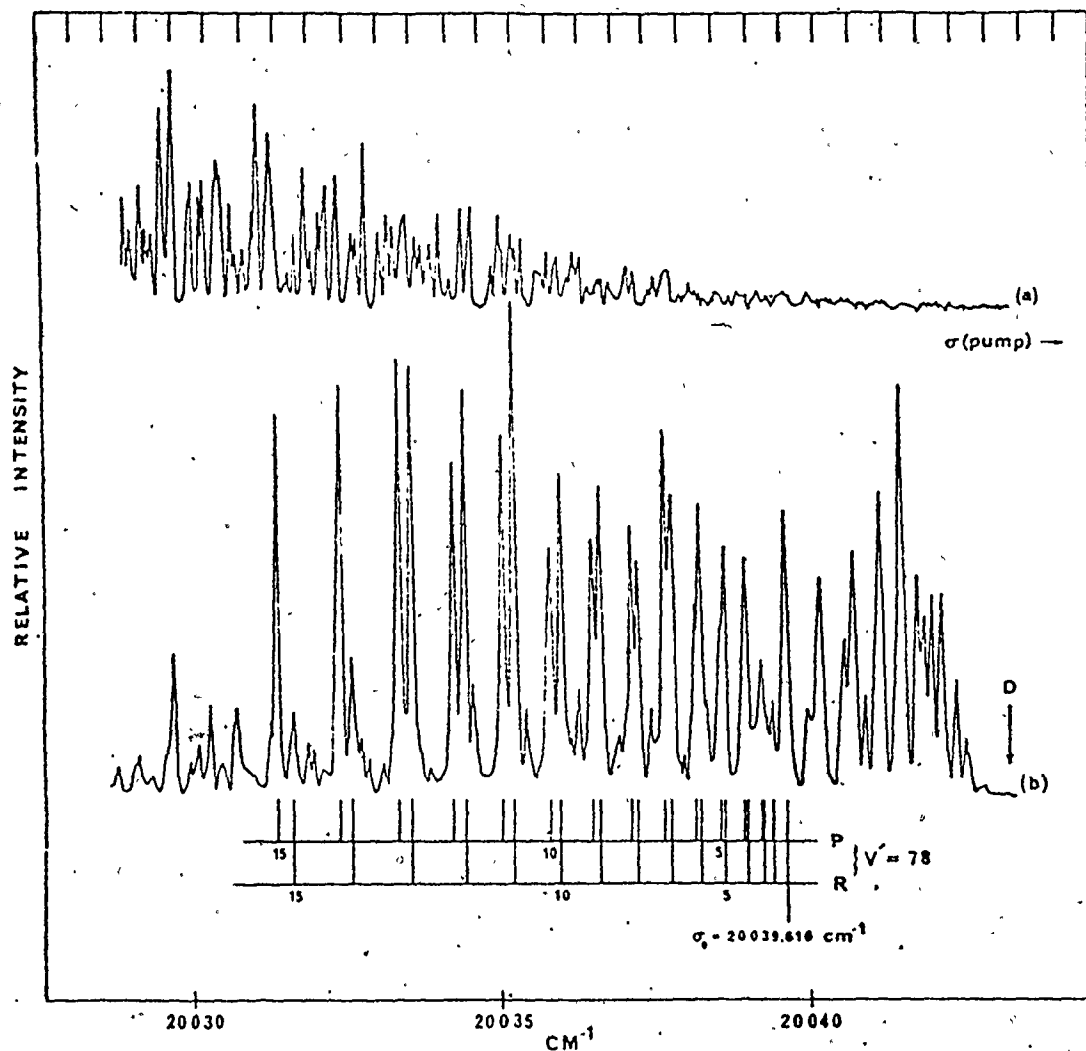
Figure VI-2: Rotational structure near the dissociation
limit of the B←X transition of iodine.

(a) B→X fluorescence from single-photon ab-
sorption obtained by scanning the pump
laser frequency σ_{pump}.

(b) E→B fluorescence from two-photon absorp-
tion obtained by fixing σ_{probe} and scan-
ning σ_{pump}. The probe transition termi-
nated on the γ_2 band for this run. The
rotational structure of the $v_B=78$ band
is labelled in the figure.

Figure VI-3: Enhanced rotational structure of the $v_B=77$ band.

The spectrum was obtained in a manner similar to Figure VI-2(b).

The probe transition also terminated on the γ_2 band for this run, but displaced slightly to higher frequency than the run illustrated in Figure VI-2(b).

RELATIVE INTENSITY

P

R

20038.162 cm⁻¹

CM⁻¹

20030   20035   20040

P: 15 10 7
R: 15 10 7

129
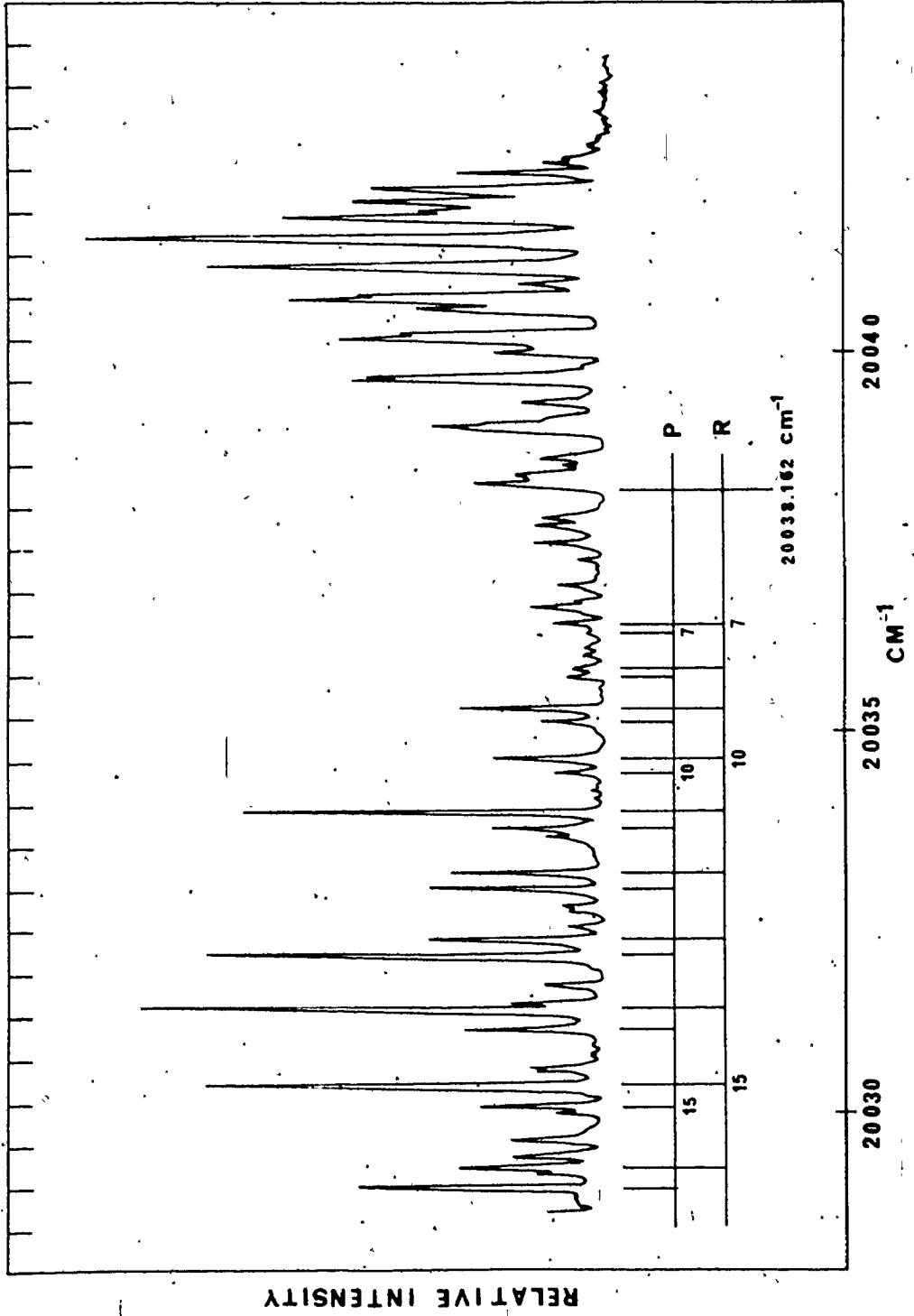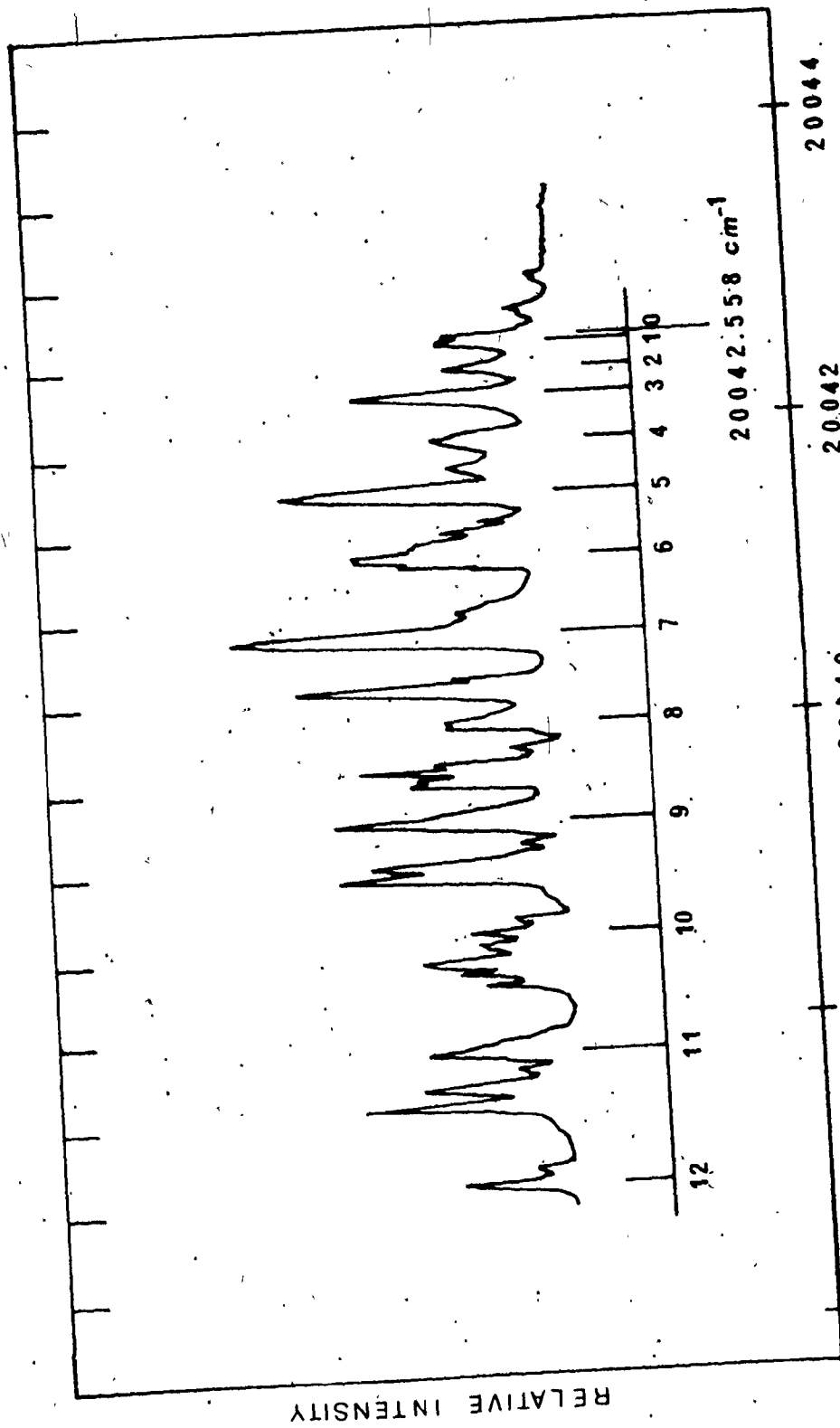
Figure VI-4: Unresolved rotational structure for the $v_B=82$ band as revealed by E→B fluorescence. The probe transition terminated on the α_9 band for this run. The intensity alteration of the unresolved components is illustrated.

Figure VI-5: Rotational structure of the v_B=79 band, showing the intensity decrease of the P and R lines with increasing J. This intensity variation is discussed in the main text with the aid of Figure VI-6.

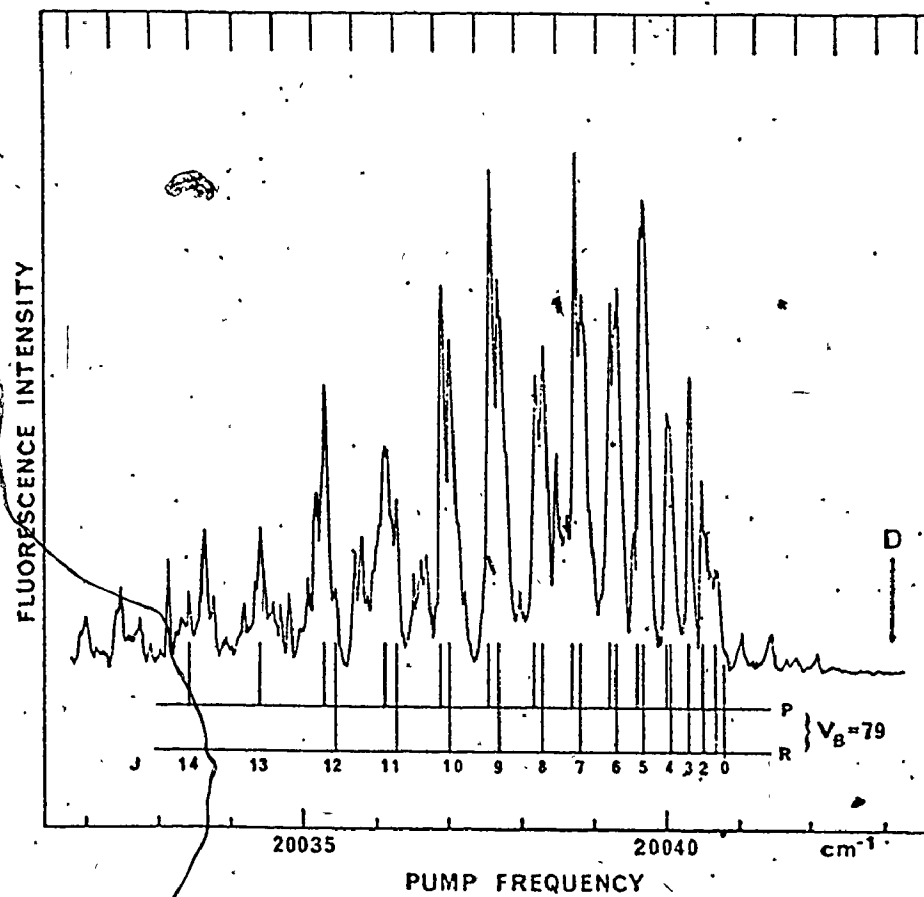lustrate enhanced two-photon B–X bands for v_B=77, 82 and 79, respectively. All of the vibrational levels from v_B=77 to v_B=83 were observed in various two-photon spectra, but the lines corresponding to v_B=83 were only weakly observed and could not be reliably analysed. No head formation was observed for the rotational lines because of the marked difference between the ground state and B state rotational constants. The intensity alteration arising from nuclear statistics (16) was readily observed, with lines of odd J strong and lines of even J weak. However it was apparent that other factors also affected the observed intensities, as discussed below.

The rotational selectivity and the intensity distribution of the two-photon B←X bands may be interpreted in terms of the rotational level structure of the three combining electronic states. Consider for example, Figure VI-6 which illustrates schematically the rotational levels for the X, B and E states. For a fixed probe frequency adjusted to resonance with an E←B transition(s) of low J_E value, the figure illustrates the effect of scanning σ_{pump} from D to lower frequencies[†] while recording

---

[†] It was generally more convenient to tune σ_{pump} from D to lower frequencies because the pressure-tuned dye laser PDL scans toward lower frequencies with increasing propane pressure.
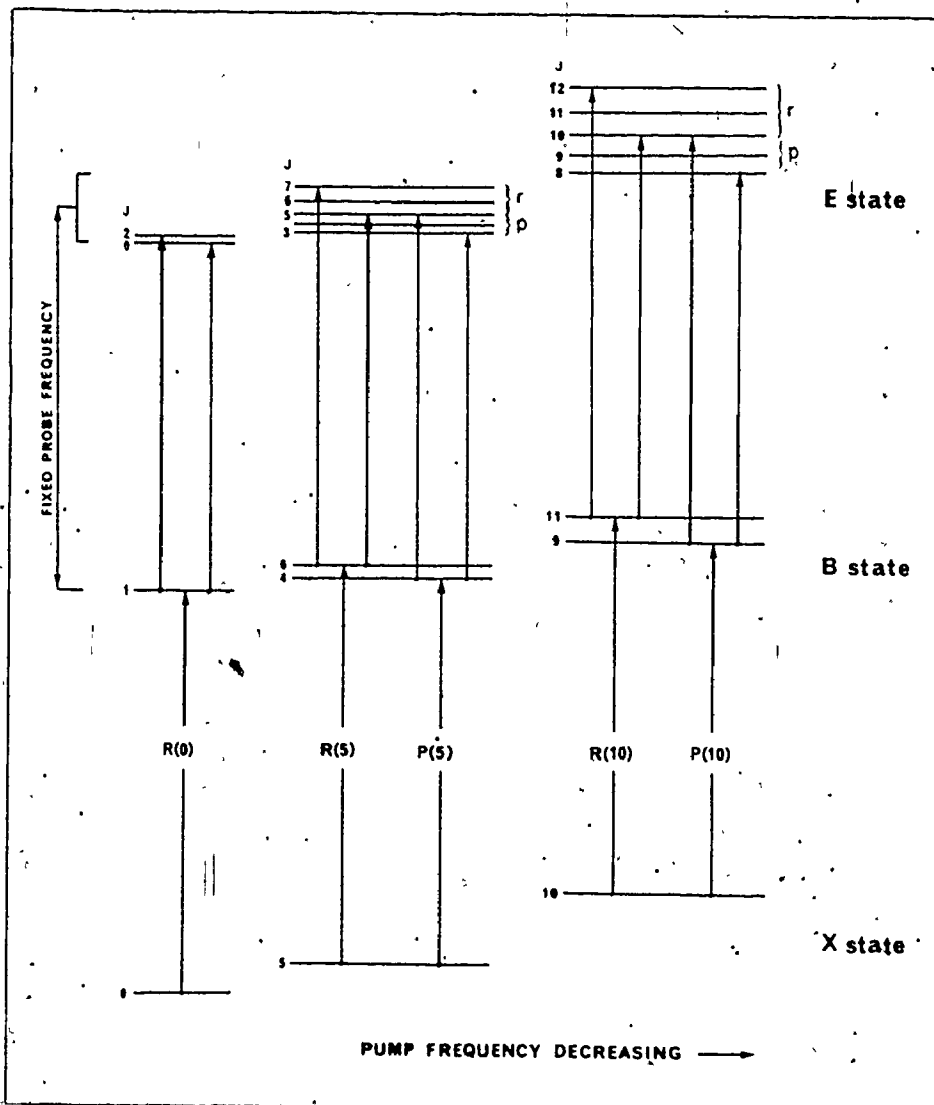
Figure VI-6: Three successive stages in the two-photon process for a single v_B level as the pump frequency decreases. The rotational level separations are greatly exaggerated in the figure and are not drawn to scale. In practice the rotational level separation of the B state is relatively much smaller than the corresponding level separations in the E state.

E→B fluorescence. The left-hand portion of Figure VI-6 illustrates that for a given vibrational level v_B, the first (highest frequency) B←X resonance excited by the pump laser will be the R(0) transition which populates the $J_B=1$ level. From the (v_B, $J_B=1$) level sequential transitions to $J_E=0$ and $J_E=2$ are induced by the probe laser. Broadband E→B emission was employed to detect the R(0) B←X transition.

As the pump frequency decreases successive B–X transitions are detected in similar fashion by the E→B fluorescence. For example, the R(5) and P(5) transitions when excited by the pump laser populate the $J_B=6$ and $J_B=4$ levels as illustrated in the central portion of Figure VI-6. For $v_B=79$ these J_B levels are just $.06 cm^{-1}$ apart. Since the pump laser has a bandwidth of $.07 cm^{-1}$ the R(5) and P(5) transitions for $v_B=79$ are just resolvable, see Figure VI-5. Subsequent probe induced transitions to the E state levels (v_E, $J_E=5$ or 7) and (v_E, $J_E=3$ or 5) have separations $r\sim 0.52$ and $p\sim 0.36$, respectively, since B_v for the excited E state is approximately $.02 cm^{-1}$. These separations are well within the $1.5 cm^{-1}$ bandwidth of the probe laser and so the R(5) and P(5) B←X transitions are revealed by strong E→B emission (see Figure VI-5, for $v_B=79$). Similarly, as indicated in the right-hand portion of Figure VI-6, the separations r and p have increased

to 0.92 and 0.76cm^{-1} for the R(10) and P(10) B$\leftarrow$X lines, respectively. These r and p values are still within the probe laser bandwidth but as levels of higher J_B are excited by the pump laser the separations begin to exceed the 1.5cm^{-1} probe bandwidth. With increasing J the result is that the separation r first exceeds the probe laser bandwidth so that the E$\rightarrow$B fluorescence signal for R(J) lines will decrease. The E$\rightarrow$B signal for P(J) lines will also decrease with higher J values as the separation increases and the number of molecules excited to the E state declines. Eventually, at still higher J values the E$\rightarrow$B signal drops to zero because no allowed transitions are accessible within the finite frequency bandwidth of the probe laser.

The observed E$\rightarrow$B fluorescence signal will therefore be selective and limited to only those allowed E$\leftarrow$B transitions (ΔJ=$\pm$1) whose frequencies fall within the probe laser bandwidth. The intensity distribution of the two-photon B$\leftarrow$X bands will be modulated accordingly. Near D where $B_v\rightarrow 0$ the upper J_B limit for the B$\leftarrow$X rotational transitions observed in the two-photon spectra is determined by the ratio of the probe laser bandwidth to the E state rotational constant. Only B$\leftarrow$X transitions of low J_B were observed herein because of the comparatively small bandwidth of the probe laser. In principle increasing the

bandwidth of the probe laser would permit transitions to levels of high J_B to be excited but this would also increase the line density and complexity of the observed spectra.

Most of the two-photon B—X spectra reported here were obtained with the probe laser frequency held in resonance with one of the first four members of the γ series. These probe transitions were conveniently accessible to the high-gain laser dye 7-diethylamino-4-methyl coumarin and yielded excellent two-photon signal levels. Members of the α and β series in the 21000 to 21700cm^{-1} region were also employed in these studies. Identical B←X transitions were developed by application of the two-photon technique to any of the α, β or γ bands in this spectral region. This observation supports the conclusion presented in Chapter V that the α and β bands arise from transitions to two similar but separate electronic states and do *not* result from vibrational relaxation within the B state manifold. If vibrational transfer processes within the B state were responsible for the α, β or γ bands then they could not yield the same value for D nor produce similar rotational structure as observed for the two-photon B←X bands near D.

σ_{pump} was monitored by a 6mm (nominal) solid quartz etalon during the pump laser frequency scans which

provided the two-photon B←—X spectra. The etalon's transmission fringes, spaced every .556cm⁻¹ (at 5000Å), were photoelectrically recorded and plotted simultaneously with the B←—X spectra on a two-pen chart recorder.[†] The relative frequency of the observed transitions could then be determined to within ±.005cm⁻¹ by interpolation between the known frequency separation of the marker fringes. An absolute frequency calibration to within ±.02cm⁻¹ was most conveniently obtained by calibrating the marker fringes against well resolved rotational lines in the v_B=77 band of the single-photon B←—X spectrum. The single photon rotational lines were identified from the molecular constants of Barrow and Yee (25). Periodically the pump laser frequency determined in this fashion was verified spectrographically by comparison with the known emission lines from an Fe/Ne hollow cathode lamp.

3. Analysis and Assignment of the Two-Photon B←—X Spectra

Once the two-photon mechanism which provided the B←—X spectra near D was understood, it was a relatively straightforward task to identify and assign the observed rotational structure. The two-photon method selectively

---

[†]The short vertical lines at the top of Figures VI-2 to VI-5 correspond to monitor etalon fringes every .556cm⁻¹.

revealed only B←X transitions of low J_B value for one or more adjacent v_B levels. This selectivity enabled assignments to be made with comparative ease by standard methods using combination differences (16).

Using these known methods of analysis; values for [R(J-1) + P(J)] were fitted by least squares to J^2 according to

$$[R(J-1) + P(J)] = 2\sigma_0 + 2(B_V' - B_V'')J^2 \quad . \quad . \quad . \quad (6-1)$$

to provide the band origin σ_0 and the rotational parameter $(B_V' - B_V'')$. Estimates for σ_0 determined in this fashion are indicated in Figures VI-2 to VI-5.

In equation (6-1) the B state rotational constant can only be determined indirectly by difference from the (known) ground state rotational constants.[†] It was considered preferable in the present study to determine both the band origin and rotational constants directly and an alternative treatment was therefore employed which minimized the uncertainty in the derived molecular constants.

The analytical procedure is illustrated in

[†]In principle, albeit with lower accuracy, the rotational constant could be determined from the combination relation (16): [R(J) - P(J) = $4B_V(J+\frac{1}{2})$] applied directly to the observed frequencies of P and R branches.

Table VI-1 for the $v_B=78$ band. The observed terms $T_{obs}(v_B,J_B)$ relative to $X_{v''=0,J''=0}$ were fitted to

$$T(v_B,J_B) = G_v + B_v' J_B(J_B+1) \qquad \ldots \text{(6-2)}$$

to obtain the B state vibrational energy and the rotational constant B_v. The term values $T(v_B,J_B)$ were determined as the sum of the observed line frequencies and the ground state rotational term $F_0''(J)$ calculated from LeRoy's (24) molecular constants for $v_X''=0$. The procedure is analogous to that reported in Chapter V for the rotational analysis of the γ and ε bands. Centrifugal distortion terms could not be accurately determined from higher order terms in equation (6-2) because only lines of low J were observed in the two-photon experiments.

Bands with $v_B=77$ to $v_B=82$ were analysed in similar fashion to determine G_v and B_v as the dissociation limit was approached ($v_D=87$). Only the $v_B=77$ band has been previously rotationally analysed and the results determined here agree favorably with Barrow's (25) values for these molecular constants. The molecular constants for the remaining levels have enabled the long-range potential function near D to be examined in greater detail. Section 4 reports G_v and B_v for the range $v_B=77$ to 82 and examines the region near the convergence limit in the light of these new observations.

J_B	R(J)			P(J)		
	σ (cm^{-1})	$F_0''(J)$ (cm^{-1})	$T_{obs}(\nu_B, J_B)$ (cm^{-1})	σ (cm^{-1})	$F_0''(J)$ (cm^{-1})	$T_{obs}(\nu_B, J_B)$ (cm^{-1})
2	20039.5707	.0747	20039.6454	20039.1941	.4480	20039.6421
3	.4173	.2240	.6413	--	-.7467	--
4	.2397	.4480	.6877	8.5635	1.1199	.6834
5	8.9733	.7467	.7200	.1645	1.5680	.7325
6	.6425	1.1199	.7624	7.6928	2.0906	.7834
7	.2557	1.5680	.8237	.1341	2.6880	.8221
8	7.8045	2.0906	.8951	6.5319	3.3599	.8918
9	.2304	2.6880	.9184	5.8130	4.1066	.9196
10	6.6445	3.3599	40.0044	.0686	4.9279	.9965
11	5.9605	4.1066	40.0671	4.2521	5.8239	40.0760
12	.2471	4.9279	.1750	3.3877	6.7946	.1823
13	4.4574	5.8239	.2813	2.4243	7.8399	.2642
14	3.5858	6.7946	.3804	1.4178	8.9599	.3770
15	2.6334	7.8399	.4733	(30.2317)	10.1546	(.3863)
16	1.6633	8.9599	40.6232	--	--	--
17	30.4293	10.1546	.5839	--	--	--
18	29.4084	11.4239	.8323	--	--	--
	G_v = 20039.6086 ± 73 cm^{-1}			B_v = .003577 ± 49 cm^{-1}		

Table VI-1: Rotational Analysis of the ν_B=78 Band. The table presents T_{obs}' calculated for each P and R line as the sum of the observed transition frequency σ and the ground X state rotational term $F_0''(J)$. The vibrational energy G_v and the rotational constant B_v were obtained by linear regression of the observed terms to equation 6-2.

4. The B State Long Range Potential

The distribution of energy levels and the form of the long-range interatomic potential near the dissociation limit of diatomic molecules has received considerable theoretical attention in recent years (96,97,98). Interaction potentials and dissociation energies have been derived for the electronic states of several diatomics, including the B state of iodine (25, 99).

As mentioned in section 1, experimental measurements in the region near D are very difficult so that theoretical studies typically involve extrapolation of only limited G_v and B_v spectroscopic data to the convergence limit. In practice the reliability of the theoretical analysis is determined by several factors. The proximity to the dissociation limit of the highest observed energy levels determines the range over which the extrapolation must be made. Other important factors are the accuracy with which the energy levels near D are known and the validity of the model assumed to represent the interatomic potential.

Under the assumption that the atoms comprising the diatomic molecule are sufficiently far apart that their electron clouds overlap negligibly, then the long-range potential may be expressed as a sum of inverse power terms:

$$V(R) = D - \sum_{m \geq n} C_m/R^m \qquad \ldots \quad (6\text{-}3)$$

In equation $(6\text{-}3)^{\dagger}$ D is the dissociation limit and R is the internuclear separation. For a given diatomic molecule the dissociation products of the electronic state in question determine which values of the index m contribute to equation (6-3) (98). The coefficients C_m can be obtained from perturbation theory, but recently fairly reliable experimental values for these constants have also become available (97).

The analysis of experimental data usually makes use of an effective single term potential

$$V(R) \sim D - C_n/R^n \qquad \ldots \quad (6\text{-}4)$$

where, for short intervals in R, n assumes some generally non-integer (weighted average) value representative of the locally important terms. At the asymptotic limit D, n assumes the integral value n which corresponds to the leading term in equation (6-3).

Various formulae have been derived from equation (6-4) for the distribution of vibrational and rotational levels near D (97). For example, the distribution of vi-

---

†All significant contributions to equation (6-3) are assumed to be attractive in the following discussion.

brational terms is given to good approximation by:

$$(D-G_v)^{(n-2)/2n} = H_n(V_D-V) \; , \; n \neq 2 \qquad \ldots \; (6-5)$$

where v_D is the vibrational index at the dissociation limit. The parameter H_n is given by:

$$H_n = \bar{H}_n / [\mu^{\frac{1}{2}}(C_n')^{\frac{1}{n}}]$$

where μ is the reduced mass and the constants $\bar{H}_n$ are numerical factors listed in reference (97).

Values for the four parameters D, n, C_n' and v_D may be obtained by a simultaneous least squares fit of the experimental energies to equation (6-5), but virtually identical results can also be obtained by simpler graphical methods. For example, provided the value of $\underline{n}$ is known then the experimentally observed vibrational terms for the asymptotic region may be substituted into

$$(\Delta \bar{G}_v / K_n)^{2n/(n+2)} = D - G_v \qquad \ldots \; (6-6)$$

were $\Delta \bar{G}_v = \frac{1}{2}(G_{v+1} - G_{v-1})$ and $K_n = [2n/(n-2)]H_n$. The dissociation limit may then be obtained by linear regression of G_v as a function of ΔG_v for fixed $\underline{n}$. The value of D once determined may then be used in equation (6-5) to ob-

tain C_n and v_D as the slope and intercept, respectively, from plots of v against $(D-G_v)^{(n-2)/2n}$.

For the B state of iodine the asymptotic term in equation (6-3) has $\underline{n}=5$ because this state dissociates into uncharged $^2P_\frac{1}{2}$ and $^2P_\frac{3}{2}$ atoms (97). Using $\underline{n}=5$ several authors (25, 28, 98) have obtained values for D, C_5 and v_D from analysis of B←X absorption transitions. The present investigation has revealed previously unobserved levels near D and has provided an opportunity to extend and improve upon these previous results for the B state of I_2.

Published values of D, C_5 and v_D for the B state of iodine are given in Table VI-2 together with values determined from the present study.

The value for D (see Table VI-2) given by Steinfeld et al (28) was derived from Verma's estimate (22) of the ground state dissociation energy and the known energy separation for the atomic dissociation products for the B state. LeRoy has since shown (31) that Verma's X state dissociation energy is erroneously large so that the v_D and C_5 values derived by Steinfeld et al can not now be considered reliable.

LeRoy and Bernstein's analysis of the B state (98) long-range potential employed Brown's (100) band head measurements for the region $v_B=55$ to $v_B=72$. A least squares fit of the observed band heads to equation (6-5) was used by the authors to derive the constants listed in Table VI-2.

Reference	D (cm^{-1})	C_5 $(10^{-5} cm^{-1} Å^5)$	v_D	v_H
Steinfeld et al (28), 1969	.20055.6	1.10	93 ± 2	50
LeRoy and Bernstein (98), 1971	20044.0 ± 1.2	3.11 ± 0.2	87.7 ± 0.4	72
Barrow and Yee (25), 1972	20043.208 ± .033	2.8861 ± .006	87.345 ± .007	77
Danyluk and King (9, 15), 1977	20043.063 ± .020	2.776 ± .018[†]	87.132 ± .012[†]	82

Table VI-2: Published Values of the Long-range Potential Constants for the B State of Iodine.

[†]The quoted standard deviations for C_5 and v_D assume an optimal value for D of 20043.063cm^{-1}, in a manner similar to the analyses of reference (98) and (25). The standard deviations must be increased to ±.132 and ±.106 for C_5 and v_D respectively, if the uncertainty in D is included in the evaluation of equation (6-5).

Improved estimates of D and C_5 for the B state of iodine
were subsequently obtained by Barrow and Yee (25) who em-
ployed G_v values from their analysis of the visible B←X
absorption up to $v_B=77$. With the graphical procedures
described above, Barrow and Yee determined the revised
constants D, C_5 and v_D also presented in Table VI-2.

The present analysis has made use of similar
graphical methods to obtain improved values for the long-
range constants for the B state of iodine. Table VI-3
lists G_v and B_v values included in the analysis. Levels up
to $v_B=82$ were included so that the required extrapolation
interval to D is reduced and the asymptotic value $\underline{n}=5$ can
be assumed with greater confidence in comparison with pre-
vious studies. The present analysis also followed LeRoy's
recommended procedure (97) in which the lowest energy level
was successively omitted from repetitive least squares fits
to equations (6-5) and (6-6). Although the standard error
for C_5, v_D and D increases as fewer data points are in-
cluded, a $(1/\sigma^2)$ weighted least squares analysis of all
calculated parameters yields optimal values for the long-
range constants (97).

Figures VI-7 and VI-8 illustrate the analytical
procedure. Figure VI-7 presents equation (6-6) in graphi-
cal form, in which $\Delta G_v^{1.0/7}$ is plotted against G_v for the range
$v_B=72$ to $v_B=82$. In Figure VI-7, Barrow's data (25) was
used over the sub-interval $v_B=72$ to $v_B=76$, while G_v values

v_B	G_v(obs) (cm^{-1})		G_v(calc) (cm^{-1})	B_v(obs) (10^2 cm^{-1})		B_v(calc) (10^2 cm^{-1})
	This work (15)	Barrow and Yee (25)	*	This work (15)	Barrow and Yee (25)	*
72		20024.558 ± 4	20024.558		.6569 ± 12	1.0312
73		28.312 ± 7	28.318		.6092 ± 18	.9417
74		31.473 ± 6	31.507		.5709 ± 22	.8542
75		34.141 ± 5	34.179		.5262 ± 26	.7689
76		36.396 ± 16	36.386		.4560 ± 81	.6859
77	20038.1637 ± 136	38.162 ± 35	38.177	.4266 ± 109	.4297 ± 180	.6054
78	39.6086 ± 73		39.600	.3577 ± 49		.5275
79	40.6972 ± 30		40.705	.2964 ± 59		.4523
80	41.5595 ± 26		41.536	.2591 ± 68		.3801
81	42.1618 ± 37		42.137	.1784 ± 39		.3113
82	42.5333 ± 73		42.548	.1064 ± 189		.2460
83	(42.6996)		42.811	(.0711)		.1849
84			42.962			.1284
85			43.034			.0777
86			43.059			.0343
87			43.063			.0029

*Calculated G_v and B_v values were obtained with the constants derived from the present analysis, see Table VI-2: $G_v = 20043.063 - \{0.15806(87.183-v)\}^{10/3}$
$B_v = \{2.13149 \times 10^{-3}(v_D-v)\}^{4/3}$

Table VI-3: Vibrational Energy Levels and Rotational Constants near the B State Dissociation Limit of Iodine.
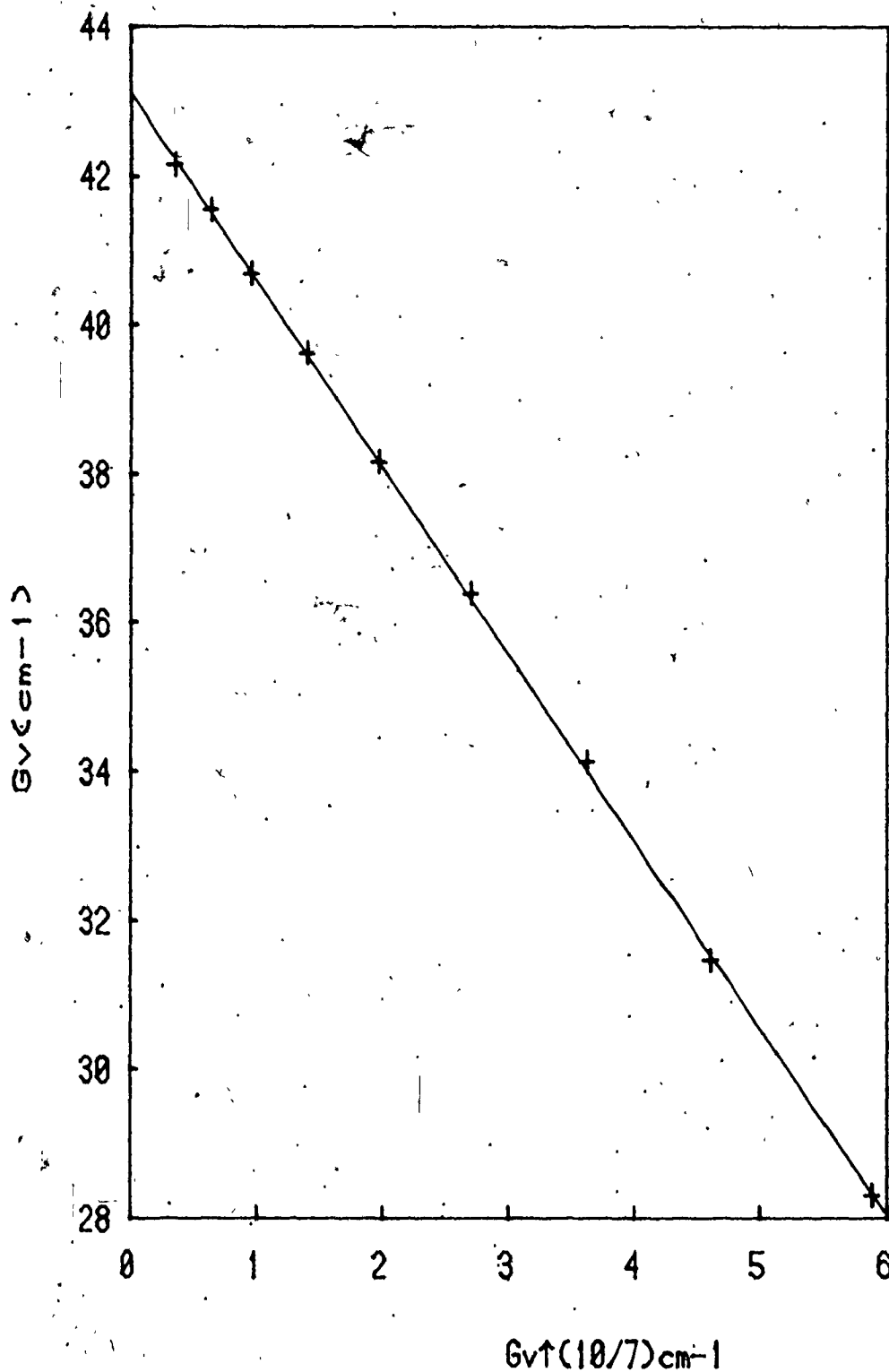
Figure VI-7: G_v versus $\Delta G_v^{10/7}$ for vibrational levels near the B state dissociation limit. The plot illustrates application of equation (6-6) to the experimental data of Table VI-3 to determine the dissociation limit D.
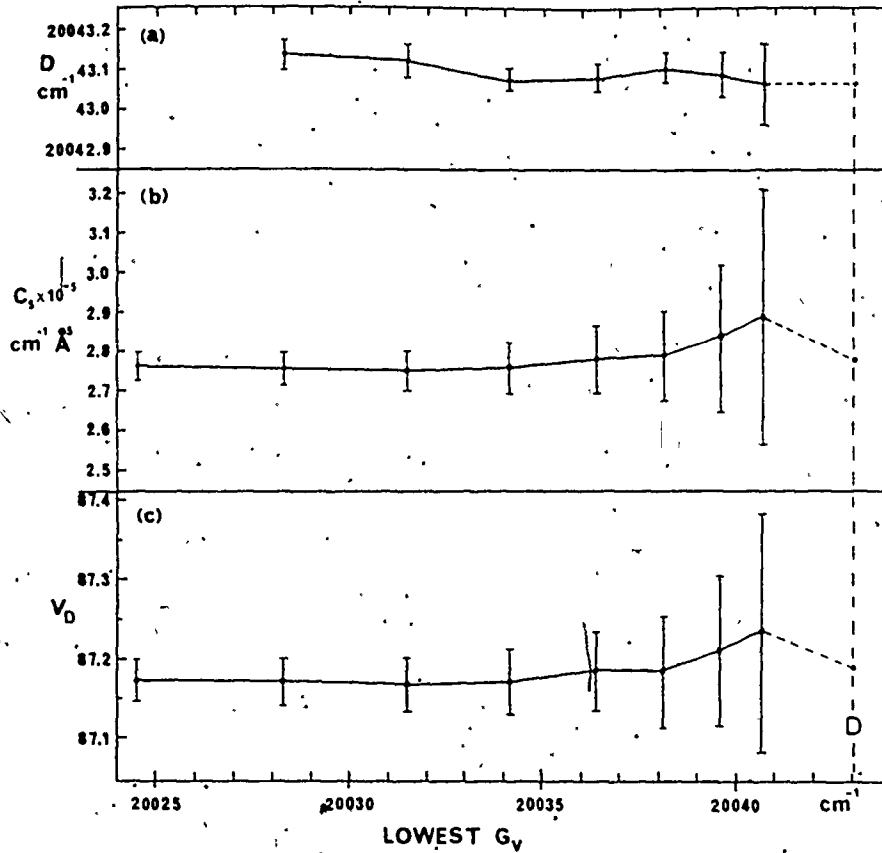
Figure VI-8: Calculated values of D, C_5 and V_D as a function of the lowest level included in the least squares fits. The error bars represent one standard deviation ($\pm\sigma$). The values at D were determined from a weighted ($1/\sigma^2$) fit to the points in each plot. The points in (a) were determined from equation (6-6), those in (b) and (c) from equation (6-5).

from the present analysis were used for the levels $v_B \geq 77$.
As the lowest energy level was successively omitted ($v_B=72$
to $v_B=79$) from the analysis, see Figure VI-8, the calculat-
ed value of D declined slightly. LeRoy and Bernstein (98)
have observed a similar trend in their calculated D values
for the B state of both I_2 and Cl_2. A weighted least
squares fit of the data points given in Figure VI-8 pro-
vided the value of $20043.063 \pm .020 cm^{-1}$ for the converg-
ence limit for the B state of iodine.

With this value for D, application of similar
procedures to equation (6-5) provided values for C_5 and
v_D. Figure VI-9 illustrates a plot of v against $(D-G_v)^{\frac{3}{10}}$
for the range $v_B=72$ to $v_B=82$. Here too Barrow's data was
used for energy levels below $v_B=77$ and C_5 and v_D were re-
peatedly clalculated while the lowest energy level was suc-
cessively omitted from the analysis. See Figure VI-8. A
$(1/\sigma^2)$ weighted least squares extrapolation of the calcu-
lated parameters to D provided the C_5 ($2.776 \pm 1.018 \times$
$10^5 cm^{-1}Å^5$) and $v_D(87.183 \pm .012)$ constants listed in Table
VI-2. As shown in the table there is good agreement be-
tween the long-range constants of the present study and the
upper bound values derived by Barrow and Yee (25) from a
$7 cm^{-1}$ extrapolation from $v_B=76$ to the dissociation limit.

Although the above discussion has considered only
the distribution of vibrational levels near the convergence
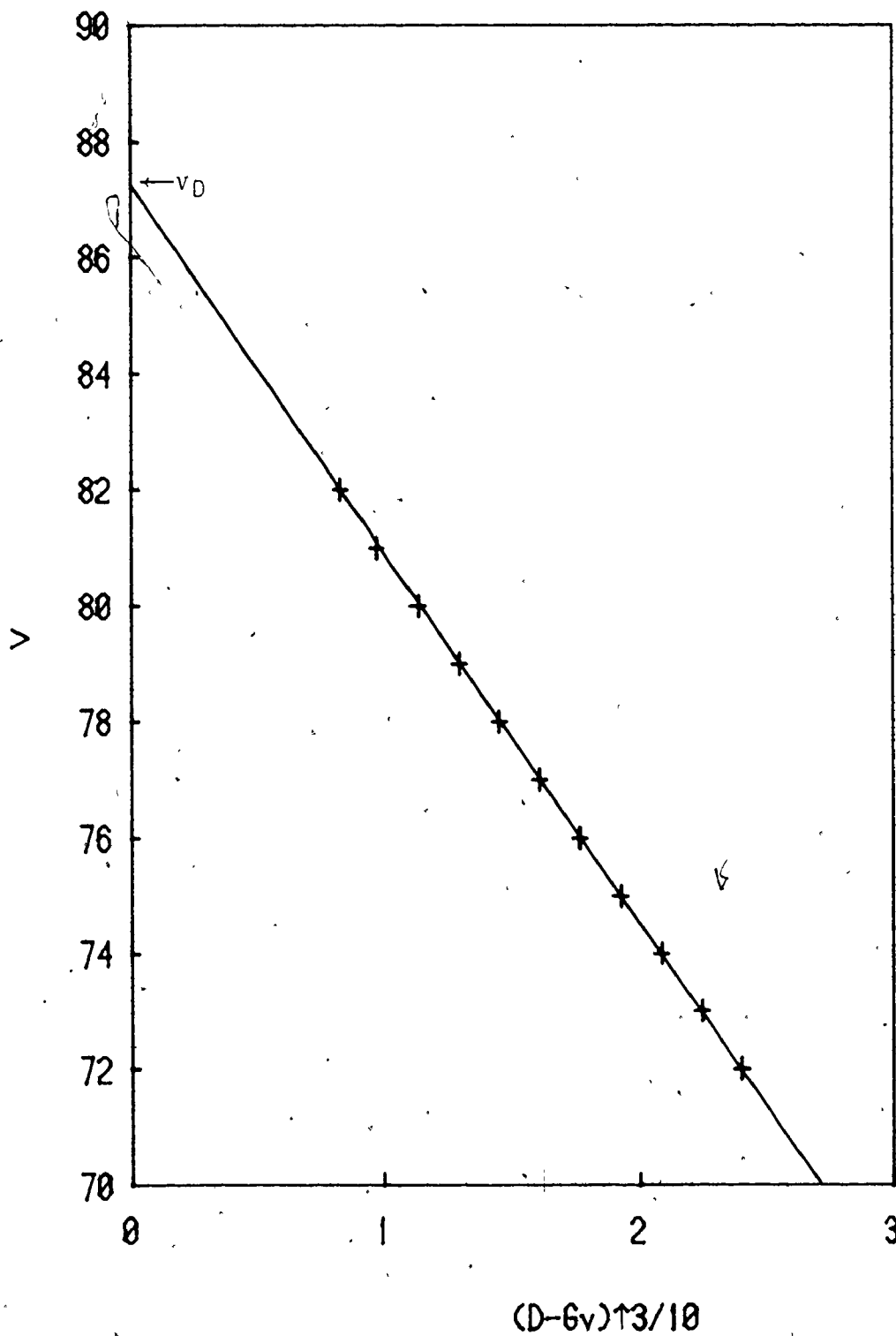limit, the rotational level distribution has also been

Figure VI-9: Application of equation (6-5) to the experimental data of Table VI-3 to determine the vibrational index v_D and the coefficient C_5.

theoretically examined. LeRoy (97) has shown that in the absence of centrifugal distortion, the rotational constants near D are given by:

$$B_v^{(n-2)/4} = Q_n^{(n-2)/4}(v_D-v) \ , \ n \neq 2 \qquad \text{. . . (6-7)}$$

where

$$Q_n = \overline{Q}_n/[\mu^n(C_n)^2]^{1/(n-2)} = \overline{P}_n(H_n)^{4/(n-2)}$$

and v_D and H_n' are as defined for equation (6-5). The constants $\overline{P}_n$ and $\overline{Q}_n$ are numerical constants tabulated in reference (97).

As discussed by LeRoy (97) equation (6-7) is a less accurate approximation than the analogous equation for the vibrational energy levels. The value for C_n determined by fitting experimental B_v values to equation (6-7) will, in general, tend to be too large. Conversely, if known C_n values [derived from equation (6-5)] are used with equation (6-7) to predict the rotational constants B_v, then the latter are expected to be higher than the experimental values.

Subject to this limitation, the main application of equation (6-7) has been to estimate unknown B_v values for energy levels near D (25; 97). For the B state of iodine Barrow and Yee (25) have employed equation (6-7) (as well as polynomial expressions) to predict B_v values for the

then unknown levels above $v_B=77$. As expected their predic-
ted values for B_v are larger than those determined here
experimentally. Similarly, the long-range parameters
of the present study (C_n, v_D, D) yield calculated B_v values
which are larger than the observed rotational constants,
see Table VI-3. (The calculated vibrational energies in
Table VI-3 agree quite favourably with the observed val-
ues.)

Throughout the preceding discussion it was as-
sumed that only the leading term ($\underline{n}=5$) in equation (6-3)
need be considered in the analysis of the B state inter-
atomic potential near D. Several authors have shown
(25, 99, 101) that both the second and third terms (R^{-6} and
R^{-8}) in equation (6-3) contribute to the potential function
for molecular iodine. These authors have used theoretical
analyses of RKR turning points to derive values for the C_6
and C_8 coefficients. LeRoy has shown that fortuitously for
iodine, the correction to the C_5 level distribution for-
mulae [equations (6-5), (6-6) and (6-7)] precisely vanishes
even if the C_6 term contributes up to 50 percent of the
total binding energy. For iodine then the level spacing
for a $\left[\dfrac{C_5}{R^5} + \dfrac{C_6}{R^6}\right]$ potential is equivalent to that for a
pure $\dfrac{C_5}{R^5}$ function. Cancellation does not occur for the
third term (C_8) correction, but this factor contributes on-
ly a minor fraction of the total binding energy at large R.
LeRoy presents an expanded discussion of these points in

reference (97). The result is that the second and higher-order inverse power terms in equation (6-3) have only an insignificant effect on the C_5 coefficient and the C_5 value reported herein is probably reliable within its stated error limit.

For the energy levels near D revealed by the present investigation it was of interest to examine the RKR turning points as well as the C_6 and C_8 coefficients of equation (6-3). Table VI-4 lists the RKR turning points for the B state levels $v_B=70$ to 82 calculated by the weighted quadrature procedure of Tellinghuisen (92). The RKR f and g integrals for $v_B \leq 50$ were evaluated (with a convergence threshold of 10^{-6}) from the polynomial expressions for B_v and G_v given by Barrow and Yee (25). For $v_B=51$ to 82 where the rapid variation of G_v and B_v can not be accurately represented by a single polynomial expression in v_B, the RKR turning points were evaluated by a cubic spline fit to the experimental constants. The turning points for $v_B \leq 76$ were derived from Barrow and Yee's experimental G_v and B_v constants and agree well with their reported RKR values (25). For the range $v_B=77$ to 82 the outer turning points reported here are slightly greater than those predicted by Barrow and Yee (25).

As the convergence limit is approached, the calculated turning points become increasingly sensitive to

v	$G_v(cm^{-1})$	$R_{min}(Å)$	$R_{max}(Å)$
70	4353.21	2.62673	7.34978
71	4358.26	2.62627	7.60342
72	4362.64	2.62586	7.88607
73	4366.40	2.62550	8.20494
74	4369.56	2.62520	8.56847
75	4372.23	2.62495	8.96191
76	4374.48	2.62473	9.41267
77	4376.25	2.62457	9.97782
78	4377.70	2.62443	10.59063
79	4378.78	2.62439	11.38076
80	4379.65	2.62431	12.23407
81	4380.25	2.62426	13.5355
82	4380.62	2.62422	15.217
D	4381.15		

Table VI-4: RKR Potential Turning Points for the Vibrational Levels of Iodine near the B State Dissociation Limit.

small errors in the experimental constants G_v and B_v. The repulsive limb of the potential is particularly sensitive to uncertainties in B_v which are generally known with less precision than the corresponding vibrational energies near D. This was observed in the present study where for levels above $v_B=80$ the calculated R_{min} values were observed to *increase* slightly. As described by LeRoy (97) reliable turning points can still be obtained in such cases by applying the extrapolation procedures first used by Verma (22). .

The R_{min} were smoothed by a cubic polynomial and the inner turning points for $v_B=79$ to 82 calculated by extrapolation. The extrapolation is valid because the inner wall of the potential rises very steeply and can be accurately represented by a low-order polynomial. Improved values for R_{max} were then obtained directly from the turning point differences [i.e. $(R_{max}-R_{min})$] which were determined accurately from the known vibrational energies.

The values reported in Table VI-4 have been corrected according to this procedure in order to provide the best possible estimates for the turning points in the asymptotic region.[†]

[†]For the $v_B=82$ level where the molecular constants are known with least accuracy the uncertainty in B_v and G_v introduces an error bound of ±.009Å and ±.06Å, respectively, in the calculated value R_{max}.

LeRoy has given (99) expressions for the analysis of long-range RKR turning points which yield values for the major coefficients in equation (6-3). For the B state of iodine when C_5 is known, the coefficients C_6 and C_8 may be determined from:

$$\left\{ R_V \left[(D-G_V)-C_5/R_V^5 \right] \right\}^{-\alpha} = C_6^{-\alpha} - \left[\alpha C_8/C_6^{(1+\alpha)} \right]/R_V^2 \quad \quad \text{(6-8)}$$

where R_V is the outer turning point of the vth vibrational level. The exponent α is given by:

$$\alpha = \frac{2C_{10}/C_8}{C_8/C_6} - 1$$

and is a measure of whether higher terms in equation (6-3), collectively denoted by C_{10}, contribute to the long-range potential. The B state of iodine has been analysed with both $\alpha=-1$ (101) and $\alpha=0$ (99) for levels $v_B \leq 77$ and $R_V \leq 10$Å to yield values for the C_6 and C_8 coefficients. It was of interest to examine these coefficients for the higher energy levels (up to $v_B=82$) and larger internuclear separations (up to 15Å) reported here.

For the B state of iodine Table VI-5 sumarizes published values for the long-range potential coefficients C_5, C_6 and C_8. The values given by Yee (101) [line (a), Table VI-5] assume $\alpha=-1$, but LeRoy has since concluded (99)

Reference	Range (Å)	$10^{-5} C_m (cm^{-1} Å^m)$		
		C_5	C_6	C_8
Yee (101), 1974	$5.4 \leq R_v \leq 10.0$	3.40	10.9	460 a)
Leroy (99), 1974	$5.4 \leq R_v \leq 10.0$	2.8861	17.5	267 b)
Danyluk and King (15), 1977	$8.0 \leq R_v \leq 15.3$	2.776	17.8	243 c)

a) based on experimental data of reference (25).

b) C_6 and C_8 coefficients derived from equation (6-8) with the C_5 value of reference (25).

c) This work plus experimental data for $v_B=72$ to 76 from (25).

Table VI-5: Published Values for the B State Long-range Potential Coefficients C_5, C_6, C_8.

that the long-range potentials for the B states of halogen
molecules are best represented by $\alpha=0$ in equation (6-8).
LeRoy's recommended values [line (b), Table VI-5] were
derived on this assumption from a re-analysis of the ex-
perimental data of Barrow and Yee (25) and their best
estimate for C_5 (2.8861 × 10 cm^{-1}Å^5).

In the present study the coefficients C_6 and C_8
were obtained by linear regression of the turning points of
Table VI-4 to equation (6-8) with $C_5 = 2.776 \times 10^5$ cm^{-1}Å^5.
The calculation was repeatedly evaluated over the range
$\alpha=1$ to $\alpha=-1$, in 0.1 steps, as the lowest energy levels were
successively dropped. (The procedure was similar to that
described previously for the calculation of C_5, v_D and D.)
The standard deviations for the fits to equation (6-8)
always were a minimum for $\alpha=0$ and the present study sup-
ports LeRoy's recommendation that $\alpha=0$ for the B state halo-
gens.

The standard deviations for the calculations de-
scribed above increased markedly as fewer levels were in-
cluded. At large R_v (high v_B) $(D-G_v)\rightarrow 0$ so that equation
(6-8) becomes increasingly sensitive to errors. The best
probable values for the long-range constants were derived
from data for $v_B=72$ to 82 and are presented in Table VI-5.
The values for C_6 and C_8 are consistent with previously
reported values, but due to the sensitivity of equation

(6-8) to slight errors in R, D and G_v, it is difficult to evaluate their accuracy quantitatively.

CHAPTER VII

CONCLUSIONS

This study was undertaken with two primary objectives: (1) to build a two-photon laser spectrometer and (2) to investigate two-photon sequential absorption transitions in molecular iodine. These objectives have been met sucessfully and this concluding chapter briefly highlights the results of the present investigation and suggests areas for continued research.

The laser spectrometer designed and constructed for this work has performed satisfactorily and is expected to see continued use for spectroscopic research at McMaster University. However several refinements can be suggested which would improve the convenience and range of application of the spectrometer.

A nitrogen laser of only 300kW peak power was available to excite both of the tunable dye lasers in the two-photon spectrometer. This limited optimal simultaneous operation of both dye lasers to only that spectral region accessible to the high-gain coumarin-type laser dyes. A nitrogen laser with higher output power (peak outputs in

excess of 1MW are commercially available) would consider-
ably improve the wavelength tuning range of the instrument
by permitting the use of low efficiency laser dyes. Al-
ternatively, both dye lasers could be operated with nar-
rower bandwidths than were used here and higher resolution
studies could then be undertaken. In principle nearly
Doppler-free spectra could be obtained and hyperfine struc-
ture resolved. In the present application even a modest
improvement in the bandwidth of the probe laser would have
enabled resolution of the rotational structure of the α,
β and δ bands. This would assist the unambiguous assign-
ment of the upper electronic state for these bands and is
a suggested topic for further research.

One additional instrumentational improvement is
suggested. The spectroscopic application of tunable lasers
requires a convenient and accurate means of frequency cali-
bration of the laser output. It was possible in the pres-
ent application to determine the frequency of the pump
laser indirectly from the known B-X rotational transitions
of iodine and that of the probe laser by recording spectro-
graphically calibration spectra before and after each run.
Although adequate for the present purpose these procedures
were also quite tedious and time consuming. Two very re-
cent publications have suggested different methods for the
convenient calibration of tunable dye lasers which could

be readily applied to the spectrometer used here. The first method, described by D. S. King *et al.* (102), employs the optogalvanic effect in hollow cathode lamps and can be used .to provide direct and accurate spectral calibrations. Hänsch has suggested a second method (103) based on a new self-calibrating type of grating which may soon become commercially available.

The sequential absorption experiments reported here are among the first detailed two-photon investigations of a molecular system. Iodine is perhaps an ideal candidate for a prototype demonstration of two-photon sequential absorption spectroscopy but the technique is quite general and applicable to other molecules.

There are two major advantages of sequential absorption spectroscopy that are illustrated by the present study. First, eigenstates not accessible to single-photon methods may now be investigated. In the present, application to iodine, five separate electronic states have been examined in the 5 to 5.5eV region and their spectroscopic constants evaluated. All five of the excited gerade states (labeled α, β, δ, γ, and ϵ) are of ion-pair type character and have energy levels which are closely interleaved. At least three of these excited states have been shown to likely contribute to previously reported emission spectra of iodine.

The second major advantage illustrated by the

present study is the high degree of rotational selectivity
inherent to sequential absorption experiments. Rotational
assignments for the two-photon spectra may be derived with
comparative ease provided the J numbering of the inter-
mediate pump level is known. For the γ and ϵ bands of
iodine only $\Delta J=\pm 1$ transitions originated from the inter-
mediate pump level(s). This observation has supported a
0_g^+ symmetry assignment and rotational analysis has pro-
vided rotational constants for the corresponding excited
states.

For the weak α, β and δ bands the symmetry as-
signment of the upper state is not so clear because these
bands were not rotationally resolved. Strict application of
selection rules would suggest that only 0_g^+ or 1_g^+ assign-
ments are probable for these excited states. However an
examination of Tellinghuisen's (95) reassignment of the
3400Å emission of iodine suggests that either the α or β
excited states (or both) could have 2g symmetry and that the
high sensitivity of the two-photon technique renders tran-
sitions to 2g states observable in violation of strict
selection rules.

In addition to the high resolution absorption
studies suggested above, it would be an area of further
interesting research to spectrally resolve the emission
from the α and β states excited by two-photon absorption.
Direct comparisons could then be drawn with Tellinghuisen's

emission spectra and it may be possible to conclude a
symmetry assignment for the excited state(s) accordingly.

A two-photon technique for the direct determina-
tion of molecular dissociation limits was developed from
the sequential absorption studies summarized above. The
method permits selective excitation of rotational band
structure near the convergence limit and has provided
values for the long-range potential constants (D, C_5, C_6,
C_8) for the B state of iodine out to an internuclear
separation of 15Å. The technique is generally applicable
to other molecules with high energy vibronic states (E)
accessible by single-photon absorption from an intermediate
state (B).

The main advantage of the new two-photon method
is its rotational selectivity which yields simple spectra
that can be readily analysed. By comparison, single-photon
studies of the region near D yield very complex spectra
that are often indistinguishable (because of multiple over-
lapping transitions) from the adjoining continuum. For
the new method, the upper J limit of the rotational struc-
ture selectively excited near D can be adjusted by varying
the ratio of the probe laser bandwidth to the E state ro-
tational constant. Any degree of line density and com-
plexity can therefore be selected by appropriate adjustment
of the probe laser bandwidth. For the B state of iodine

rotational structure within about 0.36cm^{-1} of the convergence limit was studied in this manner.

The future for two-photon spectroscopy appears excellent. Continued improvements and the wider commercial availability of tunable laser sources will likely see expanded application and refinement of laser-based spectroscopic techniques in general. Less time need be spent on instrumentational development and the innovative spectroscopist will have improved opportunities to contribute to the development of modern optical spectroscopy.

REFERENCES

1) Hänsch, in *Dye Lasers*, ed. F. P. Schäfer (Springer-Verlag, New York, 1973) ch. 5.

2) H. W. Walther, in *Laser Spectroscopy of Atoms and Molecules*, ed. H. W. Walther (Springer-Verlag, New York, 1976) ch. 1.

3) W. Kaiser and C. G. Garret, Phys. Rev. Lett. *7*, 229 (1961).

4) B. Cognac, G. Grynberg and F. Biraben, Phys. Rev. Lett. *32*, 643 (1974).

5) M. D. Levensen and N. Bloembergen, Phys. Rev. Lett. *32*, 645 (1974).

6) T. W. Hänsch, S. E. Lee, R. Wallenstein and C. Wieman, Phys. Rev. Lett. *34*, 307 (1975).

7) L. S. Vasilenko *et al*, JEPT Lett. *12*, 113 (1970).

8) R. W. Field, G. A. Capelle and M. A. Revelli, J. Chem. Phys. *63*, 3228 (1975).

9) M. D. Danyluk and G. W. King, Chem. Phys. Lett. *43*(1), 1 (1976).

10) M. D. Danyluk and G. W. King, Chem. Phys. Lett. *44*(3), 440 (1976).

11) M. D. Danyluk and G. W. King, Chem. Phys. *22*(1), 59 (1977).

12) J. C. McLennan, Proc. Royal Soc. (London) *A88*, 289 (1913); *A91*, 23 (1914).

13) R. S. Mulliken, J. Chem. Phys. *55*. 288 (1971).

14) K. Wieland, J. B. Tellinghuisen and A. Nobs, J. Mol. Spectr. *41*, 69 (1972).

15) M. D. Danyluk and G. W. King, Chem. Phys. *25*(3), 343 (1977).

16) G. Herzberg, *Molecular Spectra and Molecular Structure I, Spectra of Diatomic Molecules* (D. Van Nostrand, New York, 1950).

17) G. W. King, *Spectroscopy and Molecular Structure* (Holt, Rinehart and Winston, Toronto, 1964).

18) R. S. Mulliken, Phys. Rev. *46*, 549 (1934).

19) J. A. Coxon, in *Report on Electronic Spectroscopy*, ed. R. F. Barrow (Chemical Society, London, 1973) ch. 4.

20) R. S. Mulliken, Phys. Rev. *36*, 1440 (1930).

21) C. Teichteil and J. P. Malrieu, Chem. Phys. Lett. *49*(1), 152 (1977).

22) R. D. Verma, J. Chem. Phys. *32*, 738 (1960).

23) D. H. Rank and B. S. Rao, J. Mol. Spectr. *13*, 34 (1964).

23a) D. H. Rank and W. M. Baldwin, J. Chem. Phys. *19*, 1210 (1951).

24) R. J. LeRoy, J. Chem. Phys. *52*, 2683 (1970).

25) R. F. Barrow and K. K. Yee, J. Chem. Soc. Faraday II *69*, 684 1973).

26) R. Meeke, Ann. Phys. *71*, 104 (1923).

27) W. G. Brown, Phys. Rev. *38*, 709 (1931).

28) J. I. Steinfeld, J. D. Campbell and N. A. Weiss, J. Mol. Spectr. *29*, 204 (1969).

29) J. I. Steinfeld *et al*, J. Chem. Phys. *42*, 33 (1965).

30) R. L. Brown and T. C. James, J. Chem. Phys. *42*, 33 (1965).

31) R. J. LeRoy, J. Chem. Phys. *52*, 2678 (1970).

32) J. Tellinghuisen and T. Wei, J. Mol. Spectr. *50*, 317 (1974).

33) K. K. Yee and G. J. Miller, J.C.S. Chem. Comm. 1054 (1972).

34) K. Sakurai and H. P. Broida, J. Chem. Phys. *50*, 557 (1969).

35) J. I. Steinfeld and A. N. Schweid, J. Chem. Phys. *53*, 3304 (1970).

36) D. G. Fouche and R. K. Chang, Phys. Rev. Lett. *29*, 536 (1972).

37) S. Ezekiel and R. Weiss, Phys. Rev. Lett. *20*, 91 (1968).

38) G. Herzberg and L. L. Howe, Can. J. Phys. *37*, 636 (1959).

39) R. L. Brown and W. Klemper, J. Chem. Phys. *41*, 3072 (1964).

40) J. Solomon, J. Chem. Phys. *47*, 889 (1967).

41) T. W. Broadbent and A. B. Callear, J.C.S. Faraday II, *68*, 1367 (1972).

42) G. A. Capelle and H. P. Broida, J. Chem. Phys. *58*, 4212 (1973).

43) D. G. Youmans, L. A. Hackel and S. Ezekiel, J. Appl. Phys. *44*, 2319 (1973).

44) J. A. Paisner and R. Wallenstein, J. Chem. Phys. *61*, 4317 (1974).

45) J. Tellinghuisen, J. Chem. Phys. *57*, 2397 (1972).

46) G. Hancock and K. R. Wilson, in: *Proceedings of the Esfahan Symposium*, eds. M. S. Feld *et al* (John Wiley and Sons, New York, 1973) p. 257ff.

47) A. A. Paschier and N. W. Gergory, J. Phys. Chem. *72*, 2697 (1968).

48) P. Venkateswarlu, Can. J. Phys. *48*, 1055 (1970).

49) A. G. Briggs and R. Norrish, Proc. Roy. Soc. (London), *A276*, 51 (1963).

50) O. Oldenberg, Z. Physik. *18*, 1(1923).

51) K. Wieland and J. Waser, Phys. Rev., *85*, 385 (1952).

52) P. Venkateswarlu, Proc. Ind. Acad. Sci., *A24*, 480 (1946); *A25*, 119 (1947).

53) D. L. Rousseau and P. F. Williams, Phys. Rev. Lett. *33*, 1368 (1974).

54) E. U. Condon, Phys. Rev. *32*, 858 (1928).

55) D. L. Rousseau, J. Mol. Spectr. *58*, 481 (1975).

56) R. D. Verma, Proc. Ind. Acad. Sci., *A48*, 197 (1958).

57) H. Mahr, *Quantum Electronics*, Vol. 1 (Academic Press, New York, 1975), p. 285.

58) J. M. Worlock, in: *Laser Handbook*, eds. F. T. Arecchi and E. O. Schulz-Dubois (North-Holland Publ. Co., New York, 1972), Ch. 2.

59) W. M. McClain, Accounts Chem. Res. *7*(5), 129 (1974).

60) A. M. Bonch-Bruevich and V. A. Khodovoi, Soviet Phys. Usp. *8*, 1(1965).

61) W. L. Peticolas, Annu. Rev. Phys. Chem. *18*, 233 (1967).

62) M. Goeppert Mayer, Ann. Phys. *9*, 273 (1931).

63) B. Honig, J. Jortner and A. Szoke, J. Chem. Phys. *46*, 2714 (1967).

64) R. M. Hochstrasser, H. N. Sung and J. E. Wessel, Chem. Phys. Lett. *24*, 168 (1974).

65) F. Metz, Chem. Phys. Lett. *34*(1), 109 (1975).

66) R. Zito and A. E. Schraeder, Appl. Opt. *2*, 1323 (1963).

67) T. J. McIlrath, Appl. Phys. Lett. *15*, 41 (1969).

68) S. Svanberg and P. Tsekeris and W. Hopper, Phys. Rev. Lett. *30*, 817 (1973).

69) H. T. Duang, S. Liberman, J. Pinard and J. L. Vialle, Phys. Rev. Lett. *33*, 339 (1974).

70) S. Svanberg and P. Tsekeris, Phys. Rev. *A11*, 1125 (1975).

71) P. F. Liao and J. E. Bjorkholm, Phys. Rev. Lett. *34*(1), 1 (1975).

72) J. E. Bjorkholm and P. F. Liao, Phys. Rev. Lett. *33*(3), 128 (1974).

73) R. H. Barnes *et al.*, Appl. Phys. Lett. *24*(12), 610 (1974).

74) F. W. Dalby *et al.*, Can. J. Phys. *55*(12), 1033 (1977).

75) F. W. Dalby and C. Tai, to be published in Can. J. Phys.

76) P. P. Sorokin and J. R. Lankard, IBM J. Res. Develop. *10*, 162 (1966).

77) F. P. Schäfer, W. Schmidt, and J. Volze, Appl. Phys. Lett. *9*, 306 (1966).

78) F. P. Schäfer, in *Dye Lasers*, ed. F. P. Schäfer (Springer Verlag, New York, 1973), Ch. 1.

79) A. Dienes, in *Laser Applications to Optics and Spectroscopy*, eds. S. F. Jacobs, M. Sargent III, J. F. Scott, and M. O. Scully (Addison Wesley, New York, 1975), Ch. 2.

80) T. W. Hänsch, Appl. Opt. *11*(4), 895 (1972).

81) J. P. Goldsborough, Opt. Engineer. *13*(6), 523 (1974).

82) G. K. Klauminzer, Opt. Engineer, *13*(6), 528 (1974).

83) R. Wallenstein and T. W. Hänsch, Appl. Opt. *13*, 1625 (1974).

84) R. Flach, I. S. Shahin and W. M. Yen, Appl. Opt. *13*(9), 2095 (1974).

85) S. Tolansky, *An Introduction to Interferometry* (Wiley and Sons, New York, 1973), 2nd edition.

86) J. E. Mack *et al.*, Appl. Opt. *2*(9), 873 (1963).

87) M. Kroll and K. K. Innes, J. Mol. Spectr. *36*, 295 (1970).

88) G. R. Hanes *et al.*, J. Mol. Spectr. *39*, 506 (1971).

89) A. S. Dickinson and R. B. Bernstein, Mol. Phys. *18*, 305 (1970).

90) R. J. LeRoy and R. B. Bernstein, J. Chem. Phys. *54*, 5114 (1971).

91) E. A. Mason and L. Monchick, Adv. Chem. Phys. *12*, 329 (1967).

92) J. Tellinghuisen, J. Mol. Spectr. *44*, 194 (1972).

93) D. G. Youmans, L. A. Hackel and S. Ezekiel, J. Appl. Phys. *44*, 2319 (1973).

94) J. Tellinghuisen, Phys. Rev. Lett. *34*, 1137 (1975).

95) J. Tellinghuisen, to be published in Chem. Phys. Lett.

96) R. J. LeRoy and R. B. Bernstein, J. Chem. Phys. *52*, 3869 (1970).

97) R. J. LeRoy, in: *Report on Electronic Spectroscopy*, ed. R. F. Barrow (Chemical Society, London, 1973), Ch. 3.

98) R. J. LeRoy and R. B. Bernstein, J. Mol. Spectr. *37*, 109 (1971).

99) R. J. LeRoy, Can. J. Phys. *52*, 246 (1974).

100) W. G. Brown, Phys. Rev. *38*, 1179 (1931).

101) K. K. Yee, Chem. Phys. Lett. *21*(2), 334 (1973), Molec. Phys. *28*, 513 (1974).

102) D. S. King *et al.*, Appl. Opt. *16*(10), 2617 (1977).

103) T. Hänsch, Optics. Lett. *1*(6), 191 (1977).